Aus dem Institut für Integrative Neuroanatomie
der Medizinischen Fakultät Charité – Universitätsmedizin Berlin

DISSERTATION

Afferents to the presubiculum in the mouse brain

zur Erlangung des akademischen Grades
Doctor medicinae (Dr. med.)

vorgelegt der Medizinischen Fakultät
Charité – Universitätsmedizin Berlin

von

Constanze Mauthe

aus Donaueschingen

Datum der Promotion: 09. September 2016

Table of content

Abstract (English)

The need to navigate is a basic behavior in all complex animals. The presubiculum, as part of the parahippocampal region, plays an important role herein in rodents, in other mammals and probably in humans. Detailed knowledge about anatomical connections and functional organisation within the neuronal circuits involved in spatial representation are crucial to understand how the brain computes navigational information.

In this thesis, anatomical afferences to the presubiculum were identified in the mouse via retrograde tracing. Labelling was obtained following stereotactic injection of Retrobeads™ into the presubicular cortex *in vivo.* The distribution of labelled neurons was quantified across the whole brain in two mice in a layer-specific manner for selected upstream cortical areas. The most intense retrograde labelling was observed ipsilaterally in anterior thalamic nuclei, the retrosplenial cortex, and in pre- and parasubiculum. Moderate labelling was found in ipsilateral secondary visual cortices V2M and V2L, lateral entorhinal cortex, perirhinal cortex and subiculum and minor input arose from claustrum, the thalamic nuclei LDN, DLG and Nucleus reuniens, the primary visual cortex and the contralateral presubiculum and retrosplenial cortex. Afferences from the orbitofrontal and anterior cingulate cortex were not examined here due to their very anterior localisation. In granular retrosplenial cortex, labelled cells lay mainly in layer III, in dysgranular retrosplenial cortex, V2M and V2L they lay both in superficial and deep layers, although they were more abundant in superficial layers in Rdg and in deep layers in secondary visual cortices. Presubicular input from V1 originated in deep and from LEC in superficial layers.

I also worked according an optogenetic experimental protocol using lentiviral transfection for the introduction of the photosensitive molecule channelrhodopsin-2 (ChR2) into afferent regions. The transfection efficacy, spread and temporal stability of expression were examined.

My results show that in the mouse, the brain regions afferent to presubiculum are similar to those described previously in other species. I also provide additional information about the laminar origin of the projections from five cortical regions, which could reflect the hierarchy of connections of the network. Preliminary results from optogenetic experiments indicate that this approach may be useful for functional connectivity mapping of specific inputs via the optical activation of axon terminals in the presubiculum.

Abstract (deutsch)

Räumliche Orientierung ist eine grundlegende kognitive Leistung aller komplexen Lebewesen. Das Presubiculum, als Teil der parahippokampalen Region, spielt bei Nagetieren, anderen Säugetieren und wahrscheinlich auch bei Menschen hierbei eine wichtige Rolle. Um zu verstehen, wie das Gehirn die Orientierung im Raum verschlüsselt sind detaillierte Kenntnisse über anatomische Verbindungen und funktionelle Organisation der beteiligten neuronalen Kreisläufe unverzichtbar.

In dieser Doktorarbeit wurden anatomische Afferenzen des Presubiculum in der Maus durch retrograde Markierung identifiziert, welche mithilfe stereotaktischer Injektion von Retrobeads™ ins Presubiculum *in vivo* erzielt wurde. Die Verteilung markierter Neuronen im gesamten Gehirn wurde in 2 Mäusen quantifiziert und in ausgesuchten afferenten Regionen gehirnschichtspezifisch ausgewertet. Die stärkste Markierung fand sich ipsilateral in Anterioren Thalamuskernen, dem Retrosplenialem Kortex, sowie in Pre- und Parasubiculum. Moderat markiert waren ipsilateral die sekundären visuelle Areale V2M und V2L, der Laterale Entorhinale Kortex (LEC), der Perirhinale Kortex, und das Subiculum, minimale Markierung wurde in Clausturm, den Thalamischen Kerngebieten LDN, DLG, Nucleus Reuniens, dem primären visuellen Kortex (V1) und kontralateral in Presubiculum und Retrosplenialem Kortex beobachtet. Afferenzen aus dem orbitofrontalen und anterioren cingulärem Kortex wurden aufgrund ihrer weit anterioren Lage hier nicht analysiert. Im granulären Teil des Retrosplenialen Kortex lagen die markierten Neuronen hauptsächlich in Layer III, im dysgranulären Teil (Rdg), sowie in V2M und V2L waren sie sowohl in oberflächlichen, als auch tiefen Schichten zu finden, wobei sie in Rdg vorwiegend in oberflächlichen, und in sekundär visuellen Arealen in tiefen Schichten lokalisiert waren. In V1 projizierten tiefe Schichten, im LEC oberflächliche Schichten ins Presubiculum.

Außerdem wurde auf ein optogenetisches experimentelles Protokoll hingearbeitet, das über virale Transfektion den photosensiblen Kationenkanal Channelrhodopsin-2 in afferente Regionen integriert. 2 lentivirale Vektoren wurden im Hinblick auf lokale Ausbreitung, Transfektionseffizienz und die Stabilität der resultierenden Virusexpression beurteilt.

Meine Ergebnisse zeigen, dass Afferenzen des Presubiculum in der Maus ähnlich sind wie die zuvor in anderen Spezies beschriebenen. Außerdem stelle ich neue Erkenntnisse über die

zellschichtliche Lokalisation projizierender Neuronen in fünf afferenten Regionen, die Aufschluss über die hierarchische Stuktur innerhalb des Netzwerks geben könnte. Vorläufige Ergebnisse aus den optogenetischen Experimenten zeigen, dass es sich hierbei um einen nützlichen Ansatz für funktionelles Mapping spezifischer Inputs via optischer Aktivierung von Axonendigungen im Presubiculum handeln könnte.

List of abbreviations

AAV	adeno-associated virus
AC	anterior cingulate cortex
AND	anterodorsal thalamic nucleus
AMN	anteromedial thalamic nucleus
AP	anteroposterior
ATN	anterior thalamic nuclear complex
AVN	anteroventral thalamic nucleus
CA	cornu ammonis
CaMKII	calcium/ calmodulin- dependent protein kinase II
cc	corpus callosum
ChETA	Channelrhoposin-2 with E123T mutation
ChR2	Channelrhodopsin-2
Cl	Claustrum
contra	contralateral
cPPT	HIV-1 central polypurine tract
dhc	dorsal hippocampal commissure
DG	dentate gyrus
DLG	dorsal lateral geniculate nucleus
DTN	dorsal tegmental nucleus
DV	dorsoventral
EC	entorhinal cortex
GFP	green fluorescent protein
HD	head direction
HF	hippocampal formation
hSyn	human synapsin
iml	intermediate molecular layer
ipsi	ipsilateral
LEC, LEA, LEnt	lateral entorhinal cortex
LDDM,	laterodorsal thalamic nucleus, dorsomedial part
LDN	laterodorsal thalamic nucleus
LDVL	laterodorsal thalamic nucleus, ventrolateral part
LMN	lateral mammillary nucleus

LV	lentivirus
LTR	long terminal repeat
MEC, MEA, MEnt	medial entorhinal cortex
MMN	medial mammillary nucleus
MS-DBB	medial septum – diagonal band of Broca
ML	mediolateral
NRe	reuniens thalamic nucleus
NSE	neuron-specific enolase
OFC	orbito- frontal cortex
oml	outer molecular layer
PHR	parahippocampal region
PaS	Parasubiculum
PBS	phosphate buffer solution
PER, PRh	perirhinal cortex
PFA	paraformaldehyde
POR	postrhinal cortex
prox	proximal
PrS	presubiculum
Rdg, RSA	dysgranular retrosplenial cortex
Rg, RSG	granular retrosplenial cortex
Rga	granular retrosplenial cortex a
Rgb	granular retrosplenial cortex b
RSC	retrosplenial cortex
RS-d	dorsal retrosplenial cortex
RS-v	ventral retrosplenial cortex
SB	saturation buffer
Sub	subiculum
sup	superficial
V1	primary visual cortex
V2M	secondary visual cortex, medial part
V2L	secondary visual cortex, lateral part
WPRE	woodchuck hepatitis virus post-transcription regulatory element
YFP	yellow fluorescent protein

1. Introduction: The presubiculum as part of the hippocampal-parahippocampal region

Spatial navigation is a crucial skill in everyday life for both animals and humans. Over the past decades, researchers have begun to elucidate a complex network involved in spatial navigation and memory. In 2014, the Nobel Prize for Medicine was awarded to John O'Keefe and the Norwegian couple May-Britt and Edvard I. Moser for their discoveries of cells that constitute the positioning system in the brain. Early research (like O'Keefe's) concentrated on one of the central components, the hippocampal formation itself, but the field has since spread out to adjacent regions, which play an important part in the underlying cognitive processes. The presubiculum is one of those neighboring regions involved in navigational processes: it is crucially involved in head direction signaling and landmark navigation.

The anatomical basis of cognitive processing in the brain is the connectivity between different brain regions. Findings on the presubiculum's connections with other brain regions originate from studies involving broader regions of the temporal lobe conducted in rats in the 1990s. Very few studies concerned the presubiculum itself. Furthermore, the recent increase in the use of mutant mouse models raises questions on the comparability of neuroanatomical and functional features of the rat and mouse brain.

Therefore, in the present work, I studied the afferents of the presubiculum in mice using a recent retrograde tracing technique: fluorescent microspheres called Retrobeads™. Retrobeads™ are non-toxic and compatible with electrophysiological recordings in labelled or connected neurons. Furthermore, I aimed to establish an optogenetic experimental protocol to study presubicular response to specific input. I introduced the light-gated cation-channel channelrhodopsin into afferent regions of the presubiculum using viral transfection with lentiviral vectors.

In the introduction, I will review the structure, function and general connectivity of the hippocampal formation and the parahippocampal region and then focus on existing information about afferent regions to the presubiculum. At the end, I will give a short introduction to the neuronal tracing techniques used in this study.

1.1 Principles of functional organization of the cerebral cortex

The cerebral cortex is concerned with cognitive function and is responsible for the planning and execution of actions in everyday life.[1] Histologically, it is divided into allocortex, periallocortex and isocortex, depending on the numbers of cellular layers, which are numbered from the outer

surface of the cortex (pia mater) to the white matter. The typical form of isocortex consists of six layers, allocortex contains only three layers and periallocortex, as the transitional form between the two consists of four to six layers. The layering of neurons serves to organize inputs and outputs of a cortical region[1].

It has functionally distinct areas called *primary*, *secondary* and *tertiary* sensory or motor areas, which are connected serially with one another. This produces progressively more complex information along the way. Areas that are further downstream and treat more refined and processed information are called higher-order areas. Primary cortices are those areas with direct connection to the peripheral nervous system. They are *unimodal:* specialized for a specific sensory or motor modality (audition, vision, etc.). Primary cortical areas convey their information to, or receive input from, an adjacent, higher-order area: a secondary cortical area. Secondary areas refine the information of a single sensory modality and are therefore also called unimodal association areaa. These areas project to multimodal association areas (or tertiary cortical areas) which integrate information of more than one modality. A feed-forward flow of information from a region of low information processing to a higher order region is referred to as *ascending*, a feedback projection from a region of higher order to a region of earlier stages of processing in terms of a feedback of the higher processed information is called *descending*, and connections within the same hierarchical level are called *lateral* projections. Connections between different cortical areas within the same hemisphere are called *associational*, connections between homologous regions of both hemispheres are referred to as *commissural* projections[1,2].

Principally, the pattern of origin and pattern of termination can give indications about the hierarchy within connected regions. The patterns of origin can be *unilaminar* or *bilaminar*, with *unilaminar* meaning that more than 70% of projections originate in the same layer (superficial or deep). Patterns of termination describe the axonal termination in the target region. Thalamic input for instance, typically targets layer IV of primary sensory cortices.

In general, ascending projections originate in superficial layers and target superficial layers I-III[2] and IV[3]. While associational projections typically originate in layer II/III, commissural projections originate almost exclusively in layer III[2]. Descending projections originate mainly in deep layers and terminate in multilaminar layers I and VI[3]. Layer V pyramidal cells project to the basal ganglia, the brainstem or the spinal cord and layer VI is the main output structure to the thalamus[2].

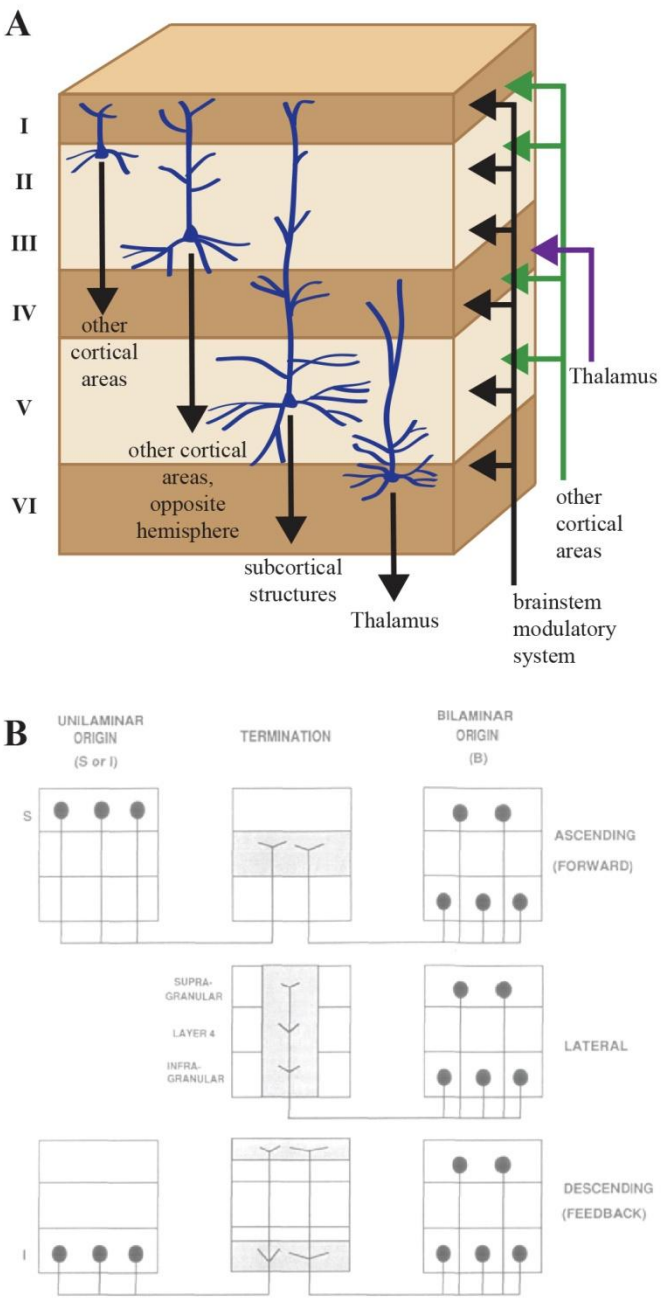

Figure 1: Principles of functional organisation within neocortex

A. Laminar organisation of the neocortex. adapted from Purves (2004)[2]. Principal neurons in layer II project to other cortical areas, projections to cortical areas of the opposite hemisphere (commissural projections) originate in layer III, layer V neurons project to subcortical structures and layer VI to the thalamus. Afferents from the brainstem terminate in all neocortical layers, cortical input terminates in layers I-V and projections from the thalamus target layer IV.

B. Patterns of origin and termination. adapted from Fellemann (1991)[3]. Unilaminar origin is defined as >70% of projections originating in one layer. Projections with bilaminar origin arise in different layers, with <70% in each layer. Ascending projections go to a hierarchically superior area, lateral projections are projections within the same hierarchical level, descending projections arise in a hierarchical superior area and target a hierarchically inferior region. B: bilaminar origin; I: Infragranular layer; S: supragranular layer.

1.2 The hippocampal-parahippocampal region

The hippocampus plays an important role in memory formation and processing, spatial navigation and emotional processing and learning[4]. While early studies focused on the hippocampus itself, the field has expanded to the surrounding areas over the last decades, and it has become more and more evident, that the parahippocampal region also plays a pivotal role in learning, memory, navigation and other cognitive functions such as object recognition[5].

1.2.1 The hippocampal-parahippocampal region: anatomy

1.2.1.1 The hippocampal formation (HF)

The hippocampal formation (HF) is located in the temporal lobe of the brain and consists of the dentate gyrus, the subiculum and the hippocampus proper or cornu ammonis (CA), which is further divided into the subregions CA1 to 4. CA4 lies adjacent to the dentate gyrus and CA1 to the subiculum. The hippocampal formation can be divided into a rostro-dorsal part, located close to the septal region (in rodents) or the corpus callosum (in primates), and a caudo-temporo-ventral part located close to the amygdala. The hippocampal formation in rodents extends its dorsal part far rostrally (Figure 2 Ab), almost abutting the septal region. In humans (Figure 2 Aa), the hippocampal formation has a less curved shape. It is located medially along the temporal horn of the lateral ventricle, with the rostrodorsal pole almost reaching the splenium of the corpus callosum and the caudoventral pole lying in the uncal portion of the temporal lobe. This uncal portion (the *pes hippocampi*) is broader than the dorsal part and shows a medial flex, such that it lies medial to the main part of the hippocampus. It exhibits a variable number of flexures and has a paw-like shape[6]. In order to simplify the reading, I will refer to the rostro-dorso-septal part as septal and to the caudo-ventro-temporal part as temporal. The topographical axes used to describe the hippocampal formation and parahippocampal region are illustrated in Figure 2. Histologically, the hippocampal formation is classified as allocortex.

1.2.1.2 The parahippocampal region (PHR)

The parahippocampal region (PHR) lies adjacent to the hippocampal formation in the parahippocampal gyrus, bordering the subiculum. It comprises five subregions: the presubiculum, the parasubiculum, the entorhinal cortex, which consist of a medial and a lateral area, the perirhinal and the postrhinal cortex[7]. In rodents, the parahippocampal region extends almost to the occipital pole of the hemisphere, where it abuts the visual cortex. In primates, the parahippocampal region is located more ventrally and occupies the ventromedial aspect of the

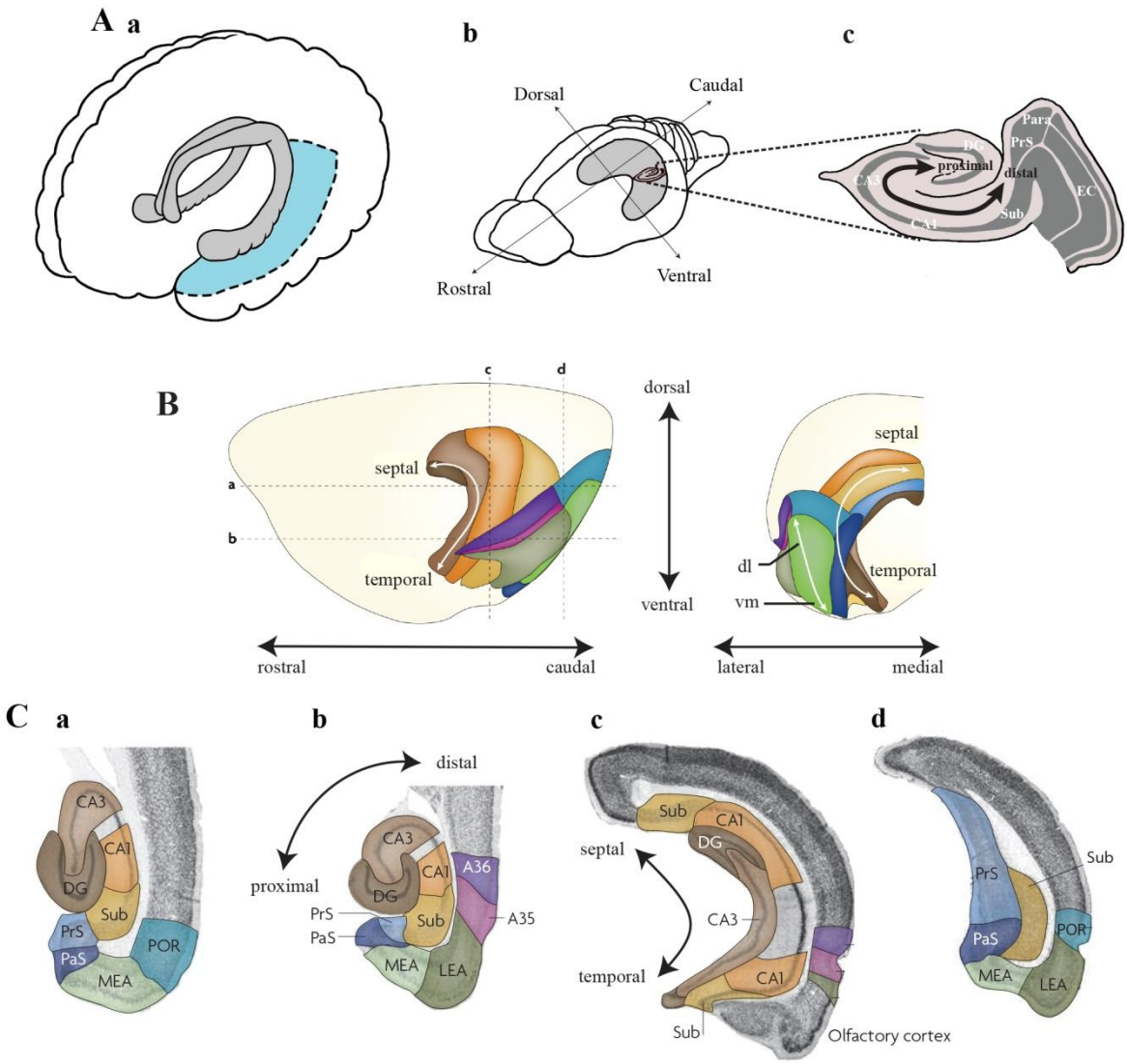

Figure 2: Hippocampal formation (HF) and parahippocampal region (PHR)
A. Representation of the hippocampus (grey) and PHR (light blue) in human (a) and rodent (b) brain. (**c**) illustrates the transverse or proximo-distal axis in the rodent hippocampus[33]. **B. and C. Representation of the hippocampal formation and parahippocampal region in the rat brain**; adapted from Strien (2009)[7] **B.** Lateral (left panel) and caudal (right panel) views. The dashed lines in the left panel indicate the levels of two horizontal (**a,b**) and tow coronal sections (**c,d**) which are shown in **C**.
For orientation, three axes are indicated: the long or septo-temporal axis (also referred to as dorso-ventral axis); the transverse or proximo-distal axis, which runs parallel to the cell layer and starts at the DG; and the radial or superficial-to-deep axis, which is defined as being perpendicular to the transverse axis. In the PHR, a similar superficial-to-deep axis is used. Additionally, the presubiculum and parasubiculum are described by a septo-temporal and proximo-distal axis. The entorhinal cortex, which has a lateral and a medial aspect, is described by a dorsolateral-to-ventromedial gradient and a rostrocaudal axis. The perirhinal cortex (consisting of Brodmann areas 35 and 36) and the postrhinal cortex share the latter axis with the entorhinal cortex and are additionally defined by a dorsoventral orientation. All subfields are colour-coded: dentate gyrus (DG; dark brown), CA3 (medium brown), CA1 (orange) and subiculum (sub; yellow); presubiculum (PrS; medium blue), parasubiculum (PaS; dark blue), lateral entorhinal cortex (LEA; dark green), medial entorhinal cortex (MEA; light green), perirhinal cortex: areas 35 (A35; pink) and 36 (A36; purple), postrhinal cortex (POR; blue-green).

temporal lobe, i.e. the uncus and the posteriorly adjacent part of the parahippocampal gyrus. Notwithstanding the differences in position, the parahippocampal region in all species is bordered dorsally and caudally by the association cortex. Rostrally, the parahippocampal region is bounded by the amygdaloid complex, the prepiriform (olfactory) cortex and, more laterally, by the insular cortex. The lateral border is constituted by the posterior rhinal sulcus, whereas medially the parahippocampal region borders the hippocampal formation[6]. Areas of the parahippocampal region are classified as periallocortex.

1.2.1.3 The presubiculum (PrS)

The presubiculum is the direct continuation of the septo-temporal axis of the hippocampal formation in rodents and consists of Brodmann areas 27 and 48[8]. Brodmann area 48, by some authors called the *postsubiculum,* is the most dorsal part of the presubiculum. Although some authors treat the postsubiculum as a subregion of the parahippocampal region[9], most authors[10] consider it part of the presubiculum and in this work, it will be treated this way. In the proximo-distal axis of the hippocampus (from dentate gyrus to subiculum), the presubiculum is located just next to the subiculum and is then followed by the parasubiculum; these three areas are classically grouped together into the *subicular complex* or *subicular cortex*. Given the anatomical and functional differences between the subiculum as a major output structure of the hippocampal formation on one hand[6] and the pre- and parasubiculum as a relay station for subcortical and cortical input to the hippocampus on the other, the usefulness of this term has been questioned in the past decade[11]. In line with contemporary literature, in this work, the subiculum will be treated as part of the hippocampal formation.

Its anatomical features and laminar cytoarchitecture make the presubiculum easily distinguishable from adjacent brain regions. The six-layered presubicular cortex shows the classical features of cortical laminar organization as it has been described by Lorente de Nó[12]. The molecular layer I contains mainly horizontally oriented axons and apical dendritic tufts of pyramidal cells and very few cell bodies: putative interneurons and glial cells. Layer II consist of pyramidal cells with at least one apical dendrite to layer I, extending to the pial surface. In the presubiculum, these pyramidal cells are particularly densely packed, which distinguishes it from the adjacent parasubiculum[13]. This transition can also be revealed by immunohistochemical staining with a specific marker of the presubicular layer II: the calcium binding protein

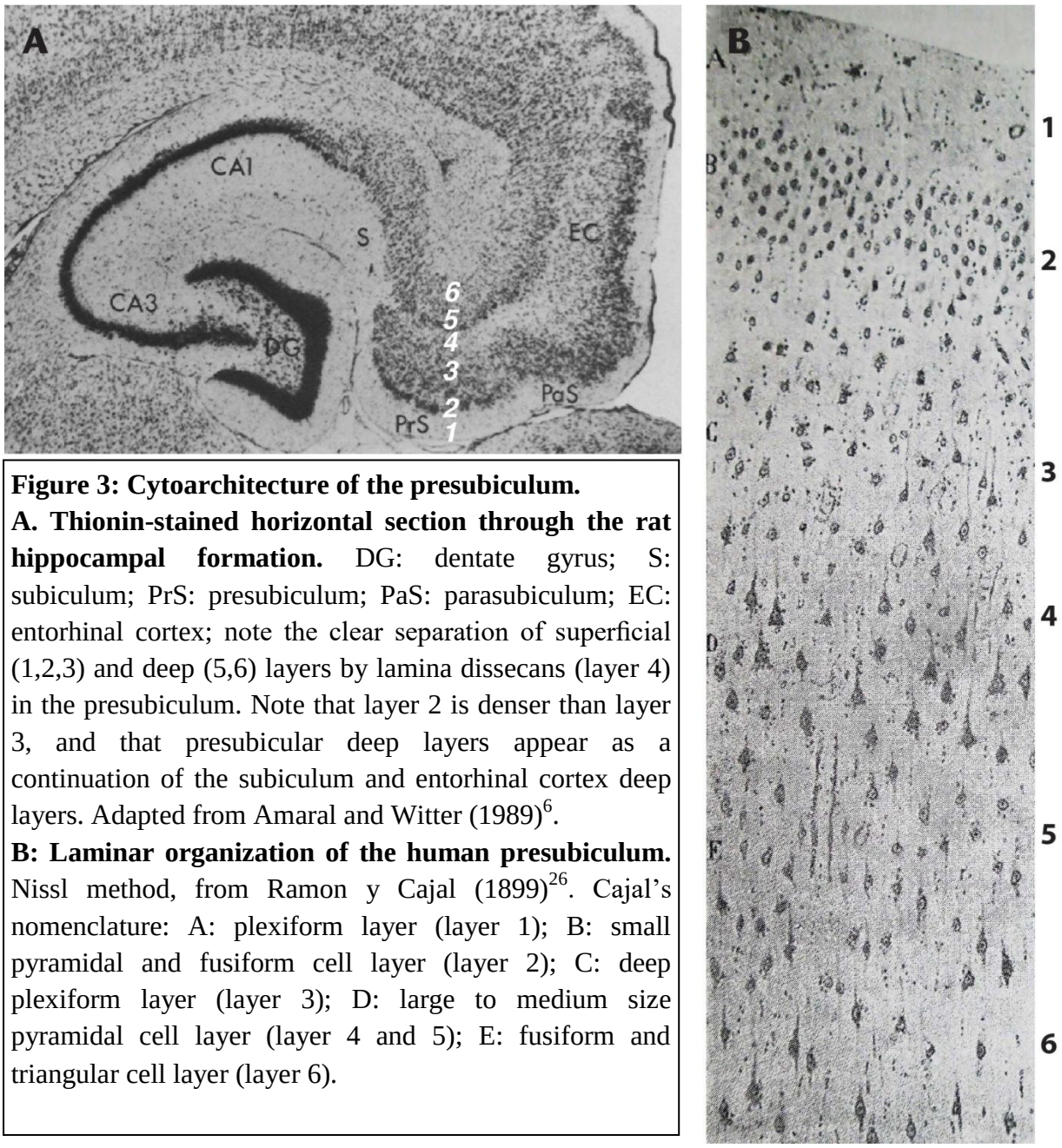

Figure 3: Cytoarchitecture of the presubiculum.
A. Thionin-stained horizontal section through the rat hippocampal formation. DG: dentate gyrus; S: subiculum; PrS: presubiculum; PaS: parasubiculum; EC: entorhinal cortex; note the clear separation of superficial (1,2,3) and deep (5,6) layers by lamina dissecans (layer 4) in the presubiculum. Note that layer 2 is denser than layer 3, and that presubicular deep layers appear as a continuation of the subiculum and entorhinal cortex deep layers. Adapted from Amaral and Witter (1989)[6].
B: Laminar organization of the human presubiculum. Nissl method, from Ramon y Cajal (1899)[26]. Cajal's nomenclature: A: plexiform layer (layer 1); B: small pyramidal and fusiform cell layer (layer 2); C: deep plexiform layer (layer 3); D: large to medium size pyramidal cell layer (layer 4 and 5); E: fusiform and triangular cell layer (layer 6).

calbindin[14]. Layer III pyramidal cells are less densely packed and have one single apical dendrite to layer I or II[13]. Layers I to III are generally referred to as superficial layers. Layer IV, the *lamina dissecans*, is a cell sparse layer and, in the presubiculum, it can be identified as the continuum of layer IV of the entorhinal cortex[13]. It is often used as a marker to separate superficial from deep layers, which are defined as layers V and VI. They contain pyramidal cells of large to medium size in layer V and smaller, fusiform ones in layer VI. The presubicular deep layers are in continuum with the pyramidal cell layer of the subiculum and the deep layers of the parasubiculum and entorhinal cortex[6]. The presubicular border to the retrosplenial cortex can be revealed by immunostaining with several markers, such as the calcium binding proteins

calretinin, calbindin or parvalbumin or markers for acetylcholinesterase, which form patches in the presubiculum, but not in the retrosplenial cortex[15].

1.3 The hippocampal-parahippocampal region: functional significance

It has been well established that the hippocampus and parahippocampal region play an important role in memory processing and formation, spatial navigation and emotional processing and learning[4].

1.3.1 Spatial navigation and neuronal schemes of spatial representation

Spatial orientation relies on two cognitive mechanisms: path integration and landmark navigation[16]. In path integration, the animal estimates its current location by integrating self-derived, internally available information such as vestibular and proprioceptive inputs, or motor outflow (*efference copy*). This information is generally referred to as *idiothetic*. Landmark navigation on the other hand, relies on *allothetic* cues: external information such as visual, olfactory, or auditory signals. Under most circumstances, the brain uses the two processes and integrates both idiothetic and allothetic information, but if information of one source is absent, it relies entirely on the other set of cues. This is the case when an animal explores a novel environment: since it cannot rely on familiar landmarks, navigation relies entirely on path integration[16].

On the neuronal level, various types of spatially tuned cells have been identified: place cells[17], grid cells[18], border cells[19], and head direction cells[20].

Place cells are the principal neurons in the hippocampal formation that are active whenever an animal is in a specific location in an environment, called the cell's *place field*[21]. A typical place field of a place cell in the hippocampus is shown in Figure 4 A. Place cells have also been described in the subiculum and the entorhinal cortex[16], but whether these recordings represented actual place cells or individual nodes of a periodic grid such as found in grid cells (see below), remains to be verified[14].

Expanded recording environments in the dorsocaudal medial entorhinal cortex (dMEC) revealed the grid cell system[18]. Grid cells have periodically spaced firing fields that span the entire environment in a grid-like fashion. The vertices of the firing fields define a triangular or hexagonal array (see Figure 4 C). Grid cells have been identified in the pre- and parasubiculum of the rat as well[14].

Border or *boundary* cells fire whenever an animal approaches a specific geometric boundary within an environment[19]. They have been found in the MEC, the presubiculum and the parasubiculum of the rat, but represent only a small part of the overall cell population within these areas. Border cell activity is often co-localized with grid- and head directional- (see below) activity[19]. A typical border cell is illustrated in Figure 4 C.

Head direction cells fire when the animal's head points to a specific geocentric (e.g. west), independent of the animal's position in an environment and its ongoing behavior. They have first been described in the dorsal part of the PrS of the rat, also known as the postsubiculum[20,22,23] where they are particularly abundant, but have been observed in a number of cortical and subcortical regions since (see below). A simulated typical head direction cell tuning curve is illustrated in Figure 4 B. The head directional signal is highly controlled by visual landmarks[22]. Rotation of visual cues in an environment leads to a corresponding shift in the preferred firing direction. On the other hand, the removal of visual cues or turning off of the lights does not cause a significant disturbance of a head direction cell's activity, although the preferred firing direction may drift after some time[22]. Grid cell firing is controlled by allothetic cues, but persists in their absence, suggesting that grid cells may be part of a generalized, path-integration-based map of the spatial environment[18]. Directional information has been postulated as being relevant to the emergence of stable grid cell properties,[24] and temporarily silencing hippocampal influence on MEC unmasks clear directional features in grid cells[25].

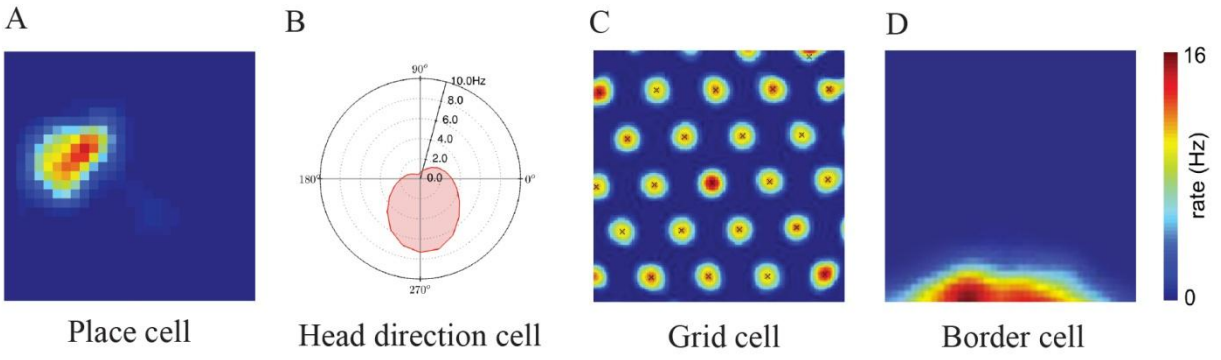

Figure 4: Spatially tuned neurons. A, C, D: Color-coded rate maps/ autocorrelograms: red indicates maximum neuronal activity, dark blue is zero. **A.** Place field of a hippocampal place cell. Place cells fire whenever an animal is in a specific location in an environment. **B.** Directional tuning curve of a head direction cell. **C.** Spatial autocorrelogram of neuronal activity of a grid cell in the medial entorhinal cortex. Grid cells fire periodically in a grid-like fashion. **D.** Colour-coded rate map of an entorhinal border cell. Border cells fire when an animal is close to the borders of the proximal environment. **A, B:** images modified from Kloostermann et al.[126] **C.** adapted from Hafting (2005)[18] **D.** adapted from Solstad (2008)[19]

1.4 The hippocampal-parahippocampal region: connectivity

Spatial information processing has been shown to occur in the entire hippocampal-parahippocampal area. The hippocampus is the confluence of the spatial navigation system. All information culminates here. But what happens before that? Where and how is the navigational information generated?

1.4.1 EC-HF connectivity

The MEC holds a neuronal coordinate system of the environment that emerges from its grid, border and head direction cells. It integrates the head directional and self-motion information from the presubiculum into its metric and directionally oriented representation of the entire environment and thus computes context-independent position information[18]. This information is projected to the hippocampus where it is integrated with event- or context- specific memory contents[4,18]. This extremely dense projection from the entorhinal cortex to the hippocampus was first described by Ramón y Cajal[26] and is referred to as the *trisynaptic circuit* or *trisynaptic loop* (schematically illustrated in Figure 5 A): a mainly unidirectional pathway. EC layer II neurons project to DG and CA3 (Cajal's *perforant pathway*). DG granule cells project to CA3 (the *mossy fibers*), which then projects to CA1 (the *Schaffer collaterals*)[6]. CA1 and subiculum are strongly interconnected with each other[11]. As the major output structure of the hippocampal formation, they project back to parahippocampal region[7] including the presubiculum[27] or the EC[7] (where they target mainly deep layers) and other cortical[28] regions.

The projections are topographically organized. The projections from EC layer II target the entire transverse axis of DG and CA3. While MEC targets the intermediate molecular layer of DG and CA3, LEC projections preferentially terminate in the outer molecular layer. Along with the EC layer II component, the perforant pathway also comprises projections from EC layer III to CA1 and the Subiculum[6,7]. These projections are segregated along the transverse axis of the

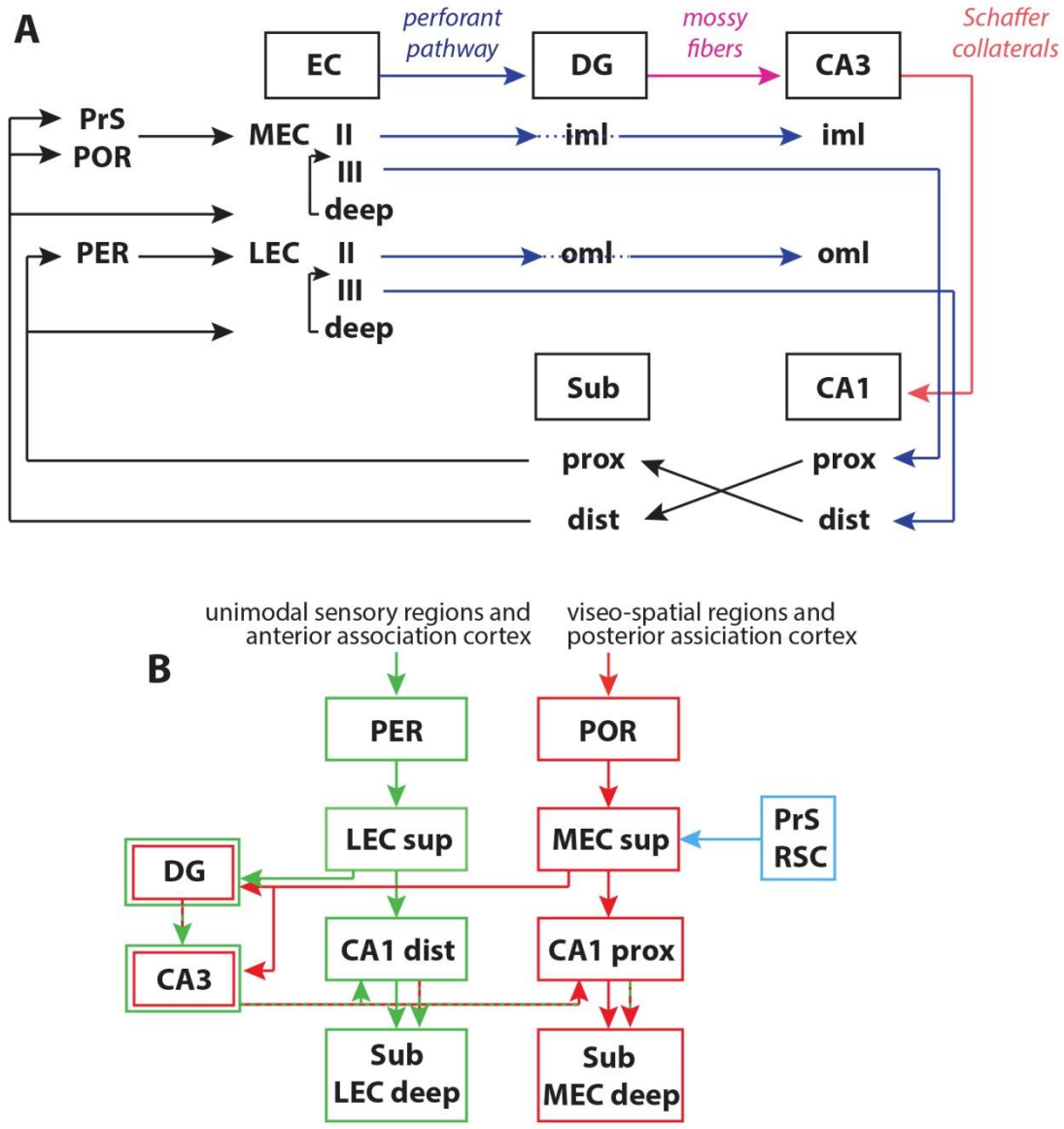

Figure 5: Connectivity between parahippocampal region (PHR) and hippocampal formation (HF). A. Schematic view of the mainly unidirectional EC- intrahippocampal loop. The EC receives input from the PrS and other regions of the PHR and has an extensive projection to the HF. Components of the *trisynaptic pathway* are color-labelled: blue: *perforant pathway;* pink: *mossy fibers;* rose: *Schaffer collaterals*. Perforant pathway fibers from MEC and LEC layer II target the entire transverse axis of DG and CA3, but axon terminals are confined to different levels of the molecular layer. Mossy fibers and Schaffer collaterals also target the entire transverse axis of CA3 and CA1 respectively, but EC layer III projections target different levels of the transverse axis of CA1. Sub as the main output structure of the HF closes the loop to deep layers of the EC and also projects to the rest of the brain. Diagram based on Ramón y Cajal (1899)[26], Amaral and Witter (1989)[6], O'Mara (2001)[11], van Strien (2009)[7], Kim (2012)[29], Dolorfo (1998)[30] **B. Anatomical segregation of cortical inputs to the hippocampus.** adapted from Deshmukh and Knierim (2011)[35]. LEC receives major input from PER, part of the brain's ventral ("what") pathway. MEC receives input from POR, part of the dorsal ("where") pathway. MEC also receives major spatial inputs from PrS and RSC. The projections of LEC and MEC remain segregated along the transverse (proximo-distal) axis of the HF, whereas the projections to DG and CA3 converge onto the same anatomical regions.

hippocampus, such that MEC innervates proximal parts of CA1 and distal parts of the subiculum and LEC innervates distal CA1 and proximal subiculum. This transverse organization also holds true for projections from CA1 to the subiculum: cells in the proximal portion of CA1 (adjacent to CA2) project to the distal part of the subiculum (bordering the presubiculum) and cells in the distal portion of CA1 (bordering the subiculum) project just across the CA1/subiculum border into the proximal part of the subiculum (see Figure 5 A)[7,11]. The distal subiculum projects primarily to PrS, POR and MEC, while the proximal subiculum prefers PER and LEC[29].

In addition to the organization along the transverse axis, the projections from the EC to the hippocampal formation follow a longitudinal pattern of organization. The dorso-lateral parts of both medial and lateral EC innervate preferentially septal parts of the hippocampus, and the ventro-medial parts of the EC target temporal parts of the hippocampal formation[7,30]. The longitudinal topography is thought to play a pivotal role in functional segregation of processed information.

1.4.1.1 Functional segregation

Anatomical and behavioral results suggest the existence of two functionally different streams of navigation- relevant information converging in the hippocampus[31,32] (see Figure 5 B). The *dorsal* pathway conveys spatial and navigational information through the postrhinal cortex and the dorsal presubiculum to the medial entorhinal cortex, which projects to septal parts of the hippocampal formation (POR- dorsal PrS- MEC- septal HF). This pathway probably relies on internal information and is involved in path- integration. The *ventral* stream through the perirhinal cortex, ventral parts of the presubiculum, the lateral entorhinal cortex to temporal parts of the hippocampus (PER- ventral PrS- LEC- temporal HF) plays an important role in non-spatial cognitive processes[33,34], but also provides sensory input and information about individual objects to the hippocampus and could thus play a role in object- related spatial navigation (landmark navigation)[35,36].

1.4.2 PrS connectivity

The presubiculum is one of the major input structures of the EC. Projections from the presubiculum to the entorhinal cortex are topographically organized. A dorsal-to-ventral gradient in PrS corresponds to a lateral-to-medial gradient in the EC[37]. The presubiculum contains a large number of HD cells[20] and relays head directional, visual and potentially somatosensory information (my results) to the EC.

In the following chapter, I will review existing data on afferents to the presubiculum and give a detailed overview layer specificity and topographical organization for the most important regions. If not otherwise specified, projections refer to connections with the ipsilateral side. Table 1 is a summary of all data.

Afferent region	**layer of origin**	**layer of termination**	**topography**	**density**	**source**	**Function**
ADN		I, III/VI (rat) I, III-VI (rabbit)	rostral → ventral PrS; caudal →dorsal PrS	++ +++	[38] [39]	HD
AVN		I, III/IV I	ventral PrS dorsal PrS	++ +	[38]	HD
AMN			ventral PrS	+	[40]	HD
NRe		sup		+	[9,27,41].	HD
Rdg	V	ipsi I/II, V/VI contra V	only dorsal PrS rostral → rostrodorsal[42,43] → entire PrS[34] caudal → caudodorsal bilateral	++	[34,42,43]	visual
Rga	V	I- III[9,44] IV-VI[27,43,45]	rostral → entire PrS caudal → dorsal PrS bilateral	++	[9,27,34,43–45]	visual
V2M (area 18b)		I, III		++	[43]	visual
V1			dorsal PrS	+	[9,43]	visual
Rgb		ipsi I, III/IV contra V	only dorsal PrS rostral → septal PrS caudal → temporal PrS bilateral	+++	[9,27,43,45]	visuo-spatial
POR		deep	dorsal PrS	++	[36]	spatial
PaS	II/III, V	ventral PrS: I, III ; dorsal PrS: V	bilateral	+++	[9,27,46]	spatial
Sub		I, V	prox. Sub → prox. PrS	+++	[9,11,27,46–49]	spatial
CA1		dorsal PrS: II, V[9,27]	intermediate/ventral CA1	+	[9,27,50]	spatial

	ventral PrS: I, IV, V[50]	→ ventral PrS[50]			
MEC	I		+	[51,52]	spatial
LDN	deep I, III/IV	rostral, dorsalmost LDN → ventral PrS; more caudal dorsal LDN → dorsal PrS	+++	[53]	SS
PER		only area 36	+	[36]	SS
LEC	I		+	[36,51,54]	SS
AC	ventral PrS: I, III, deep; dorsal PrS: I, V	dorsal AC > ventral → ventral PrS > dorsal PrS caudal AC → dorsal PrS bilateral	+++	[34,43]	other
OFC	I- III	ventral orbital area	++	[55]	other
MS- DBB				[9,27,56–58]	theta waves

Table 1. Afferent regions to the presubiculum.

1.4.2.1 Head direction circuit

Head directional activity was first described in the PrS[20,23], but has been observed in numerous brain regions (colored in blue in Figure 6) since: the dorsal tegmental nucleus (DTN)[59], the lateral mammillary nucleus (LMN)[60], the anterodorsal (ADN)[61], anteroventral (AVN)[62] and lateral dorsal (LDN)[63] thalamic nucleus, the medial entorhinal cortex (MEC)[64], the retrosplenial cortex (RSC)[65], and the dorsal striatum[66]. Smaller numbers of head direction cells have been described in the nucleus reuniens of thalamus[67] and the hippocampal area CA1[68].

The connectivity within the head direction circuit has been the subject of extensive research over recent decades. A schematic overview is shown in Figure 6. The head directional signal is thought to be generated subcortically in the LMN on the basis of angular head velocity information from the DTN. Theoretical models suggest that the computational basis of the generation of the head-direction signal may be an attractor network, and that cells which signal angular velocity update the directional setting of the attractor[69]. The angular head velocity signal in the DTN probably originates from vestibular and motor information[70]. The head direction

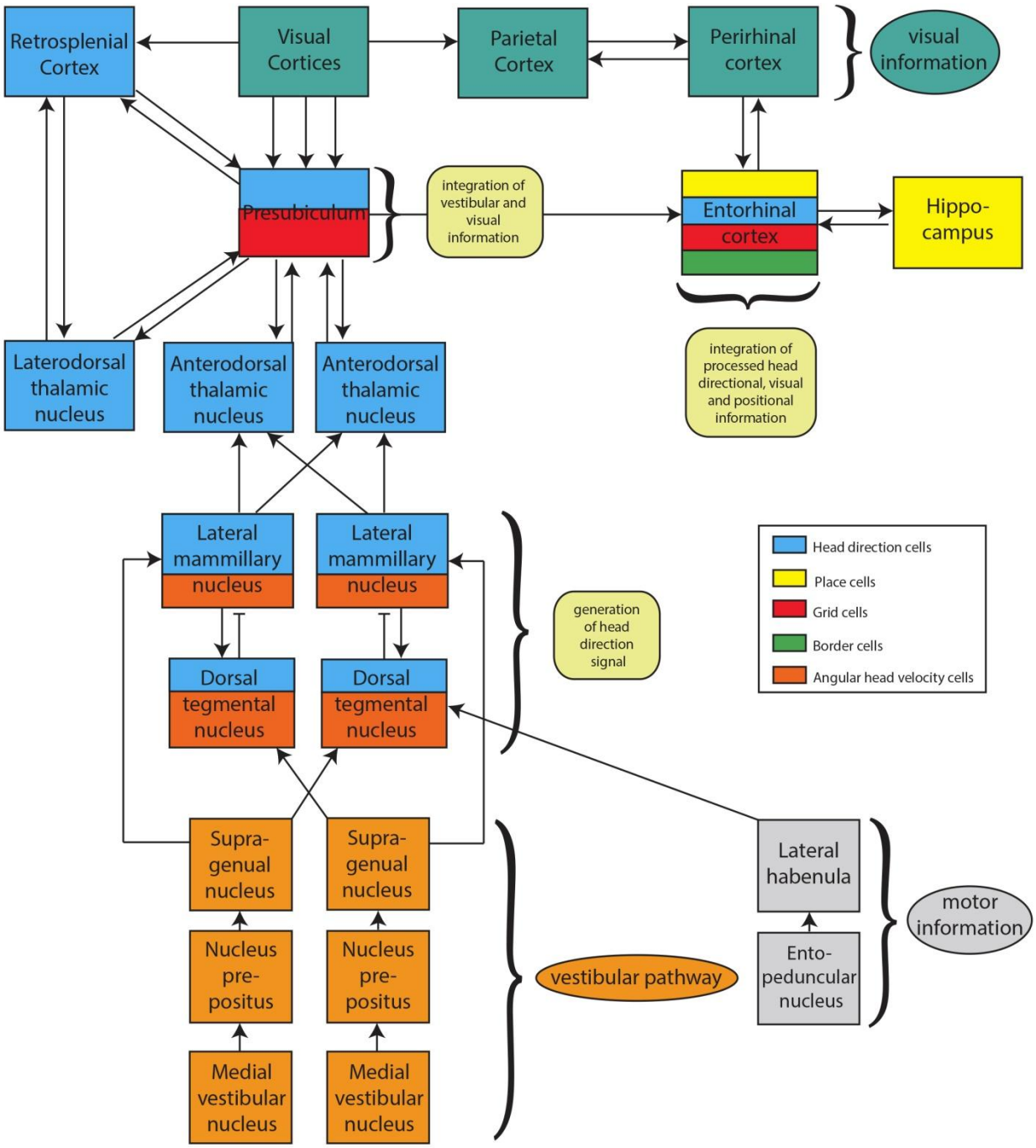

Figure 6: Schematic illustration of the head direction circuit.
The head direction signal is generated subcortically in the dorsal tegmental nucleus (DTN) and lateral mammillary nucleus (LMN) on the basis of idiothetic cues, notably vestibular input from the supragenual nuclei (SGN). It reaches the presubiculum through the anterodorsal thalamic nucleus (ADN) where it is integrated with visual landmark information from the retrosplenial cortex, the laterodorsal thalamic nucleus (LDN) and primary and secondary visual cortices. The dorsocaudal medial entorhinal cortex (dMEC) is thought to contain a directionally oriented, topographically organized neural map of the spatial environment, in which the head directional signal is integrated. The dMEC projects the integrated spatial information to the hippocampus. Schema based on Taube (2007)[16], Biazoli (2006)[67], Yoder (2011)[71], Jankowski (2014)[72], Bezdudnaya (2008)[73].

signal is then projected bilaterally from the LMN to the ADN[16], and the nucleus reuniens[67], which project to the dorsal presubiculum[9,27].

The HD signal enters the PHR/HF area through the presubiculum. The presubiculum receives input from both cortical and subcortical structures. It integrates the vestibular information from the tegmento-mammillary pathway[71], visual landmark information from both retrosplenial and visual cortices[72], somatosensory information from the trigeminal nucleus interpolaris and the LDN[73] and possibly information about objects and sensory input from the LEC (see results). It projects the processed information both in a feed-forward direction to the medial entorhinal cortex (MEC)[44,74,75] and as feedback to the ADN[76], the retrosplenial cortex[27,42,43,45], the nucleus reuniens[67] and the LDN[9].

1.4.2.2 Head directional input to the presubiculum

1.4.2.2.1 Anterior thalamic nuclear complex (ATN)

The ATN consists of the anterodorsal (ADN), anteroventral (AVN) and anteromedial (AMN) thalamic nuclei. Due to its anatomical location and similar connection pattern, the laterodorsal (LDN) nucleus is often described as part of the ATN[73]. The prevailing theory is that the anterior thalamus, through its interactions with the hippocampus and the parahippocampal region, is involved in learning and memory, particularly of spatial tasks[77]and discriminative avoidance conditioning[39]. Lesions in the anterior thalamus result in impairments of spatial memory[78,79].

The ADN projects to the presubiculum in rat[9,27], the retrosplenial cortex in rat[38] and rabbit[39], and other parts of the hippocampal formation of the rat[41]. Both in rat and rabbit, rostral parts of ADN project to the ventral presubiculum, and caudal parts have a very strong projection to layers I, III and IV of the dorsal presubiculum in rats[38], and to layers I and III-VI in rabbit[39]. In rabbit presubiculum, they show no topographical organisation[39].

The AVN receives input from all areas of the limbic cortex in both hemispheres[80], including the ipsilateral presubiculum[27]. Efferences of the AVN to the presubiculum are mainly confined to the ventral part, where they terminate in layers III, I and IV[38]. Minor projections have been described in layer I of the dorsal presubiculum[27,40]. AVN HD-by-theta cells discharge predominantly in spike trains at theta frequency (6–12 Hz), integrating head-directional and theta information[62].

The AMN has a strong projection to the entorhinal cortex and much weaker ones to the ventral presubiculum and Area 18b (V2M)[40].

Neurons of the LDN exhibit prominent short-latency responses to whisker stimulation, which has been shown to be a monosynaptic input from the trigeminal nucleus interpolaris (SpVi), but there is only a small projection from LDN to barrel cortex[73]. It also receives input from the ipsilateral presubiculum[9,27] and granular retrosplenial cortex, which is topographically organized: rostral RSGb projects to medial LDN and caudal RSGb to lateral LDN[45]. It has been suggested that LDN provides the hippocampal formation with whisker-based somatosensory information through the PaS[81]. Efferent projections to the PrS terminate in layers I, III and IV[53].

1.4.2.3 Other spatial input to the presubiculum

1.4.2.3.1 Postrhinal cortex (POR) (parahippocampal cortex)

The postrhinal cortex occupies the very caudal pole in the rat brain and borders the rhinal sulcus. In the primate brain, the comparable region is the parahippocampal gyrus. As part of the dorsal stream conveying in spatial information to the hippocampus, it is strongly and reciprocally connected with septal parts of the hippocampal formation and the MEC. A recent tracing study described a strong efferent and afferent connection between POR and deep layer of the dorsal PrS and caudal parasubiculum[36], that had not been described in earlier works.

1.4.2.3.2 Parasubiculum (PaS)

The parasubiculum lies between the PrS and the EC. In rat, pre- and parasubicular cortices are reciprocally connected. Parasubicular layers II/III and V project bilaterally to the PrS, where terminal fields of axons in ventral parts of the PrS were found in layers I and III, whereas as in dorsal PrS, they were found in layer V[9,27,46]. Input to the PaS originates bilaterally in large PrS layer V pyramidal cells and targets superficial layers[27].

1.4.2.4.3 Hippocampal formation

The subiculum seems to be the major output structure between the hippocampus proper and the entorhinal and other cortices, as well as a range of subcortical structures. It plays a key role in the mediation of hippocampal–cortical interaction and seems to be the major relay station for hippocampal input to the presubicular cortex, since direct innervations from the hippocampus to the PrS are sparse. The subiculum of the rat brain is the origin of a very dense projection to the PrS, which is organized topographically, such that the proximal subiculum (adjacent to CA1)

projects to proximal parts of PrS (those bordering the subiculum)[11,49]. Subicular input is confined mainly to PrS layers V and I. The fibers reach the deep layers of the PrS through the angular bundle[9,27,46–48]. Superficial, but not deep layers of the PrS seem to project back bilaterally to the distal subiculum[46]. Barthesaghi et al. suggested that the presubicular response to hippocampal stimulation would be relayed through the subiculum[82].

Direct projections from CA1 to the PrS have been described by van Groen & Wyss and Cenquizca & Swanson, but they do not report corresponding information: while van Groen & Wyss report projections to layers II to V in dorsal parts of the presubiculum (which they call the *postsubiculum*)[9,27], Cenquizca & Swanson did not find such projections. They, on the other hand, report a rather sparse projection from intermediate and ventral parts of CA1 to layers II, IV and V in the ventral presubiculum[50]. They also report a direct projection from dorsal CA1 to the retrosplenial area. Swanson et al. described projections from the entire cornu ammonis to the PrS[83], but they have not been confirmed by later studies.

No direct connectivity between the PrS and the DG has been described. Nevertheless, presubicular input can widely influence the entorhinal cortex- dentate gyrus- hippocampal system. Stimulation of the dorsal hippocampal commissure, which contains presubicular fibres in a topographically organised manner, activates perforant pathway neurons of the MEC. The discharge in the DG is then followed by a discharge along the trisynaptic pathway as described above[84].

1.4.2.4.4 Medial entorhinal cortex (MEC, MEA)

The PrS lies upstream to the MEC. It is one of its major afferents, but projections from MEC back to PrS are sparse. Wyss (1981) described projections from the MEC to layer I of dorsal and ventral parts of the PrS[51] and Funahashi et al. report that functionally, EC bursts trigger bursts of activity in deep layers of the PrS, probably thanks to an interconnectivity between deep layer neurons[52].

1.4.2.4 Visual input to the presubiculum

1.4.2.4.1 Retrosplenial cortex (RSC)

The retrosplenial cortex lies immediately behind the splenium, the most caudal part of the corpus callosum, occupying the caudal part of the cingulate or limbic cortex. Based on morphological and functional studies, the RSC is further divided into two parts, the more dorsally located dys-

or agranular retrosplenial cortex (Rdg or Rag according to the nomenclature by van Groen and Wyss), and the ventrally located granular retrosplenial granular cortex (Rg). The latter is further subdivided into granular a (Rga) and granular b (Rgb) regions. A schematic illustration of the rodent RSC is shown in Figure 7. Some authors use a different nomenclature: Paxinos Mouse Brain Atlas refers to Rdg as RSA and to Rg as RSG[85]. Rga is designated dorsal retrosplenial cortex (RSd) by Jones (2005)[86], area 29d by Brodmann (1909)[8] and Vogt and Peters (1981) and area 29c by Krieg (1946). Rgb is referred to as ventral retrosplenial cortex (RSv) by Jones (2005)[86], Rga corresponds to areas 29a and 29b, and Rgb corresponds to area 29c of Vogt and Peters (1981). Recent evidence shows that RSC (both granular and dysgranular parts) contains head direction cells[65] and supports spatial navigation in rat[87] and human[88]. Each subdivision shows a unique connectivity pattern: the granular regions have reciprocal connections with sites that contain head-direction cells, whereas Rdg is more interconnected with visual areas[43]. This indicates that the retrosplenial cortex might be in a good position to construct associations between visual stimuli and the HD cell system[87].

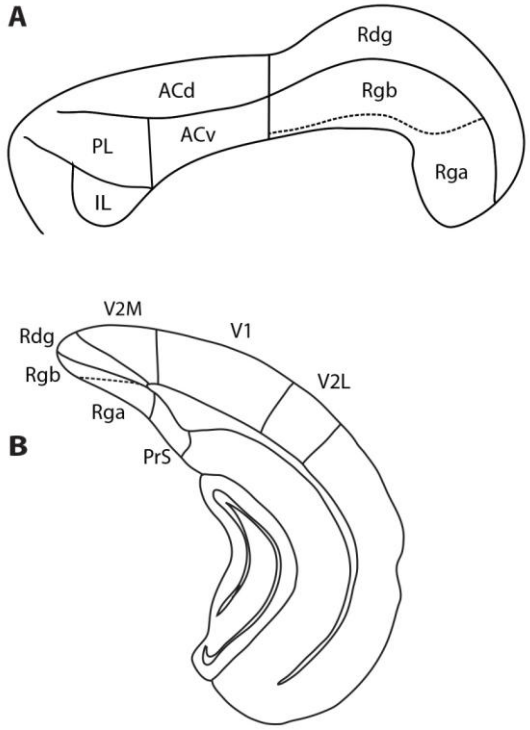

Figure 7: Schematic anatomy of the rodent retrosplenial cortex (RSC).
A. Schematic sagittal view of the cingulate cortex. adapted from Jones (2007)[34] RSC occupies the caudal half of the cingulate cortex. Nomenclature according to van Groen and Wyss.
B. Schematic coronal view at Bregma -3.65mm. adapted from Paxinos (2004)[85] Rdg is laterally bordered by V2M, Rga borders the presubiculum.
ACd: dorsal Anterior Cingulate cortex; Acv: ventral Anterior Cingulate cortex; IL: Infralimbic cortex; PrS: presubiculum; Rdg: dysgranular retrosplenial cortex; Rga: granular retrosplenial cortex a; Rgb: granular retrosplenial cortex b; V1: primary visual cortex; V2L: secondary visual cortex, lateral part; V2M: secondary visual cortex, medial part.

The Rdg has rather sparse reciprocal projections with the HF. Deep layers of the dorsal PrS project to the Rdg. While some authors describe projections from Rdg to dorsal parts of PrS only[42,43], a more recent study[34] revealed projections from rostral Rdg to the entire dorsoventral axis of the PrS and projections from caudal Rdg to the dorsal PrS. In the dorsal PrS, there is a dense axonal terminal field in layers I/II and V/VI on the ipsilateral side, and a few axon terminals in layer V on the contralateral side. The presubicular connections with the Rdg is topographically organised, such that rostral parts of dorsal PrS are connected with rostral Rdg and more caudal parts of dorsal PrS with caudal Rdg[42,43]. Rdg receives strong input from both primary (area 17) and secondary (area 18b) visual cortices[43].

Rga projections to the PrS are bilateral, originate in layer V[27,34,43] and have been described to terminate in deep layers IV-VI[27,43,45] and superficial layers I and III[9,44]. Rostral parts of the Rga seem to project to the entire PrS, whereas caudal Rga innervates only dorsal parts[34]. These projections have been shown to contact directly layer III pyramidal cells in the PrS which project to the MEC superficial layers[44]. It is one of the pathways for visual information to the hippocampus[44]. Since the retrosplenial axon terminals are located mainly near the soma, they could have a large influence on presubicular output to the MEC[44]. Presubicular afferents, like other cortical input to the Rga, originate in layer V[27,42,43].

In contrast to Rga, Rgb is connected with the dorsal PrS only, but this interconnection appears to be very strong[9,27,43,45]. The connection is bilateral in both directions and organized topographically: caudal parts of Rgb communicate preferentially with temporal parts of PrS and the PHR and HF[42], whereas rostral parts of the Rgb seem to project to the entire PrS, although connection with septal parts are stronger[34,45]. Projections to dorsal (septal) PrS originate mainly in Rgb layer V[45]. Ipsilateral projections are confined mainly to PrS superficial layers I and III-IV, while contralateral projections are found mainly in layer V[45]. Rgb superficial layers receive strong input from PrS layer V (and to a smaller amount layer VI) pyramidal cells[45].

1.4.2.3.2 Visual Cortices

Mammalian visual cortex is broadly subdivided into striate or primary visual cortex (Brodmann area 17) and extrastriate secondary visual cortex (Brodmann areas 18), which surrounds area 17. Striate and extrastriate areas are linked to a hierarchical network, which is the substrate for perception and cognitive processing of visual information[89]. The primary visual cortex (V1) is located in the occipital lobe in the posterior part of the brain, and comprises a large proportion of total cortical area in visually dependent species. In rodents, direct efferents to the dorsal PrS have

been described[9,43] (see also my results). In primates, there seems to be no direct projection from V1 to the PHR, probably due to the higher number of hierarchical levels compared to the rodent brain[3].

According to Paxinos and Franklin (2004)[85], this thesis distinguishes between a secondary visual area lying laterally of V1, the lateral secondary visual area (V2L), and the medial secondary visual area (V2M) lying medially of V1 (see Figure 6 B). V2M comprises area 18b and V2L corresponds to area 18a of Caviness (1975). Area 18b provides extensive inputs to temporal and parahippocampal cortices[90]. In the PrS, axonal terminations from area 18b are found in layers I and III[43].

1.4.2.5 Somatosensory input to the presubiculum

1.4.2.5.1 Lateral entorhinal cortex (LEC, LEA)

Presubicular connections with the lateral entorhinal cortex have been discussed controversially. Most authors postulate that connections between the PrS and the EC are found exclusively in the MEC[9,27,37,43,84] and emphasize a strict functional separation between the dorsal pathway for directional and navigational information and the ventral pathway for non-spatial information. Evidence for inter-stream connection has been provided by Wyss (1981) and Swanson and Köhler (1986), who described sparse projections from the LEC to the dorsal PrS and to layer I of the ventral PrS in the rat[51,54]. A recent tracing study showed that the lateral and intermediate entorhinal bands of the rat, which contain fibers from the LEC, have a moderate projection to the entire PrS[36]. They also described projections from the PrS to the LEC, which arose rather in ventral parts of the PrS than in dorsal ones.

1.4.2.5.2 Perirhinal cortex (PER) (Brodmann areas 35 + 36)

The perirhinal cortex lies dorsally adjacent to the LEC and comprises Brodmann area 35, which borders the LEC, and Brodmann area 36, also known as *ectorhinal cortex*, which lies dorsally of area 35. Being part of the ventral stream conveying non-spatial and sensory information to the hippocampus[35], the PER is strongly connected with temporal parts of the hippocampal formation and the LEC. A minor reciprocal connection with the PrS has been described by Agster and Burwell (2013). PER area 36, but not area 35, provides light inputs to the PrS or the PaS, and ventral parts of the PrS project back to area 35 and dorsal parts of the PrS project to both areas 35 and 36 (area 36 > area 35)[36].

1.4.2.5.3 Laterodorsal thalamic nucleus (LDN)

Neurons of the LDN exhibit prominent short-latency responses to whisker stimulation, which has been shown to be a monosynaptic input from the trigeminal nucleus interpolaris (SpVi), but there is only a small projection from the LDN to the barrel cortex[73]. It also receives input from the ipsilateral PrS[9,27] and the granular retrosplenial cortex. Rostral Rgb projects to medial LDN and caudal Rgb to lateral LDN[45]. Efferent projections terminate in layers I, III and IV in dorsal parts of the PrS, and in deep layers in ventral parts of the PrS[53]. It has been suggested that the LDN provides the presubiculum primarily with information based on somatosensory inputs[81].

1.4.2.6 Other input to the presubiculum

Other areas providing input to the PrS include the nucleus reunions, the anterior cingulate cortex (AC) [34,43], the orbitofrontal cortex (OFC)[55] and cholinergic and GABAergic input from the medial septum[56,57] and the diagonal band of Broca[9,27,58].

1.4.2.7 Intrinsic connectivity of the presubiculum

The presubiculum receives input from extensive cortical and subcortical regions. Before being projected to the entorhinal cortex, incoming information is processed within the presubiculum: Both interlaminar and intralaminar excitatory connections exist[91] (red indications in Figure 7 A). Layer V and VI pyramidal cells project intra- and interlaminarly within deep layers of the ipsilateral PrS. Layer II pyramidal cells project to layers II and V/VI of both the ipsi- and contralateral PrS[48,91,92]. Unlike the strong excitatory connection from superficial to deep layers, the connectivity from deep to superficial layers is thought to be sparse (see Figure 7 A). Axonal tracings of single layer V neurons[92] showed that these cells had very diverse projection patterns including long septotemporal intrinsic projections (see Figure 7 B). Different types of projections are highlighted: some of them are restricted to deep layers, hypothesized to send feedback information; others covered the whole presubicular plate and are thought to regulate the temporal dynamics within a extensive neuronal population in the PrS[92].

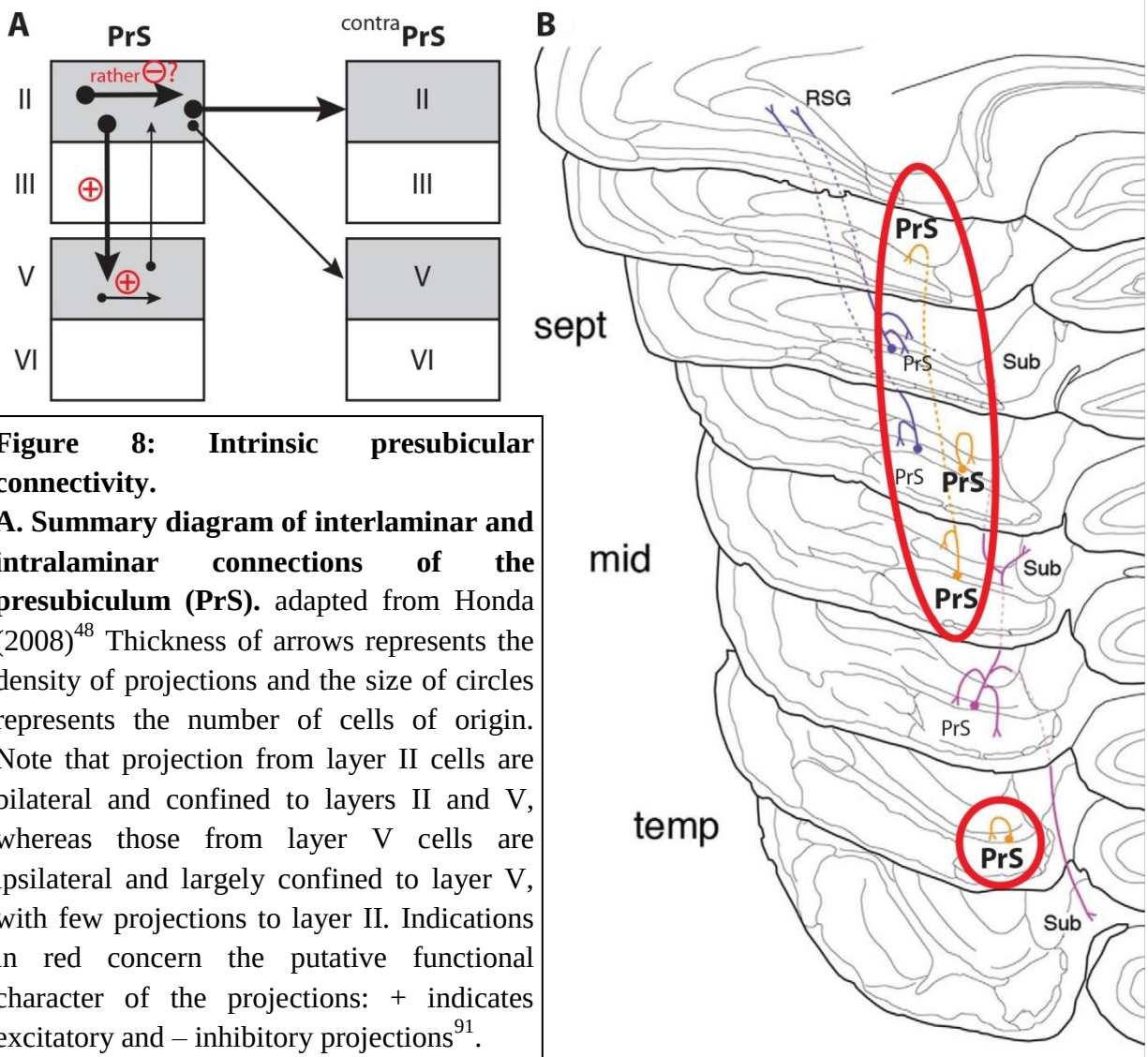

Figure 8: Intrinsic presubicular connectivity.
A. Summary diagram of interlaminar and intralaminar connections of the presubiculum (PrS). adapted from Honda (2008)[48] Thickness of arrows represents the density of projections and the size of circles represents the number of cells of origin. Note that projection from layer II cells are bilateral and confined to layers II and V, whereas those from layer V cells are ipsilateral and largely confined to layer V, with few projections to layer II. Indications in red concern the putative functional character of the projections: + indicates excitatory and – inhibitory projections[91].

B: Schematic diagram of the representative branching patterns of intrinsic and monocortically projecting neurons in layer V of septal, middle and temporal PrS. adapted from Honda (2011)[92]. The red circles highlight intrinsic projection neurons (in yellow) in mid- and temporal PrS. Purple: RSG (=Rg) projection neurons in septal and mid-PrS; magenta: subiculum (Sub) projection neurons in mid PrS. Note that all of the monocortically projecting neurons branch off recurrent collaterals. All observed layer V neurons seemed to be excitatory, because they were spiny pyramidal cells.

1.5 Novel methods for the investigation of functional connectivity

1.5.1 Neuronal tracing

An efficient way to chart anatomical connections within the nervous is neuronal tracing. In recent decades, numerous neuronal tracing techniques have been developed. *Retrograde* tracers are taken up by axonal terminations and transported back into the soma, producing a fluorescent

signal in afferent regions. *Anterograde* tracers are taken up by dendrites and transported to soma and axons, thus labelling efferent regions. Modern tracing strategies however, are not limited to strictly neuroanatomical questions, since they can be combined with a variety of additional techniques.

1.5.1.1 Retrobeads™ – fluorescent latex microspheres[93]

In order to identify afferents to the presubiculum, I used rhodamine-labelled red fluorescent microspheres called Retrobeads™. Like all fluorescent tracers, Retrobeads™ are visible without the need of further staining techniques, which makes them very suitable for in *vitro, in vivo* and cell culture experiments[93]. The possibility to record from labelled neurons or identify specific afferents makes Retrobeads™ a marker of choice for functional connectivity studies. As in the case of all fluorescent dies, strong signals can obscure details of smaller processes[94], and the fluorescent signal, although specific mounting media to limit fading processes are available, can fade over time.

1.5.2 Optogenetics

A recent innovation in experimental neuroscience has been the development of light-activated channels or pumps, derived from microbial photosynthetic systems, to modulate neural activity. The expression of these photosensitive molecules is driven through genetic manipulation of the target cells, which is why these tools are referred to as *optogenetics*. They allow for activation or silencing of neurons with unprecedented specificity and excellent temporal precision[95].

1.5.3 Viral vectors

In order to be expressed by the target cell, the genes for optogenetic molecules can be introduced into the target cells through different techniques such as viral delivery, creation of transgenic lines or *in utero* electroporation. The most commonly used strategy is viral transduction. In order to achieve cell type–specific expression, the vector constructs include a recombinant promoter coding for a gene that is expressed only in the targeted cell type. For example, neuron-specific promoters are the promoters of the genes coding for synapsin (hSyn) or neuron-specific enolase (NSE). Pyramidal cell–specific expression has been achieved with the promoter for calcium/calmodulin-dependent protein kinase II (CaMKII)[96]. For ease of identification of transfected cells, the optogenetic molecules can be tagged by a fluorescent marker protein such as eYFP, mCherry or tdTomato on its C-terminal.

1.7 About this thesis work

Anatomical data about connectivity throughout the parahippocampal network has largely been examined in rat. With a growing number of transgenic mouse models being available, questions about the comparability of rat and mouse brain have emerged. In my study, I reviewed existing data on the presubicular afferences and re-examined the afferent connections of the presubiculum in the mouse brain.

Information about the laminar organization is important to elucidate the hierarchy within a cortical network. Therefore, I paid special attention to the laminar distribution of projecting neurons in five afferent cortical regions: granular and dysgranular retrosplenial cortex, medial and lateral secondary visual areas, lateral entorhinal and primary visual cortex. This will help to understand functional connectivity and hierarchical organization within the presubicular network.

Compared to our knowledge about anatomical connectivity, electrophysiological data concerning the presubiculum is still lagging behind. The fluorescent tracer I employed in my thesis project is compatible with electrophysiological recording of labelled and connected neurons and can be combined with optogenetic tools and immunohistochemical staining techniques. I aimed to establish a protocol to introduce the light-gated cation-channel Channelrhodopsin via viral transfection into different target regions. In the future, this protocol will make it possible to characterize presubicular responses to specific neuronal input (e.g. from a particular afferent region) through light-gated activation of channelrhodopsin-expressing neurons.

1.7.1 Aims and primary questions of this study

The primary goal of my study was to elucidate the comparability of data on presubicular afferences from the rat brain and the mouse brain. In the introduction, I give a detailed review of existing literature which I will compare with results of retrograde tracing experiments in the mouse brain.

Since the tracing technique I employed is layer-specific, I also examined laminar distribution in five afferent regions, namely the granular and dysgranular retrosplenial cortex, the medial and lateral secondary visual areas, the lateral entorhinal and the primary visual cortex.

2. Methods and Material

2.1 Animals

This study was made on 64 GAD67-GFP positive male and female mice[97] of post natal age P22-P47 (mean 28 days) and weighing 9-26 g (mean 15 g). In this mouse line, GABAergic interneurons including interneurons expressing parvalbumin (PV), calretinin (CR) or somatostatin (SST) are GFP labelled.

Experimental protocols followed the EC Council Directive 08/120/EC and INSERM guidelines and were approved by a local animal care committee. 2–6 littermates were housed per cage, with a regular dark-light cycle and water and food were available *ad libitum*.

2.2 Stereotactic injection

Experiments were conducted according to institutional guidelines and policies (Université Paris 6 and INSERM) and were approved by the French Ministry for Research (MESR, authorization n° 01025.02). Mice were anesthetized by intraperitoneal injection of 100/15 mg/kg of a Ketamine hydrochloride/ Xylazine hydrochloride solution (Sigma-Aldrich Inc.; Cat No K-113). When the animals showed no response to nociceptive stimulation (pinching of the toes), ophthalmic ointment was applied in order to prevent eye drying, the head was shaved and disinfected and a medial, 1cm-long skin incision was made. The mice were placed in a custom stereotaxic apparatus (Kopf Instruments; Model 900 Small Animal Stereotaxic Instrument; see Figure 9). The height of the nose clamp was adjusted so that Bregma and Lambda were at the same dorso-ventral height, indicating that the head was flat. Injection coordinates were chosen according to Paxinos Mouse Brain Atlas[85] and confirmed by post hoc histological analysis:

	anteriorposterior (AP) [mm from Bregma]	mediolateral (ML) [mm from Bregma]	dorsoventral (DV) [mm from Bregma]
Presubiculum	-4.19	-2.75	-2.6
Retrosplenial Cortex	-3.5	-0.5	-0.6

Table 2. Stereotactic coordinates

All injections were performed on the right hemisphere. With a small drill (Dremel Stylus™ Lithium-ion Cordless drill), a hole was drilled into the skull, allowing the insertion of the needle. For virus injection I used a special steel/silicon needle (silicon fiber with inner diameter: 75 µm**,** outer diameter: 150 µm; Phymep, Paris**)** mounted into a Hamilton 30G (Hamilton™ Company, Ref. 7762-03 needle), for Retrobeads™ a 20° tapered 33 G steel needle (Hamilton™ Company, Ref.7803-05, inner diameter 108 µm). 0.5 µl of Retrobeads™ solution was injected over 10 min with a 10 µl gastight Hamilton syringe (Hamilton™ Company, model no RN 1701) under steady pump-controlled (World Precision Instruments Micro 4 – Micro Syringe pump controller) pressure and flow rate (50 nl/min). After the injection, the needle was left in place for another 10 min in order to allow for the product to diffuse. The needle was then pulled back carefully. The incision was sutured with 4-0 non-absorbable polyamide thread (Johnson&Johnson Intl.; Ethilon* Polyamide 6), 0.9% sodium chloride (NaCl) solution was injected subcutaneously to prevent dehydration and the animal was supervised during the recovery.

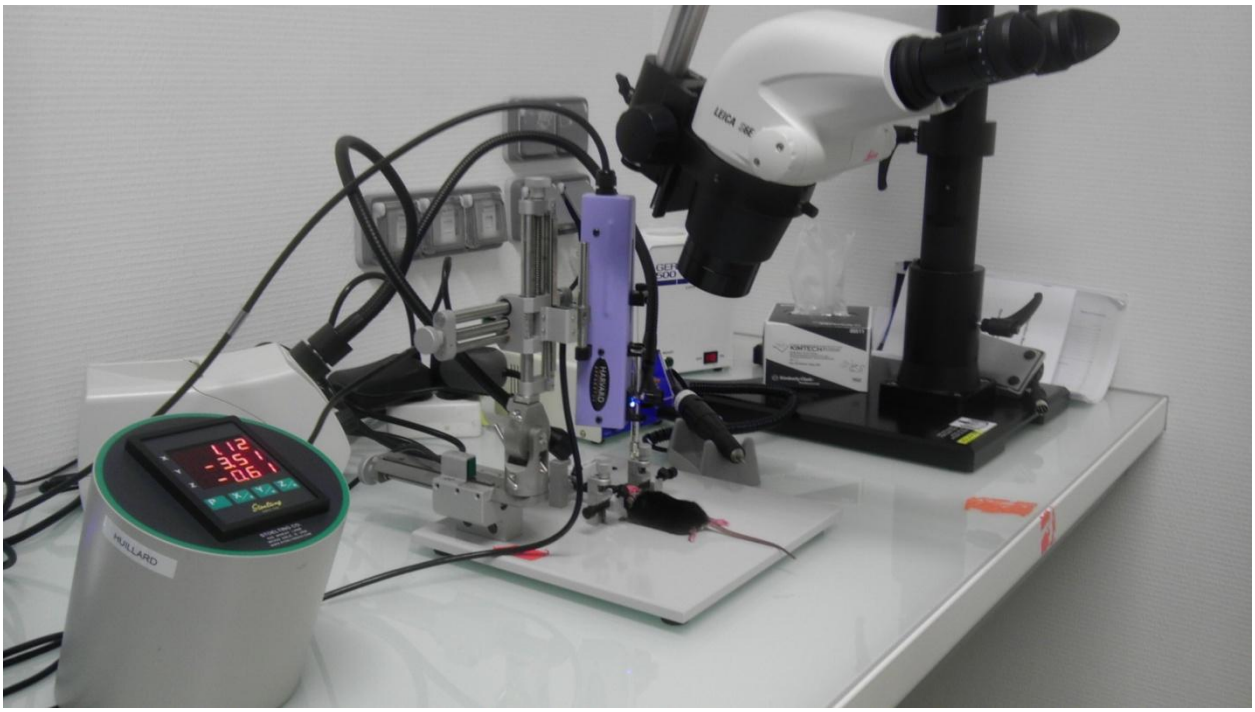

Figure 9: Stereotactic setup.
The deeply anaesthetized mouse is placed in a digital stereotactic apparatus. In order to identify the skull's fissures and define Bregma, a binocular loupe is installed.

2.3 Retrograde labelling and immunohistochemistry

2.3.1 Retrobeads™

In order to identify afferent regions of the presubiculum, 20 mice received an injection of rhodamine-labelled Retrobeads™ (LumaFluor Inc., 3628 Carlisle Drive, Durham, NC 27707, USA). The injections targeted the presubiculum (stereotaxic coordinates see section II.4). Two mice (including case #69) received 500 nl of Retrobeads™ solution. The other 18 mice (including case #105) received injections of 400 nl of Retrobeads™ solution.

Retrobeads™ are 20-200 nm large rhodamine-labelled latex beads that are suitable for tracing both local and long-range connections, depending on the injected volume of tracer solution. There is very little diffusion into the surrounding brain tissue so that sharply defined injection sites are produced. Rhodamine is a fluorescent protein that is soluble in water, ethanol and methanol. The microbeads are taken up by axon terminals within the injection site and transported retrogradely into the soma. The exact mechanism of uptake and transport remains unknown, but size and surface properties seem to play an important role[93,98]. The uptake mechanism could be a latex-triggered endocytosis followed by vesicle-bound transport of the beads into the soma. The labelling increases until 48h after injection and then persists for several weeks. Latex microspheres are not cytotoxic for the animal, and no phototoxicity for labelled cells after longer illumination times has been described. Simultaneous labelling with multiple colors is possible: Retrobeads™ are available with red and green fluorescence and they can be combined with several other fluorescent markers. Latex microspheres can also be combined with immunohistochemistry, intracellular injections, immunofluorescence, Golgi silver impregnation or in situ hybridization[99]. Like all fluorescent tracers, Retrobeads™ are directly visible without the need for further staining techniques, which makes them very suitable for in *vitro, in vivo* and cell culture experiments[93]. The possibility to record from labelled neurons or identify specific afferents makes Retrobeads™ a marker of choice for functional connectivity studies. As in the case of all fluorescent dies, strong signals can obscure details of smaller processes[94], and the fluorescent signal, although specific mounting media to limit fading processes are available, can fade over time. Severed fibers of passage, but not intact ones, seem to show some uptake of marker material. Red Retrobeads™ must be examined under appropriate conditions: the rhodamine component is best excited with a light source of 530 nm wavelength, while the maximum emission lies at 590 nm.

2.3.2 Transcardial perfusion

Two days after injection, the animal was anesthetized by intraperitoneal injection of 100/15 mg/kg of a Ketamine hydrochloride/ Xylazine hydrochloride solution (Sigma-Aldrich Inc.; Cat No K-113). When the animal showed no response to nociceptive stimulation, the thoracic cavity was opened and the descending aorta and vena cava inferior were clamped. In order to inhibit blood coagulation and hence ameliorate the slice quality, I performed a transcardial transfusion with 0.2 ml heparin sodium (Héparine Choay, Sanofi-Aventis; 25 000 UI/ 5ml). Then, I performed a transcardial transfusion with 4% paraformaldehyde (PFA) in 0.12 M phosphate buffer solution (PBS, pH 7.4) in order to fixate the tissue. The head was separated from the body, the brain was carefully removed from the skull and incubated in 4% PFA overnight.

2.3.3 Preparation of histological sections

After overnight incubation in 4% PFA, the brain was rinsed several times in PBS. Cerebellum and pons were removed and the brain was glued on the brain stem onto a cutting plate (Figure 10 A). Using a vibratome (Microm HM 650 V; Walldorf, Germany), 40 µm thick coronal slices were cut in 0.12 M PBS (Figure 10 B). Slices were then transferred into multi-well plates (TPP Switzerland, Product No.92024) containing PBS (Figure 10 C).

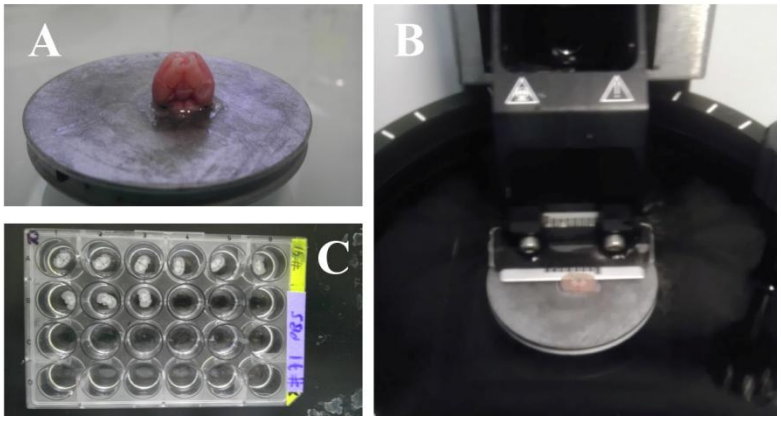

Figure 10: Setup for preparation of histological sections.
A. Ventral view of a mouse brain glued on brainstem on cutting plate for coronal sections. **B.** Vibratome cutting a coronal section in PBS bath. **C.** Slices in a multi-well plate.

2.3.4 Immunostaining

In a first step, the cell membranes were permeabilized by 3-5 cycles of freezing/ thawing over dry ice. To minimize non-specific binding of antibodies ("blocking step"), slices were rinsed in PBS and incubated with a 'saturation buffer solution' (SB) containing: 2% milk powder, 10%

bovine serum, 1% Triton X-100 in PBS for 2-3 hours at room temperature. Triton X-100 is a detergent that improves antibody penetration for immunohistochemistry and reduces background staining. Slices were then incubated at 4°C overnight with primary antibody solution containing the primary antibody against NeuN, specifically labelling neurons, in SB at 0.3% Triton X-100. Slices were rinsed in PB for 2-3 hours and then incubated for 4 hours at room temperature with the secondary antibody in SB at 0.3% Triton and the DNA intercalant 4',6-diamidino-2-phenylindole (DAPI). DAPI counterstains cellular nuclei of all cell types. A last rinsing cycle in PB was run over 2-3 hours and slices were mounted on uncoated microscopic slides (Knittelglass StarFrost, Product no.: VS11275077FKC) with ProLong Gold Antifade Reagent (Life Technologies France, Product No. P36930). For concentrations and manufacturers see table 2.

	Antibodies/ histochemicals	Concentration	Manufacturer
primary	anti-NeuN (mouse)	1:200	EMD Millipore (Catalog No. MAB377)
secondary	goat anti-mouse- Alexa Fluor 647	1:500	Jackson Immunoresearch Inc., USA (Code: 115-605-003)
	DAPI	1:1000	Invitrogen™, Life Technologies, USA

Table 3. Concentrations and manufacturers of the histochemicals used in this study.

2.3.5 Data acquisition and analysis

2.2.5.1 Microscopic image acquisition

The mounted slices were visualized with a QImaging Retiga EXI camera (QImaging Surrey, BC, Canada and scanned with an Optigrid II (Thales Optem, Qioptik, Rochester, NY, USA) mounted on an inverted Olympus IX81 microscope. The Optigrid system permitted sequential scanning and the acquisition of structured images and subsequent 3D reconstruction with the analysis software Volocity (Improvision, Perkin-Elmer, Coventry, UK). Images were acquired using an x20 NA 0.85 oil immersion objective lens with steps of 0.5 µm between every image. Overview images were acquired with an x4 objective lens with a numerical aperture (NA) of 0.16.

Fluorescent markers were visualized with filters according to their excitation and emission peaks (see table 3).

Fluorophore	Excitation max [nm]	Emission max [nm]
DAPI	345	455
GFP	488	507
YFP	514	527
Rhodamine	530	590
mCherry	587	610
Alexa Fluor 647	650	670

Table 4. Excitation and emission peaks of the fluorescent proteins used in this study.

2.3.5.2 Counting Retrobeads™- positive cells in presubicular afferent regions

20x confocal stacks and 3D reconstructed images of 5 principal afferent regions were taken: primary visual cortex (V1), medial and lateral secondary visual cortices (V2M and V2L), lateral entorhinal cortex (LEC), granular and dysgranular retrosplenial cortices (Rga/Rgb and Rgd). A reference line vertical to the pial surface was drawn and left in place in images not containing the pial surface. Cells that were represented in overlapping parts of two images were labelled as reference points for future image alignment. The coordinates of these reference points and the vertical vector were measured and exported to an Excel table.

According to cell density, patterns of immunostaining of NeuN and DAPI and with the help of the Allan Mouse Brain Atlas[100], I performed an approximative layer definition and selected representative areas of each layer for cell counting purposes. Retrobeads™-, GFP- and NeuN-positive cells were counted in each layer. Those cells containing Retrobeads™ were labelled and their coordinates were exported into Excel. With the help of reference points represented in overlapping areas and the vertical vector, the distance to the pial surface of each Retrobeads™-positive cell was reconstructed:

1. Alignment of reference points through vertical and horizontal parallel translation

2. Rotation of vector and data plot into vertical axis

For Retrobeads™ distribution in other areas, 5 intensity levels were defined and the intensity of Retrobeads™ labelling was noted.

2.4 Electrophysiological characterization of transfected neurons

In order to characterize the presubicular response to specific inputs in the future, I designed an experimental protocol for an optogenetic approach. I tested to different viral vectors for the introduction of the optogenetic molecule channelrhodopsin.

2.4.1 Channelrhodopsin-2 (ChR2) and Channelrhodopsin-2 variants

Channelrhodopsins are light-gated non-specific cation channels, conducting H^+, Na^+, K^+, and Ca^{2+} ions, derived from the green alga *Chlamydomonas reinhardtii*[101]. Channelrhodopsins are seven-transmembrane proteins with a molecule of all-trans retinal (ATR) bound at the core as a photo sensor. Upon illumination with ~460-470 nm blue light (excitation maximum), ATR isomerizes and triggers a conformational change to open the channel pore (Figure 11 A). Since channelrhodopsins are ionotropic, cellular depolarization is extremely fast (Figure 11 C). The main deficiency of ChR2 is the high level of desensitization (Figure 11 D), which reduces the current by ~80% at physiological pH. At high expression levels, several problems can occur: ChR2 can form intracellular aggregates instead of trafficking to the membrane[101], extra spikes can occur (two spikes following one light pulse)[101,102] and cells can enter 'depolarization block': repetitive stimulation does not allow repolarization of the membrane. In order to improve the kinetics of the wildtype channelrhodopsin, various variants have been designed. In this study, lentiviral vectors contained the channelrhodopsin-variant *ChR2/H134R* or *ChR2(gf),* which harbors a gain-of-function point mutation at position H134, leading to a modest reduction in desensitization, but also to a slight increase in light sensitivity and slower channel closing, favoring depolarization block[103]. Adenoviral vectors contained the variant ChETA, which is mutated at position E123. This creates faster kinetics, reduces extra-spikes and allows for temporary sustained spike trains up to 200Hz[102].

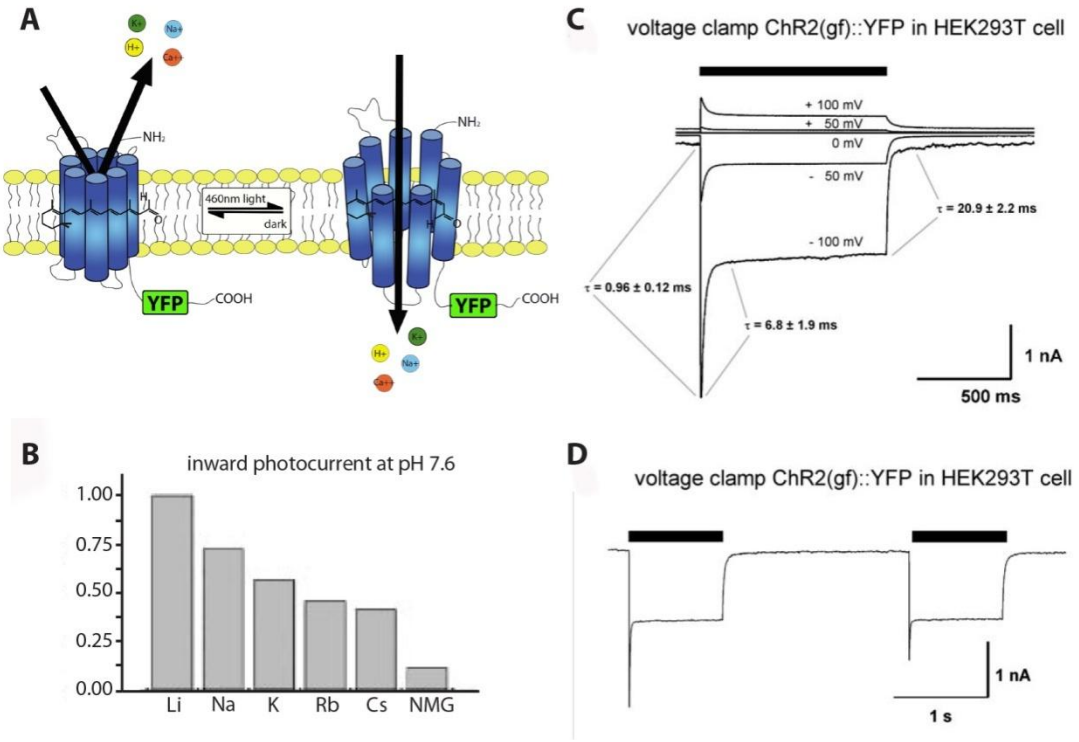

Figure 11: The light-activated cation channel channelrhodopsin.
A. Schematic illustration of molecular structure and light-driven transformation: the 7-transmembrane channel holds a molecule of all-trans-retinal (ATR); isomerisation of ATR leads to an opening of the channel. **B. Normalised inward photocurrents** at 100 mV, pH 7.6, for 115 mM salt solutions of: LiCl, NaCl, RbCl, CsCl and NMG-Cl, measured in the same Chr2-expressing oocyte. from Nagel et al. (2003)[101] **C, D: Photocurrents and membrane-potential changes in HEK-293T cells expressing gain-of-function (gf) ChR2::YFP.** from Nagel et al. (2005)[103] **C. Inward current rectification.** Photocurrents in a voltage-clamped HEK-293T cell expressing gain-of-function (gf) ChR2- YFP after defined illumination by 1 s laser pulses (442 nm, HeCd-laser) at holding potentials as indicated **D. Reduction in peak, but not steady-state photocurrents.** Repeated light stimulation of a voltage-clamped HEK-293T cell expressing gain-of-function (gf) ChR2- YFP. Peak currents were recovered in consecutive trials with a time constant t= 6.4 +/- 0.9 ms, n= 5.

2.4.2 Viral vectors

In order to introduce the channelrhodopsins into the target cells, I used the viral transfection technique. Viral vectors can be delivered directly into specific brain regions with robust transduction efficacy and limited tissue damage. The most commonly used vectors are lentiviral (LV) and adeno-associated viral (AAV) vectors. Both have particular advantages and disadvantages that need to be taken in account when designing an experimental protocol. Lentiviruses, as part of the retrovirus family, are able to integrate their genome into the host cell's genome[104] with the help of identical sequences of DNA, called *long terminal repeats*

(LTRs; see Figure 12). They have the unique ability to infect non-dividing cells[104]. Adeno-associated viruses (AAVs) provide extensive spatial spread and high expression levels[105]. Due to their significantly higher particle diameter (100 nm compared to 20-30 nm for AAVs), LV do not appear to spread as effectively as AAV vectors[106], which can lead to very small injection sites. This can be advantageous if very precise injection sites are desired, but can be a disadvantage if larger brain regions should be transfected. Furthermore, the intrinsic tropism of the virus needs to be taken into account. Although none of the two are specific for a certain type of neurons, differences in the viral tropism for different cell types have been reported in mouse somatosensory cortex: AAV transfect both inhibitory and excitatory neurons efficiently at high titer levels and show a strong preference for inhibitory cells and layer V pyramidal cells at lower viral titers, while LV seem to transfect excitatory cells preferentially[105]. For cell-type specific expression, I used the specific promoter CAMKII[96], which is expressed in pyramidal- cells only. As reporter fluorescence, I used mCherry because it allows visualization via a different wavelength (for excitation and emission levels see table 3) than the wavelength activating channelrhodopsin, and YFP. YFP requires blue light illumination (for excitation and emission levels see table 3) in order to detect the fluorescent signal, which at the same time might activate the channelrhodopsin. This could lead to cation influx and membrane depolarization of the transfected neurons upon visualization and may thus affect the health of neurons and the results of electrical recordings. A schematic illustration of the lentiviral vector construct is shown in Figure 12.

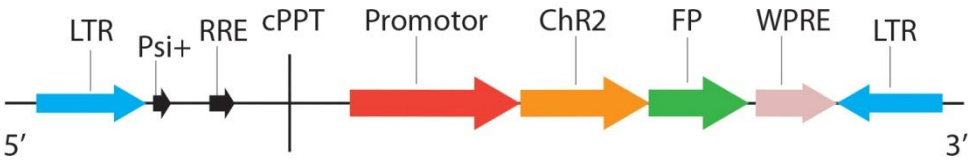

Figure 12: Lentivirus construct used in this study to deliver channelrhodopsin-2 into the mouse brain. adapted from Zhang (2006)[128]. The expression of channelrhodopsin-2 (Chr2) fused to the gene for a fluorescent protein (FP) YFP or mCherry, is driven by the pyramidal-cell specific promoter CaMKII. The channelrhodopsins I used were gain-of-function channelrhodopsin ChR2/H134R and ChETA. Long terminal repeats (LTRs) are used by retroviruses to insert their genetic material into the host genome. Psi+ and RRE form the packaging sequence an RNA sequence required for packaging the genomic material. The HIV-1 central polypurine tract (cPPT) and the woodchuck hepatitis virus post-transcription regulatory element (WPRE) increase the viral titer and gene delivery efficacy and are common elements in state-of-the-art lentiviral vectors in order to achieve long-term expression.

44 mice received a stereotactic injection (protocol of the procedure as described above) of 1 µl of one of the two different lentiviral vectors. 32 mice received a vector containing the gene for ChR2 with H134R mutation (ChR2/H134R), tagged with the red fluorescent marker protein mCherry under the control of the CaMKII promoter (LV-CaMKII-ChR2(H134R)-mCherry-WPRE). It was obtained from Institut du Cerveau et de la Moëlle Epinière (ICM) (Plateforme vecterologie, ICM Paris, France) and had a viral titer of 31 ng/µl. The success rate of the stereotactic injection in this group was of 81% (6 animals died).

12 mice received a vector construct encoding for ChR2 with E212T mutation (ChETA) tagged with the green fluorescent protein YFP (LV-CAMKII-ChETA-eYFP-WPRE). This virus construct was obtained from Institut Pasteur Paris, France (Vector core facility, Stephanie Pons and Martine Soudant). The viral titer was of 125 ng/µl. The success rate of the stereotactic injection in this group was of 83% (2 animals died).

2.4.3 Slice preparation

Acute brain slices were prepared 6- 8 weeks after injection. The animals first underwent a transcardial perfusion according to the protocol described above. The transfusion contained 0.2 ml heparin sodium (Héparine Choay, Sanofi-Aventis; 25 000 UI/ 5ml) and ice-cold oxygenated cutting solution containing (in mM): 2.5 KCl, 1.25 NaH_2PO_4, 25 $NaHCO_3$, 7 glucose, 0.5 $CaCl_2$, 7 $MgCl_2$, 110 Choline Cl). The animal was decapitated, the brain was carefully removed from the skull and immediately submerged in chilled cutting solution. Cerebellum and olfactory bulb and frontal cortex were removed and the brain was glued onto a cutting plate. For presubicular recordings, the brain was glued on its dorsal side and cut horizontally, for retrosplenial recordings, the brain was glued onto the brainstem and cut coronally. The cutting plate was placed in a vibratome (Microm HM 650 V; Walldorf, Germany; see Figure) and 250 µm thick slices were cut in ice-cold cutting solution. Slices were then transferred into oxygenated artificial cerebrospinal fluid (ACSF) containing (in mM): 124 NaCl, 2.5 KCl, 1 Na_2PO_4, 26.2 $NaHCO_3$, 11 glucose, 2 $CaCl_2$, 2 $MgCl_2$; pH 7.3; 303-315 mOsm. Slices were incubated in the dark for 60min at room temperature to allow cellular recovery.

2.4.4 *in vitro* patch clamp recordings

The slices were put into the recording chamber of ~2 ml on the stage of an Axioscope 2 FS plus microscope (Zeiss, France) for recording and heated to 32- 34°C. The presubiculum was visualized with a 10x objective lens and neurons in this area were visualized with a 40x plan-

Apochromat objective lens of NA 1.0. The reporter fluorescent protein mCherry was visualized with an appropriate filter set (Zeiss set 64: excitation BP 587/25; FT 605; emission BP 647/70), using an EMCCD- Luca- S camera (pixel size 10 x 10 µm; Andor) and allowing to see reporter fluorescence while keeping ChR2 activation to a minimum. Recorded neurons were chosen at sites with great reporter fluorescence. Neurons were patched with glass electrodes pulled with a Brown-flaming electrode puller (Sutter Instruments) from borosilicate glass pipettes with an external diameter of 1.5 mm and inner diameter of 0.86 mm (Harvard Apparatus) filled with intracellular solution containing (in mM): 130 K-Gluconate, 5 KCl, 10 HEPES, 10 EGTA, 4 Mg-ATP-$2H_2O$, 0.4 Na_3-GTP-$2H_2O$, 10 Na-Phosphocreatine, 2 $MgCl_2$, 2.7 Biocytin; pH 7.3; 290-300 mOsm. The serial resistance of the filled pipettes was between 2 and 6 MΩ.

All recordings were performed at room temperature in circulating oxygenated ACSF. In some experiments, the sodium-channel antagonist Tetrodotoxin (TTX, 0.5-1 µM; Tocris, Bristol, UK), or the GABA-A receptor antagonist bicuculline (20 µM; Sigma B-6889) was added. Whole-cell recordings were made using an Axopatch 200A amplifier (Molecular Devices, Sunnyvale, CA, USA) operated in fast current-clamp mode and filtered at 6 kHz using the built-in low-pass Bessel filter. A chlorided silver wire contacted the pipette solution and a 3 M KCl agar bridge was in contact with the bath solution, yielding an estimated junction potential of ~15 mV which was not corrected. Data was acquired at 20 kHz sampling frequency using a Digidata 1550 Digitizer controlled by pClamp 10 software package (Molecular Devices).

2.4.5 Photostimulation

Photostimulation of the transfected retrosplenial neurons was made using a blue LED light source (OptoLED, Cairn Research, Faversham, UK) or a laser (Omicron Deepstar 120 mW, single mode fiber, collimated output 1.3 mm diameter), permitting greater temporal and spatial precision. The collimated output of the fiber-coupled 405 nm laser was diverged with a negative lens in a dual LED lamp house reflecting the light with a dichromic reflector (425 DCXR, Chroma) into the epifluorescence tube of the microscope (Zeiss Axioscope). A light spot of ~10 µm diameter in 100 µm pyranine (HPTS) solution was measured at the focus plane using the Luca CCD camera. Light intensity at this point was ~11 mW. Stimulus duration and laser power were controlled by an Isolated Pulse Stimulator (A-M Systems, Model 2100).

2.5 Figures

Figures were designed using Adobe Illustrator. For overview Figures 14 and 16, labelling intensities of all areas were assigned a color code and the labelling pattern was illustrated in Adobe Illustrator files of atlas images from Paxinos (2004)[85]. Microscopic photographs shown in Figures 15 and 17- 20 were contrast-enhanced with Adobe Photoshop for illustration purposes.

2.6 Nomenclature

There are a number of different nomenclatures in the literature for the areas under scrutiny. We opted to use the nomenclature of the parahippocampal region as described by Witter and Amaral[6]. For this study it is relevant to point out that the presubiculum, as defined in this study, encompasses both the dorsal presubiculum or *postsubiculum* or Brodmann area 48[27] as well as the ventral presubiculum or Brodmann area 27. Our analysis has focused on the intermediate dorsoventral levels of the presubiculum (see results section). Regarding the retrosplenial cortex, a number of different nomenclatures have been used which to a large extent agree on how this part of the cortex should be subdivided. We follow the nomenclature as proposed in Paxinos (2001)[85].

3. Results

3.1 Afferent connectivity of the mouse presubiculum analyzed by retrograde tracing

In order to investigate the afferent connectivity of the presubiculum in the mouse brain, retrograde tracers were injected into the presubiculum. In two cases, the dye core of the injected tracer solution was located in the presubiculum and there was no significant backflow in the puncture channel. Several other cases showed heavy backflow over the dorsal hippocampal commissure with subsequent unspecific labelling throughout the entire cortical mantle, probably due to an uptake of the tracer solution by neurons in adjacent regions. Only the two cases without significant backflow over the dorsal hippocampal commissure (#69 and #105) were further analyzed in this study.

Pictures of injection sites are shown in Figure 13. The core of the injection site was defined as the anterior-posterior extent of the *dye core* visible in the bright field image. The *fluorescent halo* of the injection site extended over several coronal sections and was considered part of the injection site. Injection sites involved both superficial and deep layers. There was very little backflow into the puncture channel. Uptake in the areas traversed by the needle cannot be entirely ruled out, although it can be considered as minimal compared to the uptake in the injection site itself.

3.1.1 Description of injection sites

In case #69, the injection site was located in the caudal part of the presubiculum and, at its caudal end, involved to some extent the caudal parasubiculum and the very caudal tip of Rdg. The core extended over 120 µm, the halo was visible in 5 sections, corresponding to an anterior-posterior extent of 600 µm. The injection electrode track traversed caudal V1 (see Figure 13 A and B).

In case #105, the injection site was located in the caudal presubiculum as well, but did not involve the parasubiculum or retrosplenial cortex (Figure 13 C and D). The core extended over 240 µm and the halo extended over 4 sections, corresponding to 360 µm. The injection electrode track traversed caudal V1, but slightly more rostrally and medially than in case #69.

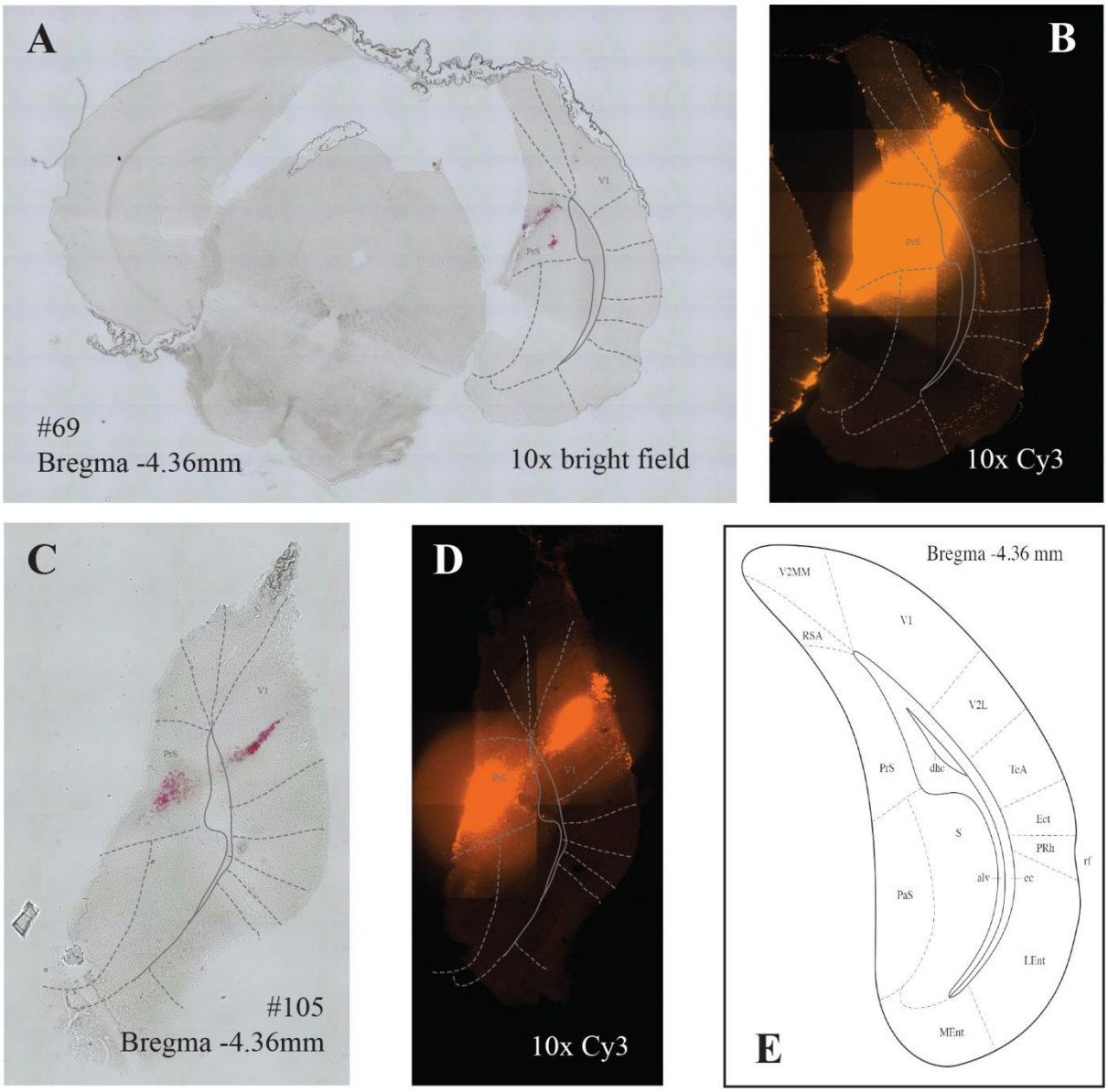

Figure 13: Injection sites.
10x microscopic images of coronal sections through the dye core. **A.** #69 10x bright-field (bf) image of coronal section at Bregma –4.36 mm showing the dye core in the presubiculum. **B.** 10x image of the same section as A. with fluorescent filters for Cy3. Fluorescent halo of the injection site. **C.** #105 10x bf image with dye core in PrS and puncture channel in V1. **D.** Cy3 fluorescence of the same slice as C. Fluorescent halo in PrS and V1. **E.** Corresponding atlas image. Modified from Paxinos Mouse Brain Atlas[85].
alv: alveolus of the hippocampus; dhc: dorsal hippocampal commissure; Ect: Ectorhinal cortex; LEnt: lateral entorhinal cortex; MEnt: medial entorhinal cortex; PaS: parasubiculum; PrS: presubiculum, PRh: perirhinal cortex; RSA: dysgranular retrosplenial cortex; S: subiculum; TeA: temporal association cortex; V1: primary visual cortex; V2L: secondary visual cortex, lateral area; V2MM: secondary visual cortex, mediomedial area

3.2 Afferents of the mouse presubiculum analyzed by Retrobeads™-labelling

In both cases, the labelling pattern of retrogradely labelled cells was similar: heavy labelling was observed in ADN, and retrosplenial cortex (dysgranular and granular parts), pre- and parasubiculum. In retrosplenial cortex, labelling in the dysgranular part (Rdg) was always heavier than in the granular parts (Rga and Rgb). Less heavily labelled were AVN, secondary visual cortices V2M and V2L, MEC and LEC, PER, and subiculum and minor input arose from claustrum, the thalamic nuclei LDN, DLG and nucleus reuniens, the primary visual cortex and the contralateral presubiculum and retrosplenial cortex. Afferents from the orbitofrontal and anterior cingulate cortex have not been examined due to their very anterior position.

If not otherwise specified in the text, projections refer to staining on the ipsilateral side. Detailed information about intensity and location of labelling is shown in Figures 14 and 16.

3.2.1 Labelling pattern in afferent regions in case #69

In case #69, the injection site was located in caudal presubiculum and involved caudal parasubiculum to a minimal extent. Heavy labelling was found in ADN, AVN, dysgranular retrosplenial cortex, secondary visual cortex V2M, and presubiculum. Moderately labelled were granular parts of retrosplenial cortex Rga and Rgb, thalamic nuclei LDN and DLG, secondary visual cortex V2M, perirhinal cortex, MEC and LEC and caudal subiculum. Minor labelling was observed in V1, the thalamic Nucleus reuniens, claustrum, parasubiculum and contralateral presubiculum and retrosplenial cortex. Figure 14 illustrates the general distribution of Retrobeads™ within the afferent regions throughout the brain.

ADN showed heavy labelling, especially in the rostromedial part. AVN was labelled less intensely than ADN, and labelling was heavier in the rostrolateral part. A 10x enlarged image of ADN and AVN is shown in Figure 15 A. Labelling in LDN was found in its entire mediolateral axis and ranged over both dorsomedial (LDDM) and ventrolateral (LDVL) parts, but was heavier dorsally. A 10x enlarged image of LDN is shown in Figure 15 C. The DLG showed some labelled cells in its anterior dorsolateral part, between Bregma -1.58 mm and 2.54 mm. The posterior half of nucleus reuniens also contained some labelled cells.

The presubiculum received bilateral input from the retrosplenial cortices. The dysgranular part (Rdg) showed labelled cells throughout its entire rostrocaudal axis with increasing intensity

Figure 14: Overview of Retrobeads™ labeling in the whole brain in case #69.
10x fluorescence images of subsequent coronal sections were analysed and labeling intensity was defined. In order to illustrate the distribution of Retrobeads™ within the afferent regions, color patches were drawn into correspondent atlas images modified from Paxinos (2004)[85] using Adobe Illustrator. Light pink indicates some labelled cells, more saturated colors indicate heavier labeling with maximum intensity shown in red. Pink represents the injection site.

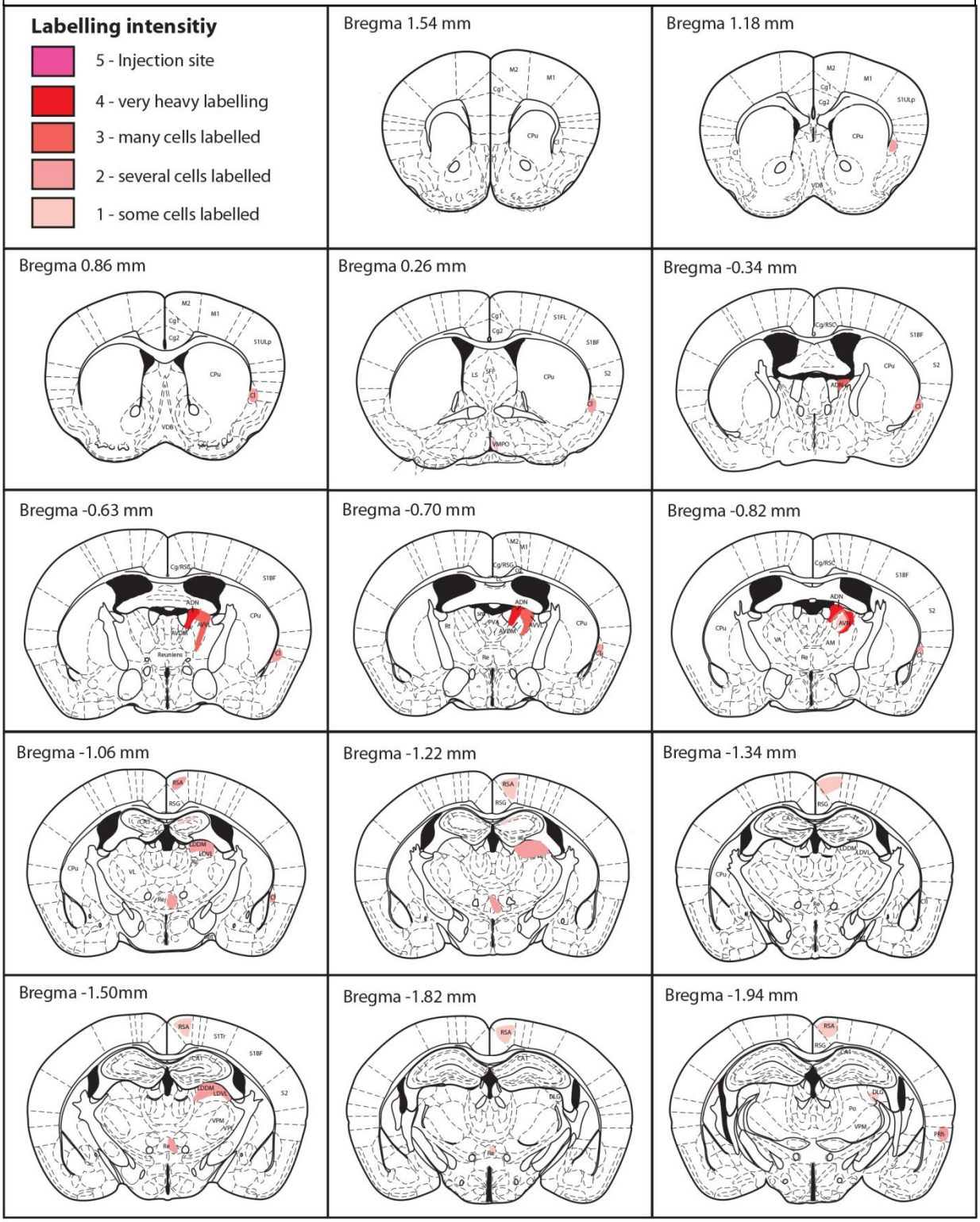

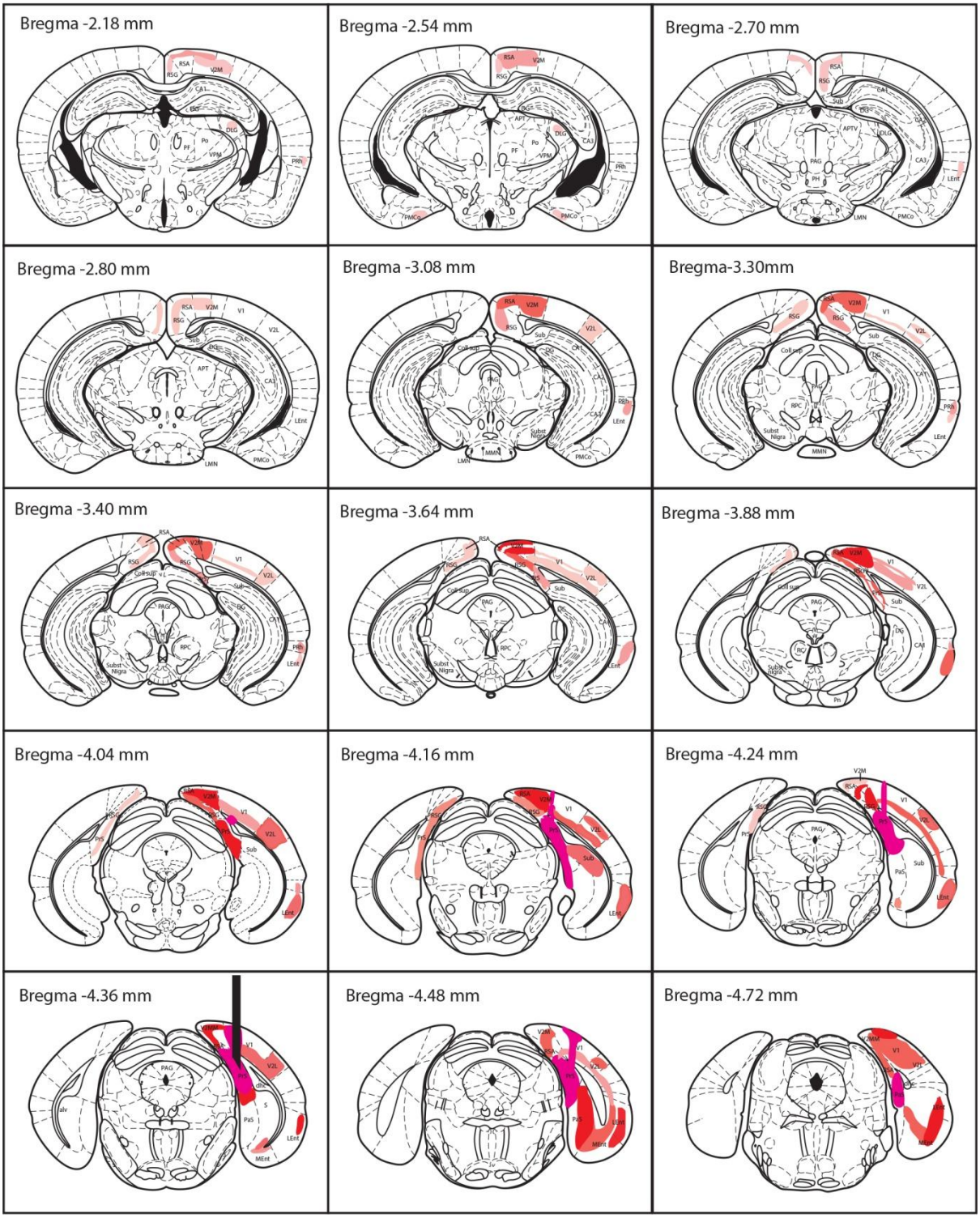

For the sake of completeness and facility of inspection of labeling pattern throughout the entire brain, images in this figure are very small. For information about abbreviations and the names of the labelled regions, please refer to Paxinos (2004)[85].

along the rostrocaudal axis and maximum intensities between Bregma -3.5 mm to -4.25 mm. Projections from the contralateral side were much less intense, but involved the entire rostrocaudal axis as well. Rdg showed heavier labelling than the granular parts.

In parts of the presubiculum lying anterior of the injection site, labelled cells were observed in deep and superficial layers, but superficial layers seemed to be more densely labelled (Figure 15 F). Along a quite long distance on the rostrocaudal axis, labelled cells were found in PRh and rostral LEC (Figure 15 E). In case # 69, labelling in PRh was found between Bregma -1.94 mm and -4.72 mm, and in LEC between -3.08 mm and -4.96 mm. Labelling in MEC was difficult to evaluate but it seemed that only deep layers of the very caudal tip of MEC contained Retrobeads™. The injection site involved caudal parasubiculum, but labelled cells in more rostral parts of the parasubiculum were rather sparse. Claustrum was labelled throughout its entire anterior-posterior axis in equal, but light intensity. Only caudal subiculum was found to project to the presubiculum. In the contralateral presubiculum, labelled cells were distributed in superficial layers only, with a clear preference for layer III (Figure 15 G). Caudal V1 and large parts of the secondary visual areas V2M and V2L contained significant numbers of labelled cells. Labelling intensities increased along the rostrocaudal axis and V2M was more heavily labelled than V2L. While labelled cells were confined to deep layers in V1, they were distributed in both superficial and deep layers in V2M and V2L.

Details on the laminar distribution of Retrobeads™- labelled cells in V1, V2M, V2L, LEC, RSA and RSG are further discussed below.

3.2.2 Labelling pattern of Retrobeads™ in afferent region in case #105

In case #105, the injection site was located in caudal presubiculum. Labelling followed the same pattern as in case #69, but was lighter in intensity, due to a smaller volume of injected tracer solution. Heavy labelling was found in ADN, dysgranular retrosplenial cortex and presubiculum. Moderately labelled were granular parts of retrosplenial cortex Rga and Rgb, secondary visual cortices V2M and V2L, the thalamic nuclei AVN, LDN and DLG, perirhinal cortex and LEC. Minor labelling was observed in V1, the thalamic Nucleus reuniens, claustrum, parasubiculum, MEC and contralateral presubiculum and retrosplenial cortex. No labelling was found in subiculum.

ADN was heavily labelled. AVN also contained labelled cells, but was marked with much lighter intensity than ADN. Compared to case #69, labelling intensity in AVN was weaker. In

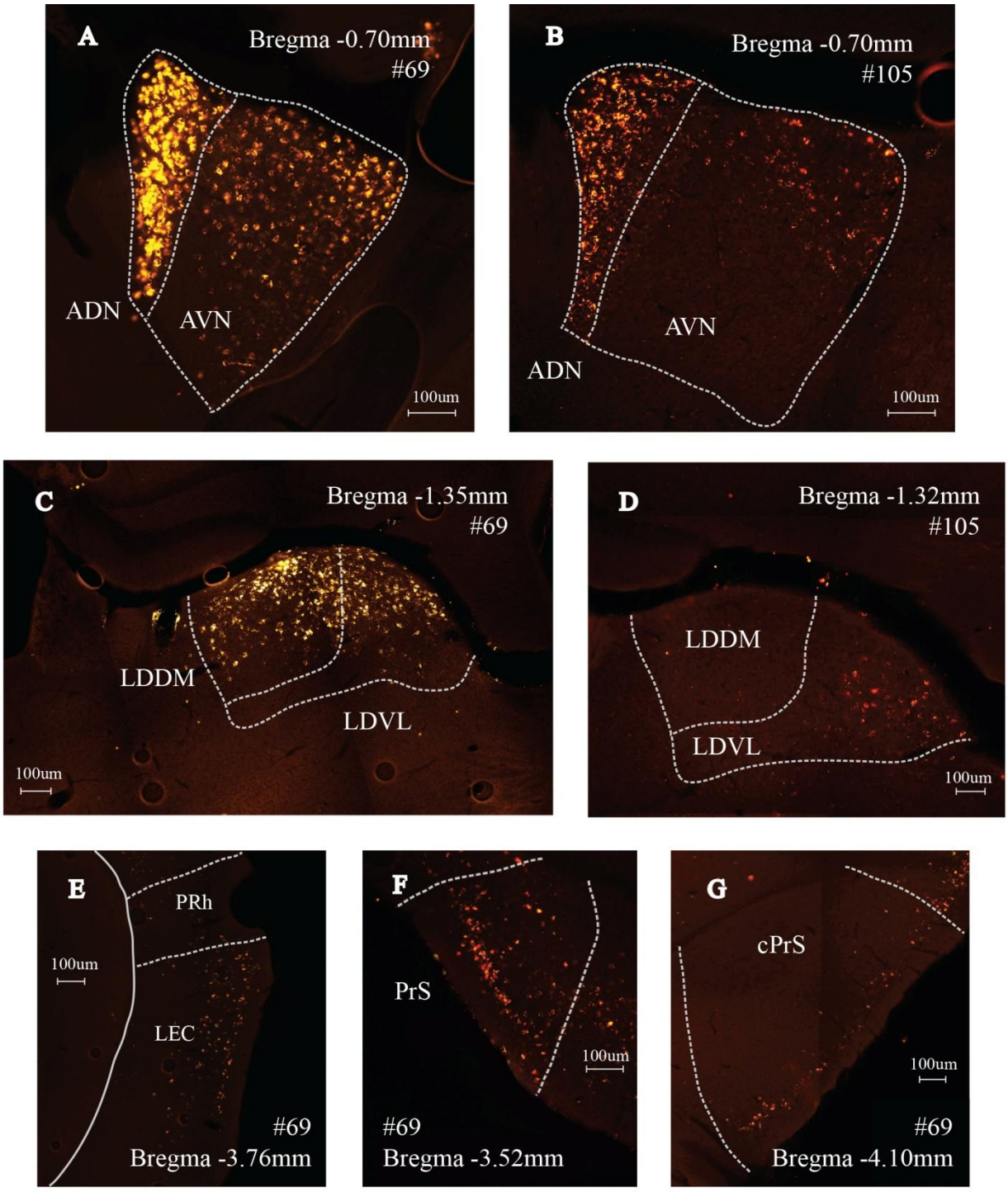

Figure 15: Labeling the anterior thalamus, LDN, LEC, PrS and contralateral PrS. 10x fluorescence microscopic images of coronal sections in the thalamus. **A.** #69 coronal section at Bregma –0.70 mm. Heavy labeling of ADN and moderate labeling of rostrolateral AVN. **B.** #105 Coronal section at Bregma –0.70 mm. Labeling of ADN and AVN is lighter than in case #69 but shows the same distribution of beads within the nuclei. **C.** #69 coronal section at Bregma –1.35 mm. Strong labeling in rostral LDN. Both dorsomedial (LDDM) and ventrolateral (LDVL) contain beads. **D.** #105 coronal section at Bregma –1.32 mm. Only LDVL is labelled. **E.** #69 coronal section at Bregma –3.76 mm. Labeling of dorsal LEC and PRh. **F.** #69 coronal section at Bregma –3.52 mm: superficial and deep layers of the ipsilateral PrS are labelled. **G.** #69 coronal section at Bregma –4.10 mm showing the labeling pattern in contralateral PrS (cPrS).

LDN, Retrobeads™-containing cells were confined to the ventrolateral part, as opposed to case #69, where Retrobeads™ were found in both LDDM and LDVL. 10x images of ADN, AVN and LDN are shown in Figure 15 B and D. Nucleus reuniens was marked only in one slice, at Bregma -1.08 mm. DLG contained some labelled cells, which were, as in case #69, confined to the dorsolateral corner. The labelling intensity in DLG was higher in case #105 than in case #69. The retrosplenial cortex provided bilateral input, but labelling was confined to the caudal half of RSC. As in case #69, Rdg was labelled with equal or stronger intensity than Rg. V1 contained labelled cells in deep layers with increasing labelling intensities along the rostrocaudal axis. From Bregma -4.48 mm to -4.60 mm, V1 contained a tracer deposit. Secondary visual cortices V2M and V2L contained beads in both superficial and deep layers. Labelling was somewhat stronger in V2L than in V2M (as opposed to case #69) and increased along the rostrocaudal axis. Labelling in PER and LEC was consistently present as well, although it was not found as far rostral as in case #69. Only deep layers of the very caudal tip of MEC contained Retrobeads™. Parasubiculum and rostral presubiculum were only sparsely labelled. Claustrum was labelled with equal intensity through its rostrocaudal axis.

Figure 16: Overview of Retrobeads™-labelling in the whole brain in case #105.
10x fluorescence images of subsequent coronal sections were analysed and labelling intensity was defined. In order to illustrate the distribution of Retrobeads™ within the afferent regions, color patches were drawn into correspondent atlas images modified from Paxinos (2004)[85] using Adobe Illustrator. Yellow indicates some labelled cells, more saturated colors indicate heavier labeling, where the maximum intensity is green. Dark green represents the injection site.

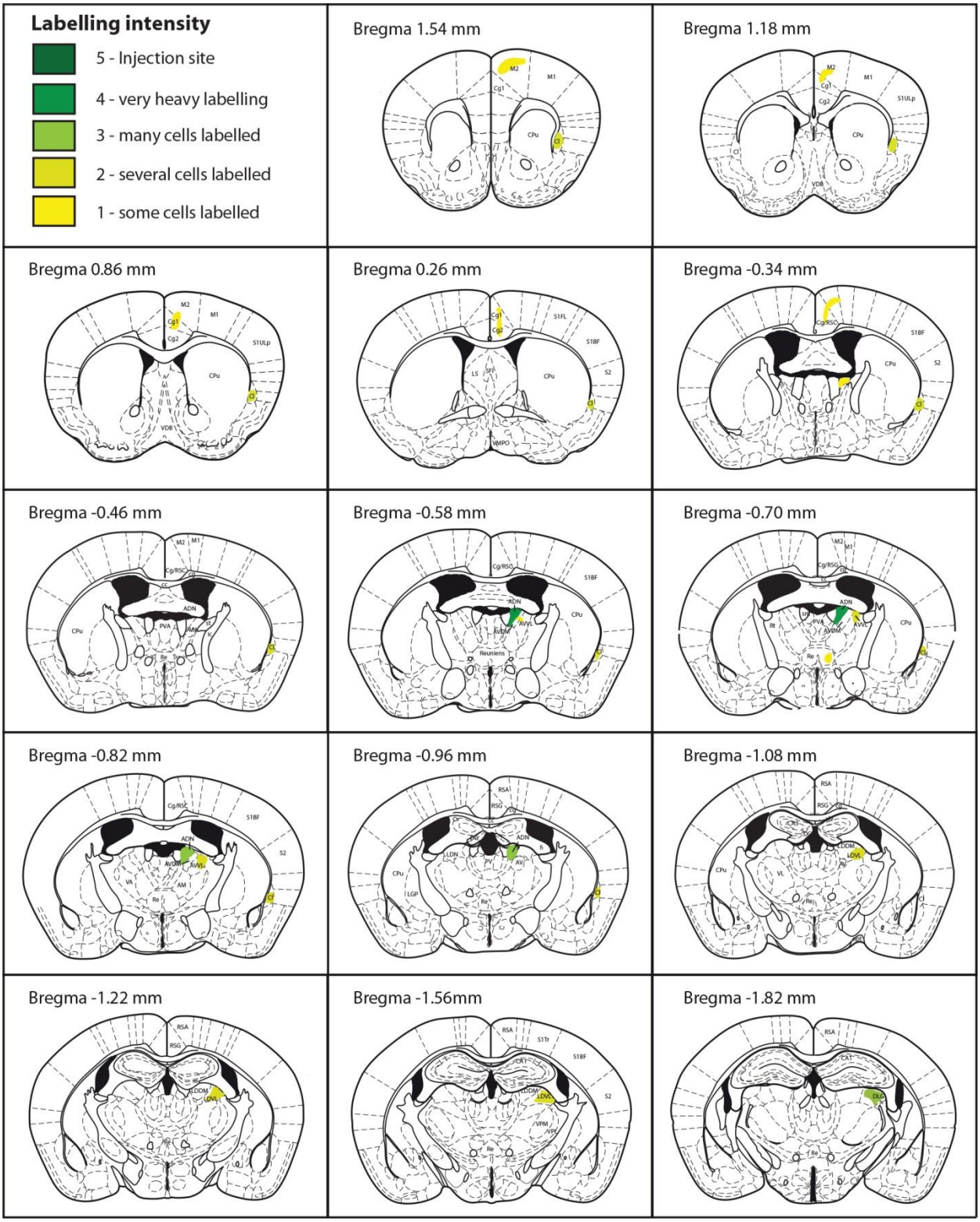

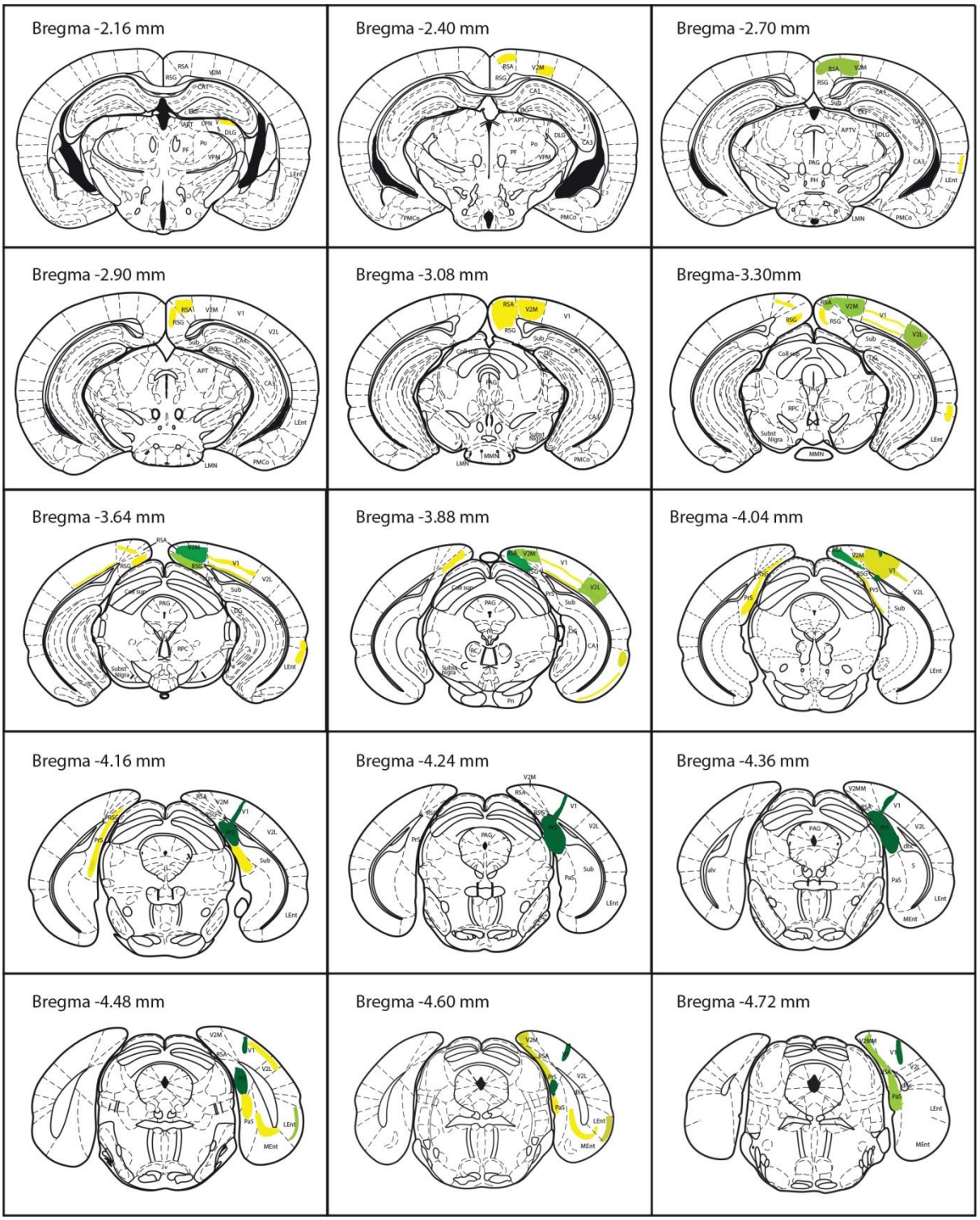

For the sake of completeness and facility of inspection of labelling pattern throughout the entire brain, images in this figure are very small. For information about abbreviations and the names of the labelled regions, please refer to Paxinos (2004)[85].

3.3 Layer-specific distribution of Retrobeads™ in the main afferent regions

I observed layer-specific differences in the density of Retrobeads™ labelling for several cortical regions afferent to presubiculum. The distribution of Retrobeads™-containing cells across layers was quantified for five regions: retrosplenial cortex, primary and secondary visual areas and lateral entorhinal cortex. Relative distributions were calculated as the ratio of Retrobeads™ labelled neurons over the total number of neurons identified by NeuN staining for layer I to VI. Differences in distribution patterns were consistent in cases #69 to #105. In granular RSC, output to the presubiculum originated mainly in layer III. In Rdg, both superficial and deep layers provided projections to the presubiculum. The percentage of projecting cells in V1 was very low (about 3%), but in both cases, projecting cells were found almost exclusively in deep layers. Secondary visual cortices V2M and V2L provided stronger input to the PrS than V1 and projecting neurons were observed in superficial and deep layers, although they were more abundant in deep layers. In contrast, projections from the LEC arose mostly in superficial layers.

3.3.1 Layer-specific distribution of Retrobeads™ in case #69

In case #69, the retrosplenial cortices showed the greatest percentage of presubicular projecting cells: 17% (148 cells) of 875 neurons in Rg and 16% in Rdg (146 labelled cells, 914 NeuN positive) contained Retrobeads™. Around 12% of V2M and LEC neurons projected to the presubiculum (V2M: 119 labelled cells, 970 NeuN positive; LEC: 68 labelled cells, 568 NeuN positive), whereas less than 5% of neurons in V1 and V2L were labelled (V1: 28 labelled cells, 867 NeuN positive; V2L: 39 labelled cells, 911 NeuN positive). Within those regions, the projecting neurons showed preferential layer distributions. Remarkably, almost 50% of layer III neurons in Rg (76 cells, 160 layer III NeuN positive) and around 25% of layer II/III neurons in LEC projected to the presubiculum (LEC: 52 cells, 205 layer II/III NeuN positive).

Around 50% (76 cells) of the 148 labelled cells in RSG lay in layer III. Only one cell was found in layer II, and 71 in deep layers V/VI (14% of labelled cells). The 76 labelled cells of layer III represented 48% of all NeuN-positive cells in this layer. In deep layers, 20% of neurons projected to the presubiculum.

In Rdg, 16% of neurons projected to the presubiculum (146 labelled cells, 914 NeuN positive). The greater part of this input (97 cells; 66%) originated in superficial layers, where 16% of the 593 neurons were labelled. 34% of the Retrobeads™ in Rdg were found in deep layers, but these

49 cells represented 15% of the 321 NeuN positive cells in these layers, so that the percentage of projecting cells was equal in deep and superficial layers.

Input from LEC originated mainly from superficial layers: 77% (52 cells) of the 68 labelled cells in LEC lay in layer II/III, which represented 25% of the 205 neurons in these layers. Deeper layers provided only light input to the presubiculum: the percentage of fluorescently marked cells of the neuronal population was around 10% in layer IV (9 labelled, 90 NeuN positive) and 8% in layer V/VI (7 labelled cells, 273 NeuN positive). 13% of projections to the PrS originated in layer IV, 4% in layer V and 6% in layer VI.

In V2M and V2L, deep layers contributed more than 50% of the projections to the presubiculum. In V2M, layer II/III contained around 24% (29 cells) of the 119 labelled cells within the region, layer IV contained 20% (24 cells), 39 labelled cells (33%) were observed in layer V and 27 cells lay in layer VI (23%). 11% of neurons in layers II/III (29 labelled cells, 263 NeuN positive), 15% of neurons in layer IV (24 labelled cells, 162 NeuN positive), 17% of neurons in layers V (39 labelled cells, 225 NeuN positive) and 8% of neurons in layer VI projected to the presubiculum (27 labelled cells, 320 NeuN positive). In V2L, the percentage of projecting cells was much smaller. Only 4% of the NeuN-positive cells contained Retrobeads™ (39 labelled cells, 911 NeuN positive): almost 60% of these afferents originated in deep layers: 38% in layer V (15 labelled cells) and 21% in layer VI (8 labelled cells). 10% originated in layer IV (4 labelled cells) and 31% in superficial layers (12 labelled cells). The percentage of projecting cells was rather small in all layers: 4% of neurons in layer II/III were labelled (299 NeuN positive), 2% in layer IV (171 NeuN positive), and in deep layers, 7% of layer V and 4% of layer VI neurons projected to the presubiculum (223 and 218 NeuN positive respectively).

In V1, an even smaller part of neurons provided input to the presubiculum: 3% of NeuN-stained cells were labelled (28 labelled cells, 867 NeuN positive). The great majority (27 cells; 96%) of those labelled cells were found in layers V and VI (12/223 cells (43%) in layer V; 15/246 cells (54%) in layer VI). In layer V, labelled cells represented 5% of neurons, in layer VI, 6% of neurons were labelled. Only one labelled cell was observed in layer II/III of the primary visual cortex.

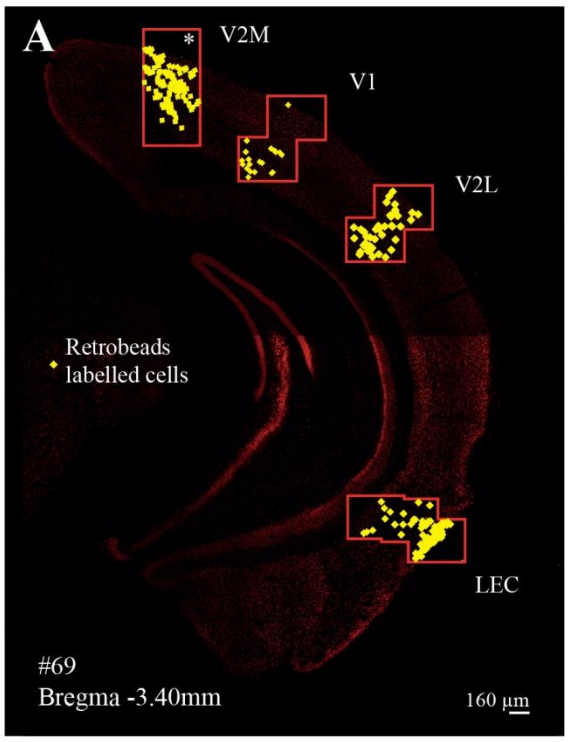

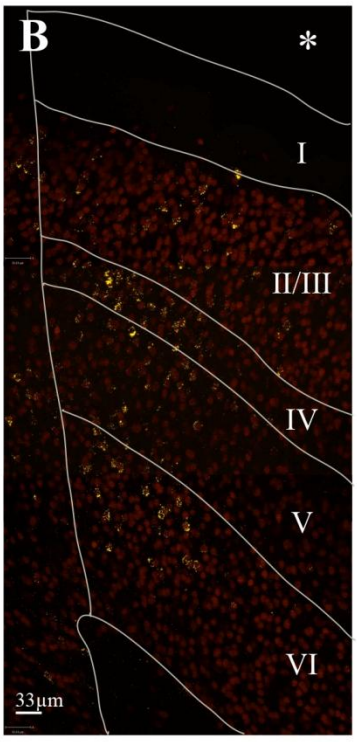

C **Percentage of labelled cells on NeuN-positive cells per layer**

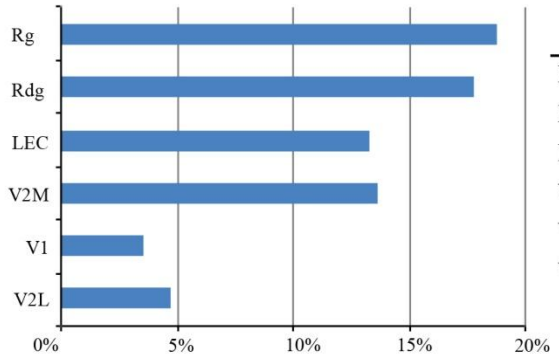

	total	layer 1	layer 2/3	layer 2	layer 3	layer 4	layer 5/6
Rg	17 %	0 %		0,3 %	48 %		20 %
Rdg	16 %	0 %	16 %				15 %
LEC	12 %	0 %	25 %			10 %	3 %
V2M	12 %	0 %	11 %			15 %	12 %
V1	3 %	0 %	0 %			0 %	6 %
V2L	4 %	0 %	4 %			7 %	5 %

D **Relative distribution of labelled cells across layers within afferent regions**

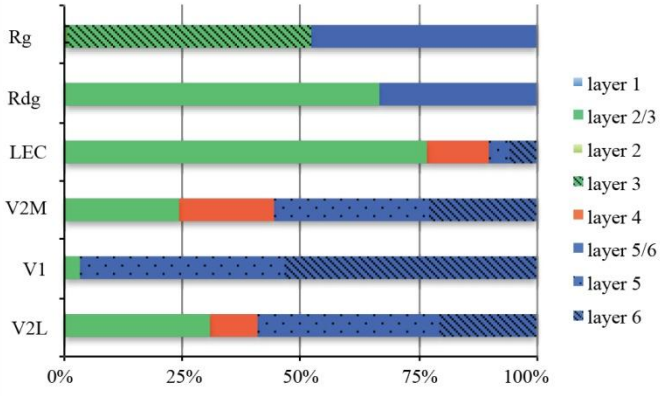

Figure 17: Layer-specific distribution of Retrobeads™ in V2M, V1, V2L, RSC and LEC. A. #69 10x microscopic photograph of NeuN stained coronal slice at Bregma -3.40 mm indicating the localization of the 20x confocal stacks of V2M, V2L, V1, RSC and LEC in which Retrobeads™ were counted. NeuN positive cells are counterstained with Alexa Fluor 64 fluorescent antibodies (dark red) in order to facilitate layer definition. Labelled cells are highlighted with yellow squares for better illustration**. B. Cortical layers I –VI in secondary visual cortex V2M.** Three stacks of images at high magnification (20x) were stitched together. Layers were defined with the help of Allen Mouse Brain Atlas[100] and according to cell morphologies and cellular density. **C. Percentage of Retrobeads™-labelled cells over NeuN positive cells.** Bar graphs indicate the percentage of neurons containing Retrobeads™ for different afferent regions. The percentage of labelled cells in each layer is given in the table on the right. Numbers take into account differences in cellular density. **D. Relative distribution of Retrobeads™- labelled cells across layers.** The bar graph shows the percentage of labelled cells in each layer of all labelled cells within a region. In V1, V2M and V2L, the majority of labelled cells were found in deep layers (>95% in V1, around 50% in V2M and V2L), whereas in LEC and the retrosplenial cortices, most labelled cells lay in superficial layers (76% in LEC, 66% in Rdg and 51% in Rg). Layer I contained no labelled cells. Note the absence of layer IV in RSC. 51.4% of all PrS projecting neurons in Rg were found in layer III (where they represented almost 50% of layer III neuronal population; see C). Layer IV of V1 contained no labelled cells, whereas 20% of PrS projecting cells in V2M, 13% in LEC and 10% in V2L were found in layer IV.

3.3.2 Layer-specific distribution of Retrobeads™ in case #105

In case #105, labelling intensities in general were lower than in case #69, probably due to a lower volume of injected tracer material. This was most striking in the Rg, where only 6% of the neuronal population contained beads (49/ 856 neurons). The greatest percentage of presubicular projecting cells was observed in the Rdg (131/ 523 cells (25%)). 10% of V2L, 8% of V2M, 7% of LEC and 4% of V1 neurons contained beads (76/ 638; 64/ 814; 25/ 368 cells respectively). In the Rdg, 25% of neurons in superficial layers (63/ 253 cells) and 28% in deep layers projected to the presubiculum (68/ 240 cells).

As in case #69, the great majority of labelled cells in the Rg were found in layer III (41/ 49 labelled cells (84%). The labelled cells represented only 20% of the 201 NeuN-positive cells in this layer, whereas in case #69, almost 50% of layer III neurons projected to the presubiculum. 14% of labelled cells were observed in deep layers, they represented 4% of the neurons in these layers (7 labelled cells, 178 NeuN positive).

In the Rdg, 52% (68 cells) of the 131 labelled cells were found in deep layers, where they represented 28% of 68 layer V/VI neurons. In superficial layers II/III 25% of neurons contained beads (63 cells, 252 NeuN positive).

In the LEC, the great majority of Retrobeads™-labelled cells was found in superficial layers (22 of 25 labelled cells in LEC), and the percentage of cells containing beads in layer II/III was 13% (22/ 165 cells). Only three cells were observed in deeper layers. One was observed in layer IV, one in layer V and one in layer VI. This represented 3% of neurons in layer IV, 2% of neurons in layer V and 1% of neurons in layer VI.

As in case #69, only 3% of neurons in the primary visual cortex (V1) were labelled (33 labelled cells, 953 NeuN positive), and 94% of labelled cells lay in deep layers. The percentage of projecting cells was 7% in layer V and 3% in layer VI. Only 3 cells in superficial layers contained the fluorescent marker (1% of neurons). No projecting cell was observed in layer IV.

In the V2M, 9% (6 cells) of the 64 labelled cells were observed in layer II/III, 36% (23 cells) in layer IV, and 42% (18 cells) in layer V and 32% (17 cells) in layer VI. 4% of neurons in layer II/III, 15% of neurons in layer IV, 9% of neurons in layer V and 7% of neurons in layer VI projected to the presubiculum (239; 153; 193; 229 NeuN positive respectively. In total, 28% of V2M neurons were labelled (64/ 814 cells). In V2L, 28% (19 cells) of the 67 fluorescently labelled cells were found in layer II/III, 7 (10%) lay in layer IV and 41 (61%) in deep layers. The percentage of projecting cells was about 9% in layers II/III, IV, and VI and 17% in layer V. In total, 10% of the cells in the V2L contained Retrobeads™ (67 labelled cells; 638 NeuN positive).

In summary, the presubiculum received minor input from deep layers of primary visual cortex V1, moderate input from deep and superficial layers of secondary visual areas V2M and V2L, and from superficial layers of the lateral entorhinal cortex. More important afferents originated in the retrosplenial cortex: In Rg, the majority of afferents originated in layer III, whereas in Rdg, deep and superficial layers were labelled. In both cases, only 4% of neurons in V1 projected to the presubiculum. There was a notable difference between both cases with respect to projections from the retrosplenial cortices: in case #69, 17% of neurons in Rg were labelled, whereas in case #105, only 6% of neurons in this region contained Retrobeads™. In Rdg on the other hand, I observed more labelled cells in case #105 (25% of neurons) than in case #69 (16% of neurons). The labelling intensity was generally weaker in case #105, but the overall labelling pattern was similar in both cases. Especially the relative distribution of labelled cells within a region was similar.

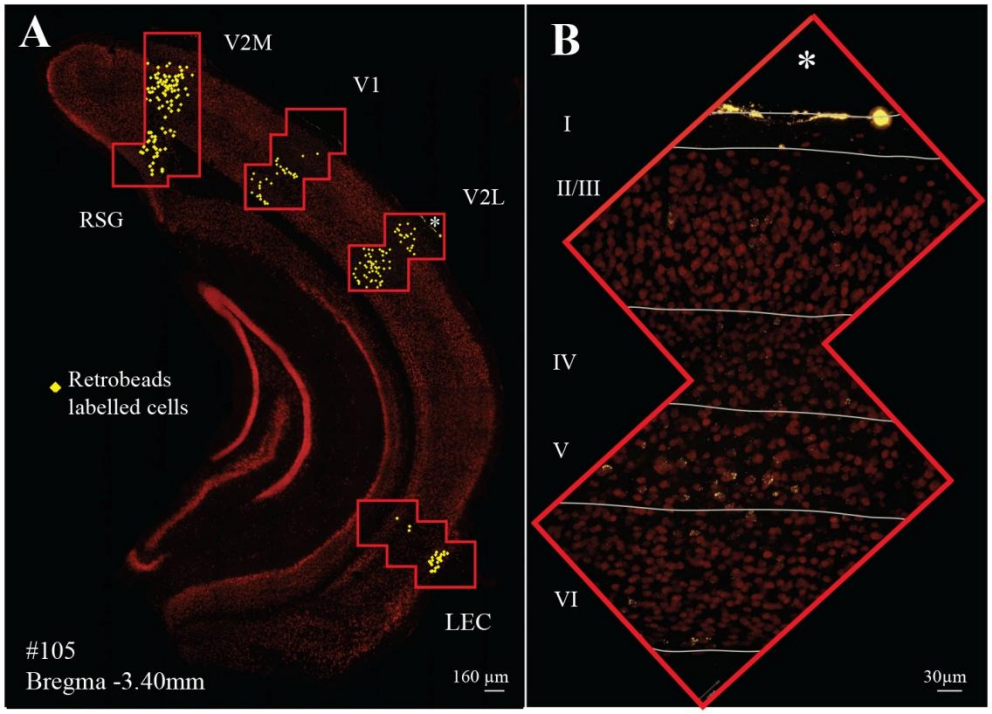

C **Percentage of labelled cells on NeuN-positive cells per layer**

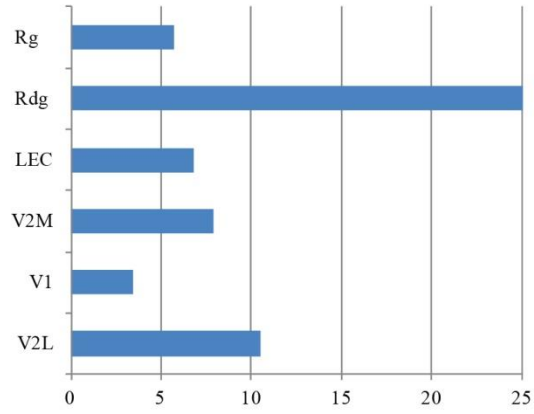

	total	layer 1	layer 2/3	layer 2	layer 3	layer 4	layer 5/6
Rg	6 %	0 %		0,2 %	20 %		4 %
Rdg	25 %	0 %	25 %				28 %
LEC	7 %	0 %	13 %			2 %	1 %
V2M	8 %	0 %	4 %			15 %	8 %
V1	3 %	0 %	1 %			0 %	6 %
V2L	11 %	0 %	9 %			8 %	12 %

D **Relative distribution of labelled cells across layers in afferent regions**

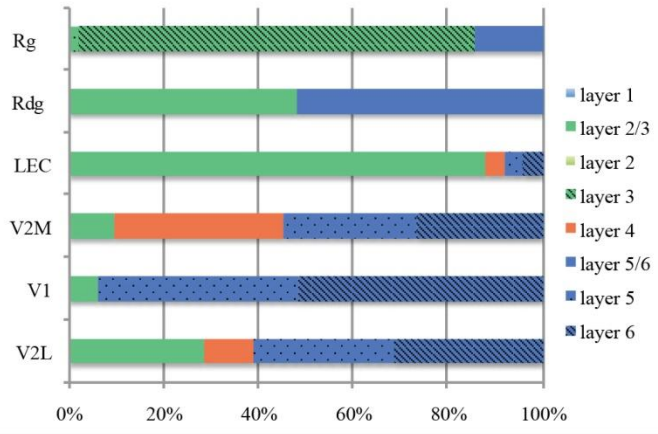

Figure 18: Layer-specific distribution of Retrobeads™ in V2M, V1, V2L, RSC and LEC. A. #105 10fold overview of NeuN stained coronal slice at Bregma -3.40 mm indicating the localization of the 20x confocal stacks of V2M, V2L, V1, RSC and LEC in which Retrobeads™ were counted. NeuN positive cells are counterstained with Alexa Fluor 647 (dark red) in order to facilitate layer definition. Labelled cells are highlighted with yellow squares for better illustration. **B. Cortical layers I-VI in V2L.** 2 stacks of images at high magnification (20x) were stitched together. Layers were defined with the help of Allen brain Atlas[100] and according to cell morphologies and cellular density. **C. Percentage of Retrobeads™-labelled cell over NeuN positive cells.** The bar graph indicates the percentage of neurons containing Retrobeads™ for different afferent regions. The percentage of labelled cells in each layer is given in the table. Numbers take into account differences in cellular density. **D. Relative distribution of Retrobeads™ labelled cells across layers.** The bar graph shows the percentage of labelled cells in each layer of all labelled cells within a region. As in case #69, in V1, V2M and V2L, the majority of labelled cells were found in deep layers (>95% in V1, ~55% in V2M and ~60% V2L), whereas in LEC and Rg, most labelled cells lay in superficial layers (88% in LEC, and 85% in Rg). Layer I contained no labelled cells. Note the absence of layer IV in RSC. 84% of all PrS projecting neurons in Rg were found in layer III (where they represented 20% of layer III neurons; see C). Layer IV of V1 contained no labelled cells, whereas 36% of PrS projecting neurons in the V2M, 4% in the LEC and 10.5% in the V2L were found in layer IV.

3.4 Viral transfection and optogenetics (collaboration with Jean Simonnet)

In order to examine presubicular response to input from afferent regions, I established an optogenetic experimental protocol using viral transfection for the introduction of the photosensitive molecule channelrhodopsin-2. I tested two lentiviral vectors with respect to their spread, transfection efficacy with incubation time and subsequent stability of viral expression. Injections were performed and recordings were performed in slices of n= 3 animals with substantial expression of the fluorescent reporter (case #8, #80, #83 and #103). 2 to 3 slices from each animal were used for recording. Patch-clamp recordings were combined with optical stimulation and subsequent visualization of the Biocytin-filled recorded neurons.

4.1 Photostimulation of LV-CaMKII-ChETA-YFP- expressing neurons in the presubiculum

With the vector LV-CaMKII-ChETA-YFP, good viral expression was observed after 4 to 5 weeks of incubation (Figure 19 A, D and G) and I was able to record light evoked events after LED stimulation in neurons near the injection site. The injection site for case #8 was the presubiculum (Figure 19 A- C). I chose a neuron close to the most intense labelling of YFP for recording. Current clamp recordings were performed at resting membrane potential (-65 mV). When a long blue light stimulation was applied, I observed a tonic depolarization of the membrane potential of about 3 mV, on top of which many rapid synaptic EPSPs occurred

(Figure 19 C, upper panel). These synaptic events were probably induced by the light-driven discharge of one or more neighboring neurons in the microcircuit. The tonic depolarization indicates that the recorded neuron itself expressed light sensitive channels which were continuously open upon the illumination. For short 20 ms light pulses applied as a train of 22 pulses with 500 ms intervals, I initiated immediate, brief depolarizing events for each pulse. On some of the pulses, the depolarizations were combined direct depolarizing and superimposed synaptic events: Superimposed events appeared for 19 out of 22 light pulses, with a delay of 10 to 15 ms with respect to the onset of the light pulse. Their rising phase was steep as in the case of synaptic EPSPs and their amplitudes ranged from 1 to 5 mV. Direct events were observed for each light stimulation with a stereotyped amplitude and shape (2 mV and slow rise time; Figure 19 C, middle and lower panel).

For case #80, the expression of the viral construct was in Rdg and Rg. For patch clamp recording, I chose a neuron in close proximity to the highest YFP signal, in layer III of Rg. Layer III also is the main layer of origin of output to the presubiculum (see section 3.3). I applied a series of hyperpolarizing and depolarizing current steps (10 ms duration, initial amplitude of -400 pA and 9 increments of +50 pA (Figure 19 F). Action potentials were initiated at a frequency of 24 Hz upon the last depolarizing current step of +300 pA. A blue light illumination of 20 ms duration was applied during the steps. It induced a small, immediate and thus direct voltage change, indicating that the cell expressed channelrhodopsin. The time course of the light-induced event was complex: it appeared as a depolarization of 1 mV in the most hyperpolarized voltage of -80 mV. At resting membrane potential (-68 mV) it was biphasic with an initial depolarizing component, and then sloped downwards to become hyperpolarizing. At more depolarized potentials (- 50mV, trace just below the threshold of action potential initiation) the light-induced voltage change was hyperpolarizing, with a maximal negative deflection of 4mV. I suggest that the event is composed of a mixture of direct opening of the ChETA cation channel and indirect inhibition by activating local GABAergic neurons.

In case #83, the expression of the transcript was most intense in the Rdg (Figure 19 G). A neuron located in Rg was chosen for recording. Figure 19 H shows the post-hoc revelation of the Biocytin-filled cell in orange, and some sparse green axons. These axons are seen mainly in layer I, where some of the dendrites of the recorded neuron are found. Furthermore, some axons are seen in layer III, close to the cell body of the recorded neuron. The application of 8 blue light pulses (LED, whole field) gave rise to 8 direct depolarizing events of 12 to 15 mV in amplitude. The depolarization began immediately with illumination and decayed when illumination stopped,

indicating that this cell also expressed ChETA. The threshold for action potential initiation was reached on pulse numbers one and three for this light intensity, while subsequent stimuli remained sub threshold. When a 405 nm laser was used for illumination, I observed similar direct depolarizations, and with this focused and higher intensity light source aimed at the cell body, the neuron was driven to action potential threshold for each of the 11 light pulses (Figure 19 I, top (LED) and bottom (laser)).

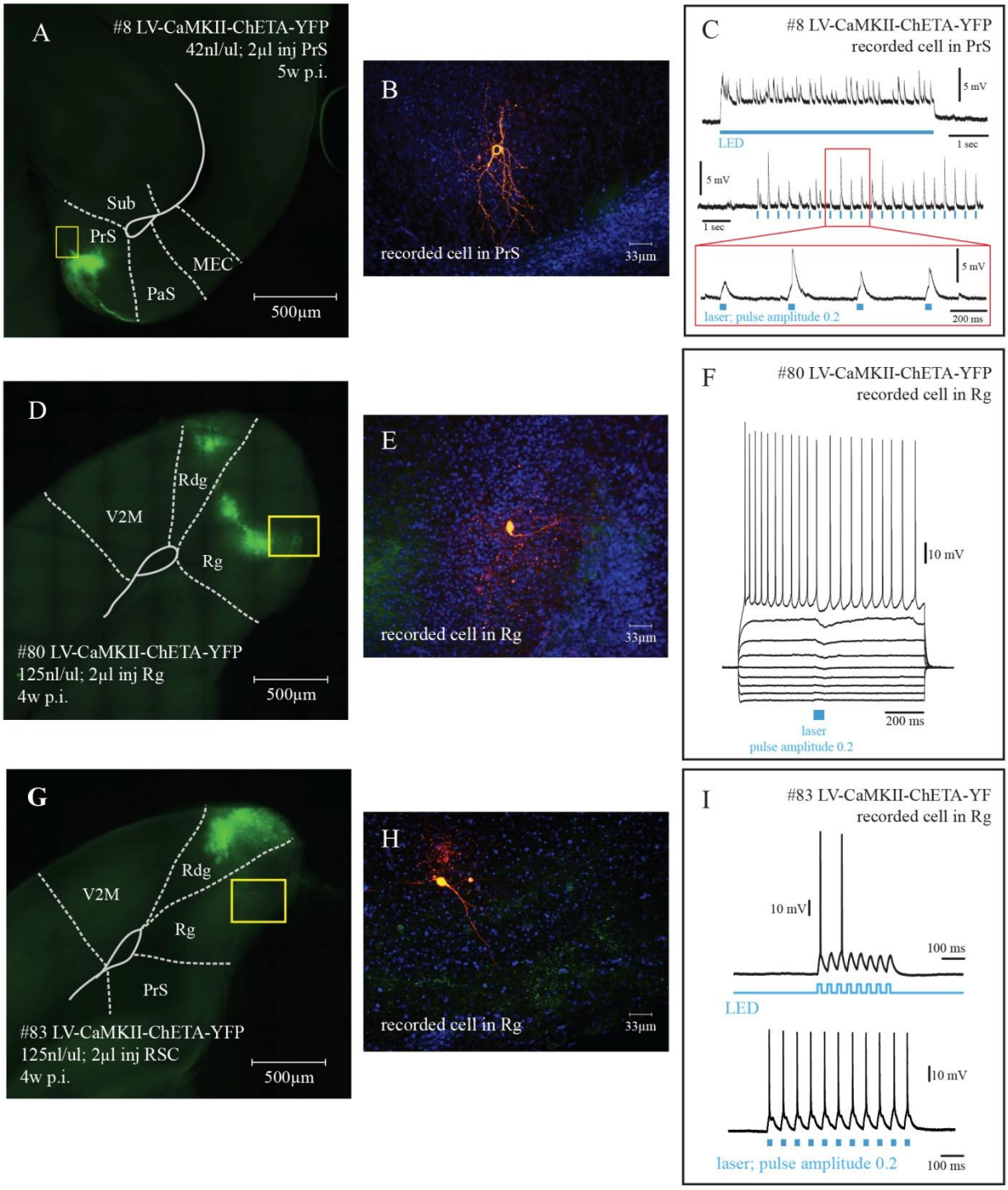

Figure 19: Three examples for expression of ChETA-YFP with subsequent electrical recording combined with blue light stimulation and biocytin revelation of the recorded neurons. **A, D, G. 10x images of slices containing the injection site. B,E,H. Biocytin revelation of the recorded neuron in 40x magnification. C, F, I. Electrical recordings near the injection site. A.** Horizontal slice with YFP expression around the injection site, 5 weeks after injection in PrS. The viral titer was of 42 ng/µl. **D, G.** Coronal slices with YFP expression in RSC 4 weeks after injection in RSC. The viral titer was of 125 ng/µl. **C.** Responses to continuous LED illumination (upper), and to trains of 20ms pulses (middle, magnification with shorter time scale, bottom). **F.** Responses to a 20ms laser pulse upon a series of current injection. **I**. Responses to a series of LED 20ms laser pulses in a Rg neuron.

3.4.2 Photostimulation of LV-CaMKII-ChR2(H134R)-mCherry- expressing neurons

The vector LV-CaMKII-ChR2(H134R)-mCherry showed some very localized expression of the fluorescent reporter at the injection site in retrosplenial cortex. In the higher magnification (Figure 20 B), several transfected cell bodies are visible. The mCherry expression appears rather clumpy than homogeneously distributed in the somatic membrane. No fluorescent axon terminals were found in presubiculum and I was not able to record any electrical responses following blue light stimulation. Possible reasons for the lack of electrical response will be discussed in section 4.1.6.

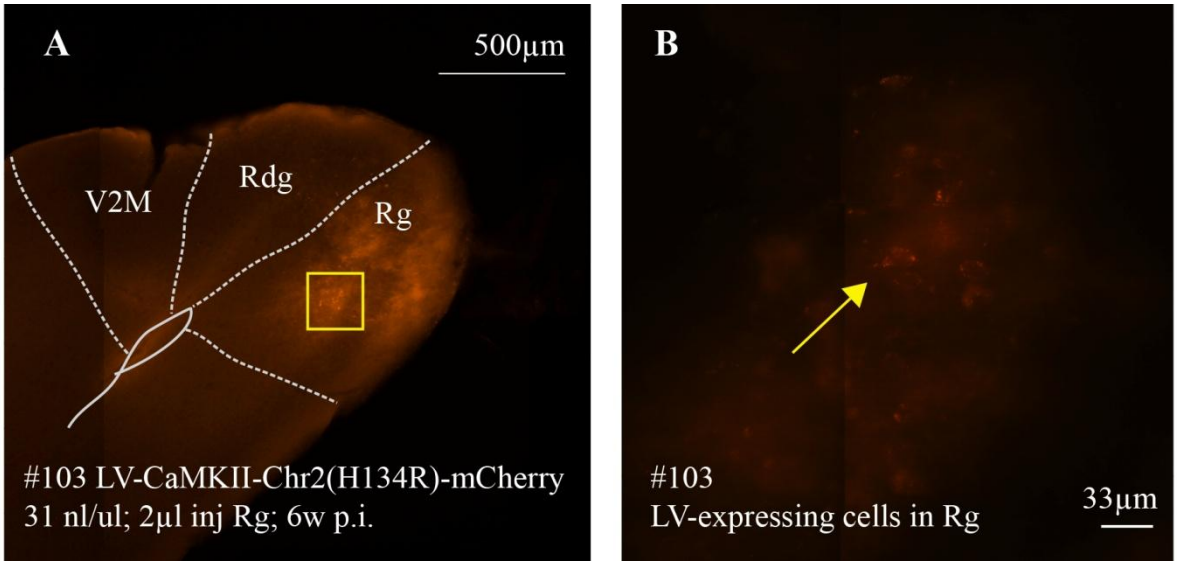

Figure 20: Example of expression of LV-CaMKII-ChR2(H134R)-mCherry 6 weeks post injection (p.i.).

A. #103 10x overview: Localised expression in Rg 6 weeks after injection of 2 µl of LV-CaMKII-ChR2(H134R)-mCherry. The viral titer was of 31 ng/µl. **B. 40x magnification of inset in A.** Several cell bodies expressing mCherry are visible (yellow arrow). Note the clumpy aspect of mCherry fluorescence. For illustration purposes, images have been treated with Adobe Photoshop. Rdg: Retrosplenial dysgranular cortex; Rg: Retrosplenial granular cortex; V2M: Secondary visual cortex, medial part.

4. Discussion

In this thesis, I report preliminary results of a series of experiments designed to characterize the functional connectivity of the presubiculum. I describe long-range afferents to the presubiculum in the mouse brain using a retrograde fluorescent marker. Furthermore, I give an initial characterization of neurons virally transfected to express the photosensitive channelrhodopsin protein using photostimulation and whole cell recordings.

My results show that the mouse presubiculum receives strongest projections from the ADN[9,27,39,53] and the retrosplenial cortex[9,27,34,44,45], some projections from the AVN[27,40], the MEC[51,107], the V2M[43], and the pre- and parasubiculum itself[48,91,92], as well as minor projections from the subiculum[27,47,49], the claustrum[27], the LDN[53], the nucleus reuniens[27,108] and the V1[43]. The distribution of retrogradely labelled cells in cortical regions was found to be in different layers, depending on the different cortical area. Projections from the contralateral pre- and parasubiculum[27,48] and the retrosplenial cortex[9,27,42] were also found. These findings confirm data from previous studies carried out in the rat brain and indicate that connectivity patterns are similar in these two species.

The presubiculum receives multimodal inputs: the ADN relays vestibular information that is thought to be the origin of the presubicular head directional signal. Visual information is provided by the visual cortex and the retrosplenial cortex. The LDN may transmit whisker-based sensory information. My results suggest that the presubiculum also receives input from the lateral entorhinal and perirhinal cortices. The presubiculum is therefore well-situated to integrate information about objects and sensory input from the LEC with visual information and self-derived and ADN-derived head directional information.

Functional connectivity can be further examined with optogenetic tools. Therefore I tested two different lentiviral vectors for the introduction of the light-sensitive cation channel Channelrhodopsin-2 into specific target regions. I showed that viral expression was present at the injection site four weeks after injection and several neurons showed responses to light stimuli. This preliminary work serves as the basis for further work that will electrophysiologically characterize the synaptic effects of the various input pathways originating in the different cortical areas.

4.1 Evaluation of methods and results

4.1.1 The injection sites for retrograde tracing

The precision of tracer injection is crucial for the interpretation of the results obtained. The injection sites for retrograde tracing described here were spatially well-defined and were situated in the presubiculum. The dye core was located dorsally in the posterior half of the region and didn't involve the most anterior parts. Very strong fluorescence – the *fluorescent halo* - masked details with lighter intensity in the slices holding the injection site (see Figure 11 B and D). At the origin of this strong fluorescent signal are probably both beads that had remained in the extracellular space at the injection site, and beads labelling locally projecting neurons within the presubiculum and locally projecting neurons in adjacent areas. Labelling in the parasubiculum, the presubiculum, the medial entorhinal and the postrhinal cortex was therefore difficult to evaluate. Intrinsic projecting neurons in the presubiculum and locally projecting neurons that might lie in adjacent regions could not be detected because, even with very weak illumination and the use of a shutter grid to limit absorbed light in the camera, details were masked by the fluorescent halo.

In both cases, the injection needle had travelled through the primary visual cortex. Although the large majority of tracer material was confined to the presubiculum, the injection needle track was visible in both cases, in case #105 more than in case #69, and might have contained a small tracer deposit. Therefore, minor tracer uptake in V1 cannot be entirely ruled out. My results will be discussed with special attention to this issue.

4.1.2 Advantages and limitations of Retrobeads™ as retrograde tracers[93,94]

With regards to their rapid axonal transport, good tolerance by the animal and compatibility with electric recordings and immunohistochemical staining, the fluorescent latex microspheres Retrobeads™ were a good choice for identification of anatomical afferents to the presubiculum in the mouse brain.

As expected, I found strong labelling in neurons of well-known afferent regions, such as the ADN, two days after injection of Retrobeads™. The labelling of Retrobeads™ was confined to the cell soma and had a granular aspect. Afferent regions and even single projecting neurons could be identified, but dendrites and axons did not contain beads and thus remained invisible. Therefore, the cell morphology of projecting neurons and the pattern of axonal termination couldn't be analyzed with this tracer. The granular, soma-localized labelling pattern is probably

due to a vesicular transport of the latex beads. Beads might be taken up via endocytosis and the vesicles containing beads would be transported to the cell body where they accumulate. Labelling has been described to be stable over several months[93,94].

Like for all fluorescent dies, strong signals can obscure details of smaller processes. This was a problem in particular in slices near the injection site (see fluorescent halo in Figure 13 B and D). In adjacent areas such as the parasubiculum or the medial entorhinal cortex, it was difficult to distinguish labelled neurons even with very short illumination times.

The two cases examined in this study showed specific labelling of presubicular afferents. In several other animals, I observed a very strong fluorescent signal (resembling a tracer deposit) along the dorsal hippocampal commissure and unspecific labelling of the entire cortical mantle (not shown). These cases were not included in this study. Since only severed fibers of passage, but not intact ones, are thought to show some uptake of marker material[93], this unspecific labelling may have been due to a lesion of the medial tip of the dorsal hippocampal commissure by the injection needle.

In the future, rabies virus might be the retrograde marker of choice. It shows high infection efficiency with specific spread to connected neurons. However, there is some cytotoxicity after more than 2 weeks after injection[109]. Rabies virus labelling includes axons and dendrites of transfected cells, enabling morphological analysis. A new pseudotyped strain which transfects genetically targeted neurons in a monosynaptically restricted manner has been developed by Wickersham et al.[110]. This rabies virus can also be used as a vector for optogenetics, providing a tool for stimulating specific afferents and thus assaying and manipulating single cells and probing the functional connectivity of specific local and long-range networks[111].

4.1.3 Input regions to the mouse presubiculum: Comparison with previous studies

The overall pattern of retrogradely labelled brain regions were the same in the two cases that I describe (cf. Figure 15 case #69 (A) vs. case #105 (B)), and mostly consistent with previous studies on rodents: the mouse presubiculum receives strong projections from the ADN[9,27,39,53] and the retrosplenial cortex[9,27,34,44,45]. Projections from the AVN[27,40], the MEC[51,107], the V2M[43], and the pre- and parasubiculum itself[48,91,92], and minor projections from the subiculum[27,47,49], the claustrum[27], the LDN[53], the nucleus reuniens[27,108] and the V1[43]. Projections from the contralateral pre- and parasubiculum[27,48] and the retrosplenial cortex[9,27,42] have also been described in previous studies. Afferents from the septal region[41] and the orbitofrontal[55] and

anterior cingulate cortices[34] have not been examined here because the cutting technique I employed didn't preserve most frontal parts of the brain.

Labelling intensities and numbers of labelled cells of the different upstream regions varied between the two animals, with denser labelling in case #69 than in #105, which may be explained by unequal quantities of infused tracer material.

For some areas, such as the LDN, the pattern of staining within the nucleus differed slightly between the two cases (see Figure 15 B and E). This might be due to a difference in the exact topographical localization of the tracer uptake in the presubiculum, given the strict topographical organization of projecting subregions of the LDN as described by van Groen and Wyss (1992)[53].

Projections from the PER and the LEC to the presubiculum have been discussed controversially in previous studies. I observed projections from dorsal LEC and adjacent PER along quite a long distance on the rostrocaudal axis (Figure 12 E). Labelling intensities were stronger in case #69, but labelling was clearly present in both cases. Most authors observed no connection[9,27], emphasizing the functional segregation between ventral and dorsal streams to the hippocampus. Only a few authors have described projections from the lateral entorhinal cortex[36,51,54] or the perirhinal cortex[9,36] to presubiculum in the rat. Agster et al. (2013)[36] observed a sparse projection from LEC to PrS and a moderate projection of the lateral and intermediate entorhinal bands, which contain fibers from LEC, to the presubiculum. They also reported light input from the perirhinal area 36 to the presubiculum. Our study confirms this observation in the mouse brain.

Thus, the findings described here challenge the classical view of two segregated streams of information to the hippocampus. There might not be a strict separation and it could be more appropriate to think of two distinct, yet intertwined, processing streams[112].

4.1.4 Discussion of divergent results in the labelling pattern

Some of the labelled regions in our experiments have not been described in previous studies concerning afferent regions of the presubiculum. In the following, I will discuss these differing results and evaluate them with special attention to a possible tracer uptake in the puncture channel in V1.

Concerning the retrosplenial cortex, previous studies in the rat have emphasized a strong connection between the presubiculum and granular parts of RSC (Rg)[42,43,45]. In my experiments, the staining in the granular and dysgranular parts of the retrosplenial cortex differed in the two

cases. The percentage of labelled neurons was similar between the two parts of RSC in case #69. However, in case #105, the dysgranular retrosplenial cortex (Rdg) showed much heavier labelling than granular parts (cf. Figures 14 and 16). Although projections from dysgranular parts to the presubiculum have been described by several authors[27,34,42,43], previous studies emphasized the strong projections from Rg to PrS[9,42,43,45]. Since the dysgranular retrosplenial cortex is interconnected with visual cortices[43], I must consider if the heavy staining of Rdg in case #105 could have been due to a tracer uptake in the puncture channel in V1. In 1983, Vogt and Miller observed strong reciprocal connections in the rat brain between dysgranular RSC, V2M and V1. However, they observed no projection from granular RSC to visual cortical areas. This strong projection to V1 could explain the retrosplenial labelling pattern in case #105: Retrobeads™ in the injection needle track could have been taken up in V1 and transported to dysgranular parts of the retrosplenial cortex. The beads deposited in the presubiculum were transported to both dysgranular and granular parts.

Retrograde fluorescent labelling was also observed in both secondary visual areas V2M and V2L. While connections between the presubiculum and V2M have been described by Vogt and Miller (1983)[43], projections from V2L to the presubiculum have not been observed before. The labelling in V2L was rather weak, but clearly present in both cases: 4% of NeuN-positive cells in case #69 and 10% in case #105 were labelled. The labelling pattern in both cases was similar: around 30% of projections originated in layers II/III, 10% of the labelled cells were found in layer IV, while deep layers provided more than 50% of projections.

Is V2L really is an afferent region of the presubiculum? Or did the labelling result from tracer uptake in V1?

In cat, projections from area 17 to area 18 originate mainly in supragranular layers[113]. If this holds true for the mouse brain, the observed labelling in V2L would rather originate in the presubiculum than in V1. Projections from secondary visual area V2L to the presubiculum would be consistent with the hypothesis that the presubiculum provides visual information to the hippocampus[72] and is strongly intertwined with other cortical areas involved in visual information processing such as the retrosplenial cortex[9,27,34,44,45] and V2M[43]. Further studies might be necessary to completely elucidate this question. This result further undermines the view that deep layers of the neocortex provide feedback projection to areas of lower hierarchical order[2,3,113] might be over-generalizing.

The pattern of laminar distribution in V2M was different in case #69 and case #105. While in case #69, 56% (66/119) of labelled cells were located in deep layers, 24% (29/119) in superficial layers and 20% in layer IV (24/119), the portion of labelled cells confined to deep layers (56/64; 74% of labelled cells) was much higher in case #105 and only 9% (6/64) lay in superficial layers. This might also be due to an additional tracer uptake in V1 and subsequent heavier labelling of V2M deep layers in case #105.

I observed some labelled cells in DLG, which were confined to the dorsolateral corner of the anterior part of the nucleus. Projections from DLG to the presubiculum have not been described in previous studies. However, given the fact that the lateral geniculate nucleus of thalamus is the third station of the visual pathway from the eye to V1, I cannot rule out that this staining was due to a retrograde labelling from V1.

Afferents from the septal region[41] and the orbitofrontal[55] and anterior cingulate cortices[34] have not been examined here because the most frontal parts of the brain were not preserved in my coronal slices.

4.1.5 Laminar origin of cortical input to the mouse presubiculum

My study provides additional information about the laminar origin of the projections from five cortical regions: Rdg, Rg, LEC, V1, V2M and V2L. The laminar organization of projections is generally taken to reflect the hierarchy of connections in cortical networks[3,114]. In the visual cortex[3,113] and the neocortex[1], unilaminar origin projections seem to be specific for their hierarchical direction: superficial layer projections are thought to be *ascending* or *feed-forward* and those from deep layers *descending* or *feedback*.

In my study, projections from the LEC had a unilaminar origin in superficial layers II/III. Layer II/III projections are typical for intracortical associational connections[2]. If unilaminar projections from superficial layers are specific for ascending projections[3], this pattern of origin would indicate that the presubiculum is higher in hierarchy than the LEC.

In V1, neurons projecting to the presubiculum lay almost exclusively in deep layers, suggesting a *descending* projection from V1 to PrS according to Fellemann et al. (1991)[3]. Since the presubiculum is a higher order cortical region than a primary sensory area such as V1, this result challenges the view postulated by Fellemann and Kandel[1], that cortical projections originating in deep layers are generally feedback projections.

Projections from Rdg and V2L had a bilaminar origin. Less than 70% originated in one compartment. Bilaminarly originating projections can be ascending or descending as well, but are most commonly observed in projections traversing no more than 2 levels of hierarchy[3]. This suggests that the hierarchical level of the presubiculum and Rdg or V2L could be close to each other.

V2M had differing patterns of origin in both cases: in case #105, 74% of projections originated in deep layers, which would suggest a feedback projection. In case #69, the majority of projections originated in deep layers as well, but the labelled cells in layer V/VI represented only 56% of the projecting neurons, which would be classified as a bilaminar origin pattern. Since bilaminar origin is found in all directions of connection and unilaminar origin in deep layers is specific for descending projections[1,3], the projection from V2M to PrS could be a feedback connection. Again, this hierarchical order seems rather unlikely, considering the high level of processing of PrS compared to a secondary visual area.

Commissural projections from the contralateral presubiculum also showed a differing pattern of origin compared to the classical view in which commissural projections originate in layer III[2]. The labelled cells in the contralateral presubiculum in my study almost exclusively lay in layer II (see Figure 15 G).

My results suggest that, in regard to hierarchical organization, the pattern of laminar origin in afferent regions of the presubiculum in the mouse brain might differ from the classical schemes described for visual and neocortex and challenge the hypothesis that deep layers provide feedback projection in the neocortex[1,2]. In fact, this hypothesis is mainly based on finding in visual cortex in cat[113] and monkey[3] .

Several explanations of the differing pattern observed in this study seem possible: the transitional character of the presubiculum between the isocortex and the allocortex might explain a differing pattern of origin. The connectional pattern in mouse might not be the same as in cat or monkey. Or the generalization from findings in visual cortex to the neocortex itself might be an over-generalization.

4.1.6 Advantages and limitations of different viral vectors for optogenetic targeting

The growing number of different technical approaches necessitate/ require detailed evaluation of competing experimental protocols. For the introduction of photosensitive molecules into specific target cells, a large number of different approaches have been elaborated. Viral transfection is an

efficient and rather simple procedure to achieve cell-type specific expression of optogenetic molecules on the condition of strong and stable expression of the viral vector in the target cells. Viral expression levels and electrical responses are two indications of the viability of a given procedure.

In my experiments, viral expression was evaluated by fluorescent labelling of transfected cells and patch-clamp recordings after light stimulation at the injection site and in long-range projection areas. I observed sharply defined areas of protein expression for the two lentiviral constructs that were tested (Figure 19 and 20), and direct responses to light stimulation at the injection site for the YFP- labelled construct (Figure 19). At recording sites in some distance to the injection site however, fluorescent labelling in axons and electrophysiological responses could not be documented in mice injected with the LV-CaMKII-ChR2(H134R)-mCherry construct. Three factors could have been responsible for these low expression levels: the virus, the promoter and the correct transfer of the product to its appropriate location.

First, the lentiviral vector could have had low infection efficiency, so that very few neurons would have been transduced in the first place. Second, the CaMKII promoter might not have been very efficient, maybe due to its high level of specificity for principal cells. In consequence, the protein would not have been expressed in sufficient quantities. Third, the protein could have been produced but have not reached its designated location: the axonal membrane. The granular aspect of the mCherry fluorescence (see Figure 20 B) could suggest that there was some aggregation or misfolding, hindering the correct membrane-bound expression of the channelrhodopsin molecules. All of these factors probably played a role in my experiments.

The present results confirm that lentiviral expression remains spatially specific and limited to areas close to the injection site (Figures 17 and 18). This may be useful or even crucial for some studies. On the other hand, local specificity can be negligible, if regions adjacent to the injection site do not project to the target region (the recording site). Since strong expression of the optogenetic protein in soma and axons is essential for recording of long-range projecting neurons, it might prove more useful to opt for a vector with stronger and more rapid expression and a more efficient but still neuron-specific promoter in the future. AAVs and hSyn might be the better choice for the optogenetic protocol of our experiments. Concerning the choice of the fluorescent reporter, I found that mCherry might possibly have hindered the correct membrane-bound expression of channelrhodopsin and that, even if some activation of channelrhodopsin

may occur during the visualization of YFP, it may be the better choice. The influence on electrophysiological results would have to be evaluated.

4.1.7 Electrophysiological results

Our electrophysiological recordings showed that action potentials could be initiated by light stimulation in transfected neurons near the injection site. In case #8, I observed small direct responses (see Figure 19 C), suggesting that the recorded neuron expressed some channelrhodopsin itself. I also observed superposed indirect excitatory events (see Figure 19 C, middle and lower panel), that were probably initiated in neighboring neurons that formed synapses with the recorded cell. These results are consistent with the fact that the channelrhodopsin should be expressed only in excitatory cells, since the CaMKII promoter is specific for pyramidal cells. In case #81on the other hand, I observed a hyperpolarizing light induced voltage change at depolarized membrane potentials (- 50 mV, see Figure 19 F, trace just below the threshold of action potential initiation). If the channelrhodopsin was expressed in excitatory cells only, this event seems surprising at first glance. I suggest that this event is a result of local inhibition. A channelrhodopsin expressing axons of a pyramidal cell could target and drive local interneurons. The firing of these interneuron could then lead to an inhibitory event in the recorded cell.

4.2 Comparison with human brain

If it is a matter of foraging for food, returning to the nest or finding the way to the correct departure gate in a big airport, the need to navigate is part of basic behavior in all complex animals. We are looking at a growing body of findings about the brain regions involved, neuronal circuits and underlying schemes of spatial representation in rodents and other members of the mammalian family. But does the human brain use the same mechanisms? Is the knowledge acquired from animal models applicable to the human brain? Do we rely on the same schemes of spatial representation as our simpler relatives? And does the presubiculum play a role in human navigation as well?

Lesion[115] and functional imaging (fMRI: functional magnetic resonance imaging)[116] studies revealed that the human hippocampus, like in lower animals, is crucial for spatial navigation and memory. Maguire et al. (1996) showed that unilateral lesions of the temporal lobe (including the hippocampus) of either hemisphere lead to impairment of topographical orientation in a real-

world environment compared to control subjects[115]. Two years later, Maguire et al. identified a network of brain areas supporting navigation in humans. Using functional imaging (fMRI) while subjects were performing virtual navigation tasks, they showed that successful navigation was associated with strong activation of the right hippocampus. In successful compared to unsuccessful trials, they observed higher activity in left hippocampus, left lateral temporal cortex, left frontal cortex, and thalamus. These results further stressed the importance of both hippocampi for successful navigation and indicated that the neural network implemented in spatial navigation involved similar regions in humans and other mammals. The presubiculum, located in the lateral temporal cortex, seemed to be involved in human navigation, too.

The question whether the human hippocampus was implemented in the acquisition *and* the retrieval of spatial knowledge was discussed controversially. Teng and Squire's (1999)[117] reported of an amnesic patient with extensive bilateral damage of the temporal lobe that included the hippocampus who had intact spatial memory for his childhood town. Their report confirmed that the hippocampus was important for the acquisition of new spatial knowledge, since their patient suffered from severe anterograde amnesia for both spatial and non-spatial information encountered after the lesion, but challenged the view that spatial information was stored in the hippocampus. The question was further examined by Maguire et al. (2000). They showed that individuals with extensive spatial knowledge – London taxi drivers – had a significant increase in gray matter in the posterior hippocampus that correlated positively with time spent as a taxi driver (time of exposure to the external stimulus). At the same time, the taxi drivers had a decreased volume of the anterior hippocampus, which also correlated with the time of practice (negatively, this time). These findings suggested that the posterior hippocampus is the site of storage of spatial information in humans and might have been spared in Teng and Squire's patient. The anterior hippocampus might be implicated in the acquisition of new spatial knowledge. It was the first evidence for a functional differentiation within the human hippocampus as it had been reported in other mammals before. Evidence for the similarity of cognitive schemes supporting spatial navigation in humans and other mammalians was accumulating. Furthermore, the proof of local plasticity after increased environmental stimulation in healthy human brains was a very interesting discovery regarding the rehabilitation of patients who have suffered brain injury or disease.

We now know that, as in simpler animals, the human temporal lobe, where the presubiculum is located, plays the pivotal role in spatial navigation. But does the human brain use the same schemes of spatial representation that have been revealed in rodents and other mammals? Do our

orientational skills rely on neuronal networks containing spatially tuned neurons such as place cells, grid cells or head direction cells, too?

Functional imaging and direct recordings in patients undergoing brain surgery indicate that this might actually be the case and that the human presubiculum might be involved in the computation of our present location and future goal direction: Ekstrom et al. (2003) discovered cells that responded to specific locations in an environment (comparable to O'Keefe's *place cells*) in the human hippocampus[118], which have since been observed in the parahippocampal[119] (holding the presubiculum) and cingulate gyrus[119] as well. Jacobs et al. (2010) discovered the existence of direction sensitive cells referred to as *path cells* in the entorhinal cortex[120], the parahippocampal gyrus[119,120], the hippocampus[119,120] and the frontal cortex[120]. *Path cells* respond to clockwise or counter-clockwise rotation regardless of the patient's location within the environment, but unlike *head direction cells* in rodents, which function like a compass, human *path cells* encode for direction in a manner that is relative to the environment's shape. These findings further stressed the presubiculum's involvement in human navigation. In a later study, Jacobs et al. observed *grid cells* and *grid-by-direction cells* in the entorhinal and the retrosplenial cortices[119], emphasizing the similar organization of spatial representation in human and rodent brain.

The human presubiculum in particular seems to be involved in the computation of (Euclidean) *goal distance*[121,122] and *future goal direction*[123]: Computational models suggested that navigation might rely on information about distance and direction of a goal[121]. Functional imaging studies showed that several brain regions actually responded in relation to *goal distance*[122] (the distance to a goal; also called *goal proximity*[121] in another study) and *goal direction*[121,123]. The distance to a goal seems to be encoded by several complementary signals: activity in the subicular/entorhinal area, where the presubiculum is located, is negatively correlated with goal proximity[121,122]. Activity increased with increasing *Euclidean distance* to the goal[122]. The *Euclidean distance* is the shortest possible distance between two points, represented by a vector. In real-world navigation, the path along which a subject has to travel might differ from the Euclidean vector. This distance to a goal along a path (the *path distance*) seems to be encoded in the posterior hippocampus[122]: while travelling, activity in this region is positively correlated with path distance, but at decision points, activity increases as the path to the goal becomes shorter and more direct. Activity in the medial prefrontal cortex (mPFC)[121] and the anterior hippocampus[122] is positively correlated with the proximity to a goal (increasing activity when

approaching the goal with maximal activity at the goal location). These finding suggest that the human presubiculum might be involved in the computation of the Euclidean goal distance.

Intended goal direction is the direction one must face in order to look at the goal location. Two complementary representational systems have been identified in the human brain: the posteromedial parietal cortex (also called precuneus) codes for *egocentric goal direction* (e.g. the angle between the current facing direction and the direction facing the goal)[121–123], while *geocentric goal direction* (e.g. west) is represented in the subicular/entorhinal area[123], suggesting a presubicular involvement in this signal. Due to a limited resolution in the MRI data, the exact anatomical location of the geocentric goal directional signal could not be determined yet. Both the presubiculum and the entorhinal cortex seem to be candidates[123]. Since head direction cells are abundant in the presubiculum and since the calculation of a future travel route might involve a simulation of the intended future route by transient activation of the neuronal population active during active travel to the goal[123], the presubiculum seems to be in a good position to be the site of that signal.

The growing data on human schemes of spatial representation and navigation reveals a great number of similarities with rodent and other mammalian brains. This supports the view that extrapolation from animal models to humans is appropriate. The medial temporal lobe including hippocampus, parahippocampal region and presubiculum, seems to play the pivotal role. In rodents, the presubiculum might integrate self-generated and incoming information about head direction and visual landmarks with information about individual objects from the lateral entorhinal cortex. In humans, it contains place cells and path cells and seems to be involved in the computation of Euclidean goal distance and intended goal direction.

Clinically, the elucidation of functional connectivity of presubiculum and other parahippocampal areas that are crucial for spatial navigation will help to better understand human pathologies involving disorientation. Neurodegeneration particularly involves the EC and HF in Alzheimer's disease[124]. In dementia with Lewy bodies, a selective loss of presubicular pyramidal cells has been reported[125]. Considering the findings on spatial representation and navigation, these observations are in line with, and may well explain, the difficulties in orientation and navigation experienced by many patients at early stages of these diseases. In the future, precise knowledge on the signal integration in the temporal lobe should allow advances in early diagnostics and for alleviating symptoms of these diseases.

1. Kandel ER, Schwartz JH, Jessell TM. The Anatomical Organization of the Central Nervous System. In: Principles of Neural Science. 2000. p. 325–31.

2. Dale P, Augustine GJ, Fitzpatrick D, et al. The Association Cortices. In: Neuroscience. 2004.

3. Felleman DJ, Van Essen DC. Distributed hierarchical processing in the primate cerebral cortex. Cereb Cortex 1991;1(1):1–47.

4. Buzsáki G, Moser EI. Memory, navigation and theta rhythm in the hippocampal-entorhinal system. Nat Neurosci 2013;16(2):130–8.

5. Burwell RD, Amaral DG. Cortical afferents of the perirhinal, postrhinal, and entorhinal cortices of the rat. J Comp Neurol 1998;398(2):179–205.

6. Amaral DG, Witter MP. The three-dimensional organization of the hippocampal formation: a review of anatomical data. Neuroscience 1989;31(3):571–91.

7. Van Strien NM, Cappaert NLM, Witter MP. The anatomy of memory: an interactive overview of the parahippocampal-hippocampal network. Nat Rev Neurosci 2009;10(4):272–82.

8. Brodmann K. Vergleichende Lokalisationslehre der Grosshirnrinde: in ihren Principien dargestellt auf Grund des Zellenbaues. 1909.

9. Van Groen T, Wyss JM. The postsubicular cortex in the rat: characterization of the fourth region of the subicular cortex and its connections. Brain Res 1990;529(1-2):165–77.

10. Blackstad TW. Commissural connections of the hippocampal region in the rat, with special reference to their mode of termination. J Comp Neurol 1956;

11. O'Mara SM, Commins S, Anderson M, Gigg J. The subiculum: A review of form, physiology and function. Prog. Neurobiol. 2001;64(2):129–55.

12. Lorente de Nó R. Studies on the Structure of the Cerebral Cortex. J für Psychol und Neurol 1933;45(6):381–438.

13. Abbasi S, Kumar SS. Electrophysiological and morphological characterization of cells in superficial layers of rat presubiculum. J Comp Neurol 2013;521(13):3116–32.

14. Boccara CN, Sargolini F, Thoresen VH, et al. Grid cells in pre- and parasubiculum. Nat Neurosci 2010;13(8):987–94.

15. Ding SL, Rockland KS. Modular organization of the monkey presubiculum. Exp Brain Res 2001;139(3):255–65.

16. Taube JS. The head direction signal: origins and sensory-motor integration. Annu Rev Neurosci 2007;30:181–207.

17. O'Keefe J, Dostrovsky J. The hippocampus as a spatial map. Preliminary evidence from unit activity in the freely-moving rat. Brain Res 1971;34(1):171–5.

18. Hafting T, Fyhn M, Molden S, Moser M-B, Moser EI. Microstructure of a spatial map in the entorhinal cortex. Nature 2005;436(7052):801–6.

19. Solstad T, Solstad T, Boccara CN, et al. Representation of geometric borders in the entorhinal cortex. Science (80-) 2008;322(1):1865–8.

20. Taube JS, Muller RU, Ranck JB. Head-direction cells recorded from the postsubiculum in freely moving rats. I. Description and quantitative analysis. J Neurosci 1990;10(2):420–35.

21. O'Keefe J, Nadel L. The hippocampus as a cognitive map. Oxford: Clarendon Press; 1978.

22. Taube JS, Muller RU, Ranck JB. Head-direction cells recorded from the postsubiculum in freely moving rats. II. Effects of environmental manipulations. J Neurosci 1990;10(2):436–47.

23. Ranck JB. Head direction cells in the deep cell layer of dorsal presubiculum in freely moving rats. Soc Neurosci Abstr 10599 1984;

24. McNaughton BL, Battaglia FP, Jensen O, Moser EI, Moser M-B. Path integration and the neural basis of the "cognitive map". Nat Rev Neurosci 2006;7(8):663–78.

25. Bonnevie T, Dunn B, Fyhn M, et al. Grid cells require excitatory drive from the hippocampus. Nat Neurosci 2013;16(3):309–17.

26. Ramón y Cajal SF. Textura del sistema nervioso del hombre y de los vertebrados. Madrid: Imprenta y Libreria;

27. Van Groen T, Wyss JM. The connections of presubiculum and parasubiculum in the rat. Brain Res 1990;518(1-2):227–43.

28. Shibata H. Terminal distribution of projections from the retrosplenial area to the retrohippocampal region in the rat, as studied by anterograde transport of biotinylated dextran amine. Neurosci Res 1994;20:331–6.

29. Kim Y, Spruston N. Target-specific output patterns can be predicted by the distribution of regular-spiking and bursting pyramidal neurons in the subiculum. 2012;22(4):693–706.

30. Dolorfo CL, Amaral DG. Entorhinal Cortex of the Rat : Organization of Intrinsic Connections. 1998;82(December 1996):49–82.

31. Burwell RD. The parahippocampal region: corticocortical connectivity. Ann N Y Acad Sci 2000;911(911):25–42.

32. Hargreaves EL, Rao G, Lee I, Knierim JJ. Major dissociation between medial and lateral entorhinal input to dorsal hippocampus. Science 2005;308(5729):1792–4.

33. Witter MP, Wouterlood FG, Naber P a, Van Haeften T. Anatomical organization of the parahippocampal-hippocampal network. Ann N Y Acad Sci 2000;911:1–24.

34. Jones BF, Witter MP. Cingulate cortex projections to the parahippocampal region and hippocampal formation in the rat. Hippocampus 2007;17(10):957–76.

35. Deshmukh SS, Knierim JJ. Representation of Non-Spatial and Spatial Information in the Lateral Entorhinal Cortex. Front. Behav. Neurosci. 2011;5(October):69.

36. Agster KL, Burwell RD. Hippocampal and subicular efferents and afferents of the perirhinal, postrhinal, and entorhinal cortices of the rat. Behav Brain Res 2013;254:50–64.

37. Honda Y, Ishizuka N. Organization of Connectivity of the Rat Presubiculum: I. Efferent Projections to the Medial Entorhinal Cortex. J Comp Neurol 2004;473(4):463–84.

38. Van Groen T, Wyss JM. Projections from the anterodorsal and anteroventral nucleus of the thalamus to the limbic cortex in the rat. J Comp Neurol 1995;358(4):584–604.

39. Shibata H, Honda Y. Thalamocortical projections of the anterodorsal thalamic nucleus in the rabbit. J Comp Neurol 2012;520(12):2647–56.

40. Van Groen T, Kadish I, Wyss JM. Efferent connections of the anteromedial nucleus of the thalamus of the rat. Brain Res. Rev. 1999;30(1):1–26.

41. Wyss JM, Swanson LW, Cowan WM. A study of subcortical afferents to the hippocampal formation in the rat. Neuroscience 1979;4(4):463–76.

42. Wyss JM, Van Groen T. Connections between the retrosplenial cortex and the hippocampal formation in the rat: a review. Hippocampus 1992;2(1):1–11.

43. Vogt B a, Miller MW. Cortical connections between rat cingulate cortex and visual, motor, and postsubicular cortices. J Comp Neurol 1983;216(2):192–210.

44. Kononenko NL, Witter MP. Presubiculum layer III conveys retrosplenial input to the medial entorhinal cortex. Hippocampus 2012;22(4):881–95.

45. Van Groen T, Wyss JM. Connections of the retrosplenial granular b cortex in the rat. J Comp Neurol 2003;463(3):249–63.

46. Köhler C. Intrinsic projections of the retrohippocampal region in the rat brain. I. The subicular complex. J Comp Neurol 1985;236(4):504–22.

47. Shipley MT, Sorensen KE. On the laminar organization of the anterior thalamus projections to the presubiculum in the guinea pig. Brain Res [Internet] 1975;86(3):473–7. Available from: http://www.ncbi.nlm.nih.gov/pubmed/1116011

48. Honda Y, Umitsu Y, Ishizuka N. Organization of connectivity of the rat presubiculum: II. Associational and commissural connections. J Comp Neurol 2008;506(4):640–58.

49. O'Reilly KC, Gulden Dahl A, Ulsaker Kruge I, Witter MP. Subicular-parahippocampal projections revisited: Development of a complex topography in the rat. J Comp Neurol 2013;521(18):4284–99.

50. Cenquizca LA, Swanson LW. Spatial organization of direct hippocampal field CA1 axonal projections to the rest of the cerebral cortex. Brain Res. Rev. 2007;56:1–26.

51. Wyss JM. An autoradiographic study of the efferent connections of the entorhinal cortex in the rat. J Comp Neurol 1981;199(4):495–512.

52. Funahashi M, Stewart M. Presubicular and parasubicular cortical neurons of the rat: Electrophysiological and morphological properties. Hippocampus 1997;7(2):117–29.

53. Van Groen T, Wyss JM. Projections from the laterodorsal nucleus of the thalamus to the limbic and visual cortices in the rat. J Comp Neurol 1992;324(3):427–48.

54. Swanson LW, Köhler C. Anatomical evidence for direct projections from the entorhinal area to the entire cortical mantle in the rat. J Neurosci [Internet] 1986;6(10):3010–23. Available from: http://www.ncbi.nlm.nih.gov/pubmed/3020190

55. Kondo H, Witter MP. Topographic organization of orbitofrontal projections to the parahippocampal region in rats. J Comp Neurol 2014;522(4):772–93.

56. Meibach RC, Siegel A. Efferent connections of the septal area in the rat: an analysis utilizing retrograde and anterograde transport methods. Brain Res 1977;119(1):1–20.

57. Gonzalez-sulser XA, Parthier XD, Candela A, et al. GABAergic Projections from the Medial Septum Selectively Inhibit Interneurons in the Medial Entorhinal Cortex. J Neurosci 2014;34(50):16739–43.

58. Beckstead RM. Afferent connections of the entorhinal area in the rat as demonstrated by retrograde cell-labelling with horseradish peroxidase. Brain Res 1978;152(2):249–64.

59. Sharp PE, Tinkelman A, Cho J. Angular velocity and head direction signals recorded from the dorsal tegmental nucleus of gudden in the rat: implications for path integration in the head direction cell circuit. Behav Neurosci 2001;115(3):571–88.

60. Stackman RW, Taube JS. Firing properties of rat lateral mammillary single units: head direction, head pitch, and angular head velocity. J Neurosci 1998;18(21):9020–37.

61. Taube JS. Head direction cells recorded in the anterior thalamic nuclei of freely moving rats. J Neurosci 1995;15(1 Pt 1):70–86.

62. Tsanov M, Chah E, Vann SD, et al. Theta-modulated head direction cells in the rat anterior thalamus. J Neurosci 2011;31(26):9489–502.

63. Mizumori SJ, Williams JD. Directionally selective mnemonic properties of neurons in the lateral dorsal nucleus of the thalamus of rats. J Neurosci 1993;13(9):4015–28.

64. Sargolini F, Fyhn M, Hafting T, et al. Conjunctive representation of position, direction, and velocity in entorhinal cortex. Science 2006;312(5774):758–62.

65. Chen LL, Lin LH, Barnes CA, McNaughton BL. Head-direction cells in the rat posterior cortex - II. Contributions of visual and ideothetic information to the directional firing. Exp Brain Res 1994;101(1):24–34.

66. Ragozzino KE, Leutgeb S, Mizumori SJ. Dorsal striatal head direction and hippocampal place representations during spatial navigation. Exp Brain Res 2001;139(3):372–6.

67. Jankowski MM, Islam MN, Wright NF, et al. Nucleus reuniens of the thalamus contains head direction cells. Elife 2014;3:e03075.

68. Leutgeb S, Ragozzino KE, Mizumori SJY. Convergence of head direction and place information in the CA1 region of hippocampus. Neuroscience 2000;100(1):11–9.

69. Sharp PE, Blair HT, Cho J. The anatomical and computational basis of the rat head-direction cell signal. Trends Neurosci. 2001;24(5):289–94.

70. Clark BJ, Taube JS. Vestibular and attractor network basis of the head direction cell signal in subcortical circuits [Internet]. Front. Neural Circuits. 2012 [cited 2014 Sep 25];6(March):7. Available from: http://www.pubmedcentral.nih.gov/articlerender.fcgi?artid=3308332&tool=pmcentrez&rendertype=abstract

71. Biazoli CE, Goto M, Campos AMP, Canteras NS. The supragenual nucleus: A putative relay station for ascending vestibular signs to head direction cells. Brain Res 2006;1094(1):138–48.

72. Yoder RM, Clark BJ, Taube JS. Origins of landmark encoding in the brain. Trends Neurosci. 2011;34(11):561–71.

73. Bezdudnaya T, Keller A. Laterodorsal nucleus of the thalamus: A processor of somatosensory inputs. J Comp Neurol 2008;507(6):1979–89.

74. Canto CB, Koganezawa N, Beed P, Moser EI, Witter MP. All layers of medial entorhinal cortex receive presubicular and parasubicular inputs. J Neurosci 2012;32(49):17620–31.

75. Rowland DC, Weible AP, Wickersham IR, et al. Transgenically targeted rabies virus demonstrates a major monosynaptic projection from hippocampal area CA2 to medial entorhinal layer II neurons. J Neurosci 2013;33(37):14889–98.

76. Yoder RM, Taube JS. Projections to the anterodorsal thalamus and lateral mammillary nuclei arise from different cell populations within the postsubiculum: Implications for the control of head direction cells. Hippocampus 2011;21(10):1062–73.

77. Shibata H, Naito J. Organization of anterior cingulate and frontal cortical projections to the anterior and laterodorsal thalamic nuclei in the rat. Brain Res 2005;1059(1):93–103.

78. Mizumori SJ, Miya DY, Ward KE. Reversible inactivation of the lateral dorsal thalamus disrupts hippocampal place representation and impairs spatial learning. Brain Res 1994;644(1):168–74.

79. Warburton EC, Baird AL, Aggleton JP. Assessing the magnitude of the allocentric spatial deficit associated with complete loss of the anterior thalamic nuclei in rats. Behav Brain Res 1997;87(2):223–32.

80. Allen G V, Hopkins D a. Mamillary body in the rat: topography and synaptology of projections from the subicular complex, prefrontal cortex, and midbrain tegmentum. J Comp Neurol 1989;286(3):311–36.

81. Shires KL, Hawthorne JP, Hope AMJ, Dudchenko P a, Wood ER, Martin SJ. Functional connectivity between the thalamus and postsubiculum: Analysis of evoked responses elicited by stimulation of the laterodorsal thalamic nucleus in anesthetized rats. Hippocampus 2013;23(7):559–69.

82. Bartesaghi R, Gessi T. Electrophysiological analysis of the hippocampal output to the presubiculum. Neuroscience 1990;37(2):335–45.

83. Swanson LW, Wyss JM, Cowan WM. An autoradiographic study of the organization of intrahippocampal association pathways in the rat. J Comp Neurol 1978;181(4):681–715.

84. Bartesaghi R, Di Maio V, Gessi T. Topographic activation of the medial entorhinal cortex by presubicular commissural projections. J Comp Neurol [Internet] 2005 [cited 2014 Sep 15];487(3):283–99. Available from: http://www.ncbi.nlm.nih.gov/pubmed/15892102

85. Paxinos G, Franklin KBJ. The mouse brain in stereotaxic coordinates. Academic Press; 2004. p. 1–138.

86. Jones BF, Groenewegen HJ, Witter MP. Intrinsic connections of the cingulate cortex in the rat suggest the existence of multiple functionally segregated networks. Neuroscience 2005;133(1):193–207.

87. Troy Harker K, Whishaw IQ. A reaffirmation of the retrosplenial contribution to rodent navigation: Reviewing the influences of lesion, strain, and task. Neurosci. Biobehav. Rev. 2004;28(5):485–96.

88. Clark BJ, Bassett JP, Wang SS, Taube JS. Impaired head direction cell representation in the anterodorsal thalamus after lesions of the retrosplenial cortex. J Neurosci 2010;30(15):5289–302.

89. Wang Q, Burkhalter A. Area map of mouse visual cortex. J Comp Neurol 2007;502(3):339–57.

90. Wang Q, Sporns O, Burkhalter A. Network Analysis of Corticocortical Connections Reveals Ventral and Dorsal Processing Streams in Mouse Visual Cortex. J. Neurosci. 2012;32(13):4386–99.

91. Funahashi M, Stewart M. Presubicular and parasubicular cortical neurons of the rat: Functional separation of deep and superficial neurons in vitro. J Physiol 1997;501(2):387–403.

92. Honda Y, Furuta T, Kaneko T, Shibata H, Sasaki H. Patterns of axonal collateralization of single layer V cortical projection neurons in the rat presubiculum. J Comp Neurol 2011;519(7):1395–412.

93. Katz LC, Burkhalter A, Dreyer WJ. Fluorescent latex microspheres as a retrograde neuronal marker for in vivo and in vitro studies of visual cortex. Nature 1984;310(5977):498–500.

94. Köbbert C, Apps R, Bechmann I, Lanciego JL, Mey J, Thanos S. Current concepts in neuroanatomical tracing. Prog. Neurobiol. 2000;62(4):327–51.

95. Boyden ES, Zhang F, Bamberg E, Nagel G, Deisseroth K. Millisecond-timescale, genetically targeted optical control of neural activity. Nat Neurosci 2005;8(9):1263–8.

96. Dittgen T, Nimmerjahn A, Komai S, et al. Lentivirus-based genetic manipulations of cortical neurons and their optical and electrophysiological monitoring in vivo. Proc Natl Acad Sci U S A 2004;101(52):18206–11.

97. Tamamaki N, Yanagawa Y, Tomioka R, Miyazaki JI, Obata K, Kaneko T. Green Fluorescent Protein Expression and Colocalization with Calretinin, Parvalbumin, and Somatostatin in the GAD67-GFP Knock-In Mouse. J Comp Neurol 2003;467(1):60–79.

98. Katz LC, Iarovici DM. Green fluorescent latex microspheres: A new retrograde tracer. Neuroscience 1990;34(2):511–20.

99. Vercelli a, Repici M, Garbossa D, Grimaldi A. Recent techniques for tracing pathways in the central nervous system of developing and adult mammals. Brain Res. Bull. 2000;51(1):11–28.

100. Allen Institute for Brain Science. Allen Mouse Brain Atlas [Internet]. 2015;Available from: http://mouse.brain-map.org

101. Nagel G, Szellas T, Huhn W, et al. Channelrhodopsin-2, a directly light-gated cation-selective membrane channel. Proc Natl Acad Sci U S A 2003;

102. Gunaydin L a, Yizhar O, Berndt A, Sohal VS, Deisseroth K, Hegemann P. Ultrafast optogenetic control. Nat Neurosci 2010;13(3):387–92.

103. Nagel G, Brauner M, Liewald JF, Adeishvili N, Bamberg E, Gottschalk A. Light activation of Channelrhodopsin-2 in excitable cells of caenorhabditis elegans triggers rapid behavioral responses. Curr Biol 2005;15(24):2279–84.

104. Sakuma T, Barry MA, Ikeda Y. Lentiviral vectors: basic to translational. Biochem. J. 2012;443(3):603–18.

105. Cardin J a, Carlén M, Meletis K, et al. Targeted optogenetic stimulation and recording of neurons in vivo using cell-type-specific expression of Channelrhodopsin-2. Nat Protoc 2010;5(2):247–54.

106. Cetin A, Komai S, Eliava M, Seeburg PH, Osten P. Stereotaxic gene delivery in the rodent brain. Nat Protoc 2006;1(6):3166–73.

107. Shipley MT. Presubiculum afferents to the entorhinal area and the Papez circuit. Brain Res 1974;67(1):162–8.

108. Herkenham M. The connections of the nucleus reuniens thalami: evidence for a direct thalamo-hippocampal pathway in the rat. J Comp Neurol 1978;177(4):589–610.

109. Ginger M, Haberl M, Conzelmann K-K, Schwarz MK, Frick A. Revealing the secrets of neuronal circuits with recombinant rabies virus technology. Front Neural Circuits [Internet] 2013;7(January):2. Available from: http://www.pubmedcentral.nih.gov/articlerender.fcgi?artid=3553424&tool=pmcentrez&rendertype=abstract

110. Wickersham IR, Lyon DC, Barnard RJO, et al. Monosynaptic Restriction of Transsynaptic Tracing from Single, Genetically Targeted Neurons. Neuron 2007;53(5):639–47.

111. Rancz EA, Franks KM, Schwarz MK, Pichler B, Schaefer AT, Margrie TW. Transfection via whole-cell recording in vivo: bridging single-cell physiology, genetics and connectomics. Nat Neurosci 2011;14(4):527–32.

112. Strange B a., Witter MP, Lein ES, Moser EI. Functional organization of the hippocampal longitudinal axis. Nat Publ Gr 2014;15(10):655–69.

113. Bullier J, Kennedy H, Salinger W. Branching and laminar origin of projections between visual cortical areas in the cat. J Comp Neurol 1984;228(3):329–41.

114. Rockland KS, Pandya DN. Laminar origins and terminations of cortical connections of the occipital lobe in the rhesus monkey. Brain Res 1979;179(1):3–20.

115. Maguire E a., Burke T, Phillips J, Staunton H. Topographical disorientation following unilateral temporal lobe lesions in humans. Neuropsychologia 1996;34(10):993–1001.

116. Maguire EA, Burgess N, Donnett JG, Frackowiak RS, Frith CD, O'Keefe J. Knowing where and getting there: a human navigation network. Science 1998;280(5365):921–4.

117. Teng E, Squire LR. Memory for places learned long ago is intact after hippocampal damage. Nature 1999;400(6745):675–7.

118. Ekstrom AD, Kahana MJ, Caplan JB, et al. Cellular networks underlying human spatial navigation. Nature 2003;425(6954):184–8.

119. Jacobs J, Weidemann CT, Miller JF, et al. Direct recordings of grid-like neuronal activity in human spatial navigation. Nat Neurosci 2013;16(9):1188–90.

120. Jacobs J, Kahana MJ, Ekstrom AD, Mollison M V, Fried I. A sense of direction in human entorhinal cortex. Proc Natl Acad Sci U S A 2010;107(14):6487–92.

121. Spiers HJ, Maguire E a. A navigational guidance system in the human brain. Hippocampus 2007;17(8):618–26.

122. Howard LR, Javadi AH, Yu Y, et al. The hippocampus and entorhinal cortex encode the path and euclidean distances to goals during navigation. Curr Biol 2014;24(12):1331–40.

123. Chadwick MJ, Jolly AEJ, Amos DP, Hassabis D, Spiers HJ. A Goal Direction Signal in the Human Entorhinal/Subicular Region. Curr Biol 2015;25(1):87–92.

124. Braak H, Braak E. Staging of Alzheimer-related cortical destruction. Int Psychogeriatr 1997;9 Suppl 1:257–61; discussion 269–72.

125. Harding AJ, Lakay B, Halliday GM. Selective hippocampal neuron loss in dementia with lewy bodies. Ann Neurol 2002;51(1):125–8.

126. Kloosterman F. A code for space [Internet]. [cited 2015 Apr 13];Available from: https://kloostermanlab.files.wordpress.com/2011/07/cell_types_tuning1.png

127. Kloosterman F, Van Haeften T, Witter MP, Lopes Da Silva FH. Electrophysiological characterization of interlaminar entorhinal connections: An essential link for re-entrance in the hippocampal-entorhinal system. Eur J Neurosci 2003;18(11):3037–52.

128. Zhang F, Wang L-P, Boyden ES, Deisseroth K. Channelrhodopsin-2 and optical control of excitable cells. Nat Methods 2006;3(10):785–92.

Eidesstattliche Versicherung

„Ich, Constanze Mauthe, versichere an Eides statt durch meine eigenhändige Unterschrift, dass ich die vorgelegte Dissertation mit dem Thema: *Afferents to the presubiculum in the mouse brain* selbstständig und ohne nicht offengelegte Hilfe Dritter verfasst und keine anderen als die angegebenen Quellen und Hilfsmittel genutzt habe.

Alle Stellen, die wörtlich oder dem Sinne nach auf Publikationen oder Vorträgen anderer Autoren beruhen, sind als solche in korrekter Zitierung (siehe „Uniform Requirements for Manuscripts (URM)“ des ICMJE -*www.**icmje**.org*) kenntlich gemacht. Die Abschnitte zu Methodik (insbesondere praktische Arbeiten, Laborbestimmungen, statistische Aufarbeitung) und Resultaten (insbesondere Abbildungen, Graphiken und Tabellen) entsprechen den URM (s.o) und werden von mir verantwortet.

Meine Anteile an etwaigen Publikationen zu dieser Dissertation entsprechen denen, die in der untenstehenden gemeinsamen Erklärung mit dem/der Betreuer/in, angegeben sind. Sämtliche Publikationen, die aus dieser Dissertation hervorgegangen sind und bei denen ich Autor bin, entsprechen den URM (s.o) und werden von mir verantwortet.

Die Bedeutung dieser eidesstattlichen Versicherung und die strafrechtlichen Folgen einer unwahren eidesstattlichen Versicherung (§156,161 des Strafgesetzbuches) sind mir bekannt und bewusst.“

Datum Unterschrift

Lebenslauf

Mein Lebenslauf wird aus datenschutzrechtlichen Gründen in der elektronischen Version meiner Arbeit nicht veröffentlicht.

Acknowledgment

A scientific script is never the work of one alone. I want to thank all those who rendered this dissertation possible. First, I would like to thank Prof. Dr. Vida for the possibility to do my doctorate at the Institute of Integrative Neuroanatomy of the Charité Berlin and his availability for productive discussion and constructive critics. I also want to thank PD Desdemona Fricker for providing the subject of this work and her comprehensive supervision throughout the entire work process. My special thanks go to Dr. Jean Simmonet who patiently introduced me into the aspects of experimental research. Thank you for your competent advice, your extraordinary commitment during the experimental phase and your rigorous feedback on my written work. I also want to thank all other colleagues at the ICM, especially Roxanne Lofredi for your faithful companionship during this somewhat tricky time for us. Last, I would like to thank my family, my friends and Boris who were always at my side and motivated me in times of doubt. Their unconditional support enabled me to accomplish this dissertation.

Danksagung

Eine wissenschaftliche Arbeit ist nie das Werk einer einzelnen Person, deshalb möchte ich mich bei allen Menschen bedanken, die mir die Erstellung meiner Dissertation ermöglicht haben. Zuerst möchte ich Herrn Prof. Dr. Imre für die Möglichkeit danken, am Institut für Integrative Neuroanatomie der Medizinischen Fakultät der Charité Berlin zu promovieren. Herr Professor Vida stand mir jederzeit mit konstruktiver Kritik und zielführenden Diskussionen zur Verfügung. Mein herzlicher Dank gilt vor allem Frau PD Desdemona Fricker für die Bereitstellung des Themas der vorliegenden Dissertation, ihre umfassende Betreuung und Unterstützung während der Entstehung dieser Arbeit. Ganz besonders bedanken möchte ich mich bei Jean Simmonet, der mich geduldig in die Experimentelle Forschung eingearbeitet hat, mir jederzeit mit fachlich kompetentem Rat zur Seite stand und außergewöhnliches Engagement bei der Klärung von technischen Problemen während der experimentellen Phase, sowie beim Korrekturlesen zeigte. Bedanken möchte ich mich auch bei allen anderen Mitarbeitern des ICMs für die gute Zusammenarbeit und insbesondere bei Roxanne Lofredi für die treue Kameradschaft während der für uns nicht immer einfachen Zeit. Zuletzt möchte ich mich auch bei meiner Familie, meinen Freunden und Boris bedanken, die mir immer zur Seite standen und mich an Tiefpunkten unermüdlich neu motivierten. Ohne ihren bedingungslosen Rückhalt wäre die Fertigstellung dieser Dissertation nicht möglich gewesen.